REPORT NO. UCSESM 70-18

STRUCTURES AND MATERIALS RESEARCH
DEPARTMENT OF CIVIL ENGINEERING

LARGE DEFLECTION DYNAMIC ANALYSIS OF THIN SHELLS USING THE FINITE ELEMENT METHOD

by
CHANG-HUA YEH

Report to
Agbabian-Jacobsen Associates
Los Angeles, California

OCTOBER 1970

STRUCTURAL ENGINEERING LABORATORY
COLLEGE OF ENGINEERING
UNIVERSITY OF CALIFORNIA
BERKELEY CALIFORNIA

Structures and Materials Research
Department of Civil Engineering

Report No. UCSESM 70-18

LARGE DEFLECTION DYNAMIC ANALYSIS OF THIN SHELLS USING THE FINITE ELEMENT METHOD

by

Chang-hua Yeh

Faculty Investigator: Ray W. Clough

Report to

Agbabian-Jocobsen Associates
Los Angeles, Calif.

Structural Engineering Laboratory
University of California, Berkeley, California

October 1970

TABLE OF CONTENTS

ABSTRACT

An analytical procedure is presented for the evaluation of the nonlinear dynamic response of thin shells of arbitrary geometry. Geometric nonlinearity associated with finite deflections of the structures is considered; the material is assumed to remain elastic throughout the analysis.

A quadrilateral finite element, developed by C. A. Felippa is used for the elastic stiffness derivation. A lumped mass formulation is used in the dynamic analysis. The natural frequencies and vibrational mode shapes of the structure are calculated using an inverse iteration technique. Damping in the structure is assumed to be proportional to mass and/or stiffness. The nonlinear dynamic response is obtained using a direct step-by-step integration of the equations of motion.

Several examples are analyzed. The results show excellent agreement when compared with existing solutions. Convergence in the dynamic analysis with respect to the refinements of the mesh size and the time step are also studied.

ACKNOWLEDGEMENTS

This work was carried out during the author's graduate study for the Ph.D. degree in the Division of Structural Engineering and Structural Mechanics at the University of California, Berkeley.

The author wishes to express his deep appreciation to Professor Ray W. Clough for his supervision, support and patience throughout the course of this research. He is also grateful to Professors G. H. Powell and C. K. Miller, members of his thesis committee, and Professor E. L. Wilson for their helpful guidance.

This research was supported by a grant-in-aid provided by Agbabian-Jacobsen and Associates of Los Angeles. The Computer Center of Berkeley Campus generously provided the computer time and facilities necessary for this study. These contributions to the research effort are also appreciated by the author.

1. INTRODUCTION

The extensive use of thin shell structures in modern construction has created a need for better understanding of their behavior - both linear and non-linear as well as both static and dynamic. For a linear problem, the solutions (displacements, stresses, etc.) are proportional to the applied loads, but for a non-linear problem, this proportionality does not exist. The reason for considering geometric non-linearity due to finite deformation of the structure is that the behavior of shells is very sensitive to their shapes. Therefore, a non-linear solution may be very much different from a linear one when the deflection of the structure becomes finite (as against the infinitesimal deformation considered in a linear analysis). In this case, results based on a linear analysis may be misleading and unconservative. For many types of shell structures, the critical stress and deflection response may result from time varying loads such as wind gusts or earthquake ground motion. In order to evaluate the dynamic response behavior, it is necessary to formulate special analysis procedures which account for the effects of inertia and damping forces. The inclusion of these forces which are dependent on the displacement behavior of the structure leads to a further complication in the analysis procedure. In order to study the response of shell structures under the time varying loadings, such as wind and earthquake, their dynamic behavior has to be studied.

In classical shell theory, even for linear static case, the governing differential equations can only be solved for a limited number of shells with simple geometry and subject to some special types

of loads. Following the development of high speed computers, various numerical procedures have been used to analyze certain classes of shells but their usage is still limited. No method for systematic analysis of shells of arbitrary shapes with arbitrary boundary conditions, changing thickness and subject to arbitrary loadings was available until the introduction of the Finite Element Method.

During the past ten years, the Finite Element Method has been used in solving many kinds of structural and mechanics problems. A flat element suitable for the analysis of thin shells of arbitrary geometry may be constructed by superposing a plate bending element and a plane stress element. Two elements of this type, developed by C. P. Johnson (19) and A. J. Carr (3) have been successfully used. With their own advantages and disadvantages, both elements are applicable to general shell analysis. These two elements represent one type of approach to finite element shell analysis in which the structure is represented by an assemblage of flat elements. An alternate approach using a curved element based on a degenerated three-dimensional solid element (1) has recently been developed, and shows considerable promise of success.

The dynamic response of a structure may be obtained either by a mode superposition method (16) or by a direct step-by-step integration of the equation of motion (27). In the mode superposition analysis, the vibration modes of a structure are obtained by solving an eigenvalue problem and the equations of motion are then decoupled and solved. The dynamic response may then be obtained by superposing the contribution from different modes. This method can be applied only to linear systems. On the other hand, the direct step-by-step

integration technique reduces the coupled equations of motion to an equivalent static problem and may be used for both linear and non-linear systems.

The classical way of solving a non-linear problem in which the non-linear equations were set up and solved, can be applied only to simple structures. In a more general case, a linearized approach, either by an iteration procedure (26) or by an incremental analysis (9), has to be used. The iteration procedure uses a series of linear analysis and calculates the out-of-balance force to get the equilibrium position. This method can only be applied to the static problems. The incremental analysis is carried out by applying the load in small increments and a linear analysis is performed for each load increment. This technique can be used for both static and dynamic problems.

With regard to the field of non-linear dynamic behavior of shells, some work (3, 13, 20, 26, 34, 39, 41, 42) using the Finite Element Method has been carried out for several special problems. A linear dynamic analysis for shells of arbitrary geometry was presented in Ref. 3. All the other references listed above deal with either plates or axisymmetric shells, and most of them consider static non-linear problems only. The dynamic non-linear behavior of many shell structures remains unknown.

It was the purpose of the present research to develop a general procedure to study the non-linear dynamic response of thin shells of arbitrary geometry. Only geometric non-linearity due to large deflection of the structure is considered. The material is assumed to remain elastic throughout the analysis. The primary interest was to

study large shell structures subject to finite deformation under working loads.

A quadrilateral shell element, developed by Johnson and later modified by C. A. Felippa, is used for the elastic stiffness derivation. The lumped mass formulation is used and damping is assumed to be proportional to stiffness and/or mass. A step-by-step integration technique is combined with the incremental analysis for non-linear problems, to calculate the non-linear dynamic response. This is a completely general procedure and can be carried out for other kinds of structures. All operations are carried out in matrix form and the resulting simultaneous equations are solved by standard Gauss Elimination.

Convergence with successive refinement of meshes formed with this element for static solution has been discussed extensively in Ref. 19. The dynamic aspects of convergence are studied in the present research by examining the natural frequencies of shells calculated with successively refined meshes, and by checking the dynamic response calculated with different time steps. The accuracy of the non-linear analysis has been studied by comparison with existing solutions.

Computer programs have been written to carry out the calculations, and results checked against existing special solutions have proved to be satisfactory. Finally analyses of a simply supported cylindrical shell roof and a doubly curved cooling tower are presented to demonstrate the capability of the analytical procedure.

2. THE ELEMENT

2.1 Finite Element Idealization of Shell Structures

An assemblage of quadrilateral elements each consisting of four planar triangular elements, is used to approximate the thin shell structure as shown in Fig. 2-1a. In addition, single triangular elements are also used whenever the quadrilateral element is not able to approximate the shell geometry properly. The quadrilateral element has four external nodes and five internal nodes (Fig. 2-1b). Internal nodes 6, 7, 8 and 9 are the middle points of the lines connecting nodes 1-5, 2-5, 3-5 and 4-5 respectively. These nodes will be referred to as the middle point nodes from now on.

The external nodes lie on the middle surface of the shell and the position of the first internal node (node 5) may be either specified independently or set equal to the average of the four external nodes. The thickness is specified at the four external nodes, and the thickness at node 5 may be either specified or set equal to the average thickness of the four external nodes. The thickness is assumed to vary linearly between nodes. The geometry of the quadrilateral element is completely defined by the data specified at these five nodes. The material properties are assumed to be constant for each element.

The planar element can only approximate the curved shell surface but will converge to the actual geometry as the size of the element is decreased.

The shell element is constructed by superposing a plane stress element and a plate bending element at the triangle level. This

assumption implies that the membrane action and the bending action are decoupled at the sub-element level. However for a curved shell structure, membrane and bending actions are coupled when the structure stiffness matrix is assembled.

2.2 Coordinate Systems

A local element coordinate system $(\bar{x},\bar{y},\bar{z})$ is defined for each quadrilateral element (Fig. 2-2a). All physical and kinematic properties such as stresses, material law, etc. are defined in this system. The $\bar{x}$ axis is defined by connecting the middle points of side 1-4 and side 2-3. A $\tilde{y}$ axis is defined temporarily by connecting the middle points of side 1-2 and side 3-4. The $\bar{z}$ axis is taken normal to $\bar{x}$ and $\tilde{y}$ and finally $\bar{y}$ is selected normal to $\bar{x}$ and $\bar{z}$ to complete a right handed system. The system is defined such that looking from the positive $\bar{z}$ direction, nodes 1-2-3-4 will run counterclockwise.

For a single triangle, it is assumed that nodes 1 and 4 share the same position and $\bar{x},\bar{y},\bar{z}$ are defined similarly.

A local subtriangle coordinate system $(\bar{x}_m,\bar{y}_m,\bar{z}_m$, where m = 1,2,3,4) is defined for each triangle of the quadrilateral (Fig. 2-2b). These systems are used to calculate the stiffness matrix, consistent load vector and internal stresses of the triangles. The $\bar{z}_m$ axis is normal to the plane of the m-th triangle. The $\bar{x}_m$ axis is taken normal to the $\bar{z}_m$ and $\bar{y}$ axes and finally $\bar{y}_m$ is selected normal to the $\bar{z}_m$ and $\bar{x}_m$ axes. If the quadrilateral is planar, all $(\bar{x}_m,\bar{y}_m,\bar{z}_m)$ axes have the direction of $(\bar{x},\bar{y},\bar{z})$.

For a single triangle element, only $(\bar{x}_1,\bar{y}_1,\bar{z}_1)$ exist and coincide with axes $(\bar{x},\bar{y},\bar{z})$.

2.3 Plane Stress Element

A constrained linear strain triangle (LST) is used to evaluate the in-plane stiffness of the quadrilateral shell element. The derivation of the element stiffness matrix and the consistent load vector of LST are discussed in detail in Refs. 10 and 19, therefore only a brief description of the element will be given here. Those who are interested in more detail should refer to the original works.

The linear strain triangle has six nodal points and twelve degrees of freedom (Fig. 2-3). The in-plane displacements u and v have a quadratic variation within the element and the strains, ϵ_x, ϵ_y and γ, have a linear variation. This element is constrained by requiring the displacements u and v to vary linearly along one side of the triangle. Thus, two equations are introduced to eliminate u_6 and v_6 as independent degrees of freedom. The resulting constrained linear strain triangle has ten independent degrees of freedom and will be used to construct the quadrilateral element.

For a single triangle element, a constant strain triangle (CST) with three nodes and six degrees of freedom is used. The CST assumes linear variation of in-plane displacements and strains remain constant within the triangle. Its derivation can be found in any elementary finite element analysis book (e.g. Ref. 43).

2.4 Plate Bending Element

The linear curvature compatible triangle (LCCT) is used for the out-of-plane stiffness mechanism of the shell element. The LCCT, which is fully compatible between elements, is the most efficient flat plate bending element yet developed and is discussed in detail in Ref. 11.

The triangle is divided into three sub-triangles with ten degrees of freedom each (Fig. 2-4a). The transverse displacement within each sub-triangle has a complete cubic expansion, and its second derivative, the curvature, has a linear variation. The three internal degrees of freedom w_o, θ_{xo} and θ_{yo} (Fig. 2-4b) are eliminated by applying internal compatibility constraints between the sub-triangles. Thus the resulting triangle element (LCCT-12) has twelve degrees of freedom (two rotations and one translational displacement at each corner and one rotation about the edge at the middle point of each side, see Fig. 2-4b). This triangle is constrained by forcing the normal rotation to vary linearly along one side. Thus θ_{m6} is eliminated and the resulting triangle element (LCCT-11) has eleven degrees of freedom and is ready for the constructing of the quadrilateral element.

For a single triangle element, the normal rotations are constrained to vary linearly along all three sides and all θ_{m4}, θ_{m5} and θ_{m6} are eliminated. The resulting triangle has nine degrees of freedom (LCCT-9).

2.5 Quadrilateral Element and Discussion

In the previous sections, the triangle elements are prepared such that there will be no external middle point node at the quadrilateral level. The reason is that these nodes tend to increase the number of equations and the band width of the structural stiffness matrix, as well as to complicate the computer programming for mesh generation.

Four triangles together form a quadrilateral element which has five nodal points and four middle point nodes (Fig. 2-1b). Each corner nodal point has five degrees of freedom (three translations and two

rotations) and each middle point has three degrees of freedom (two translations and one rotation). The quadrilateral element has a total of thirty seven degrees of freedom (twenty externals and seventeen internals). The seventeen internal degrees of freedom are eliminated by the standard static condenstation procedure after the quadrilateral element stiffness matrix is formed and may be recovered in the stress calculation.

The single triangle element has three nodal points and fifteen degrees of freedom. Due to the constant strain assumption in the plane stress element, the triangle element should be used only in areas with small strain variation or with a very fine mesh in order to represent the membrane behavior properly. Its use should be generally avoided unless it is absolutely necessary to form a satisfactory mesh.

The quadrilateral element has a superior stiffness property and it gives good results in comparison with closed form solutions (19). This element possesses two significant properties to be discussed below:

a) Each nodal point has only five degrees of freedom instead of six. This introduces problems when the element stiffness matrix is transformed into a common coordinate system for the whole structure. This subject will be discussed in detail in the next chapter.

b) The in-plane displacements have a quadratic expansion while the out-of-plane displacements have a cubic expansion within each element. Incompatibility of the displacements along the edges of the elements occurs when a curved shell surface is represented by an assemblage of these elements. However, results

from a complete compatible shell element (3) which assumed cubic displacement expansions for both the plate bending as well as the plane stress elements showed little improvement over the results given by this element. Therefore it appears that the lack of compatibility between the in-plane and the out-of-plane displacements does not cause much error in the solution.

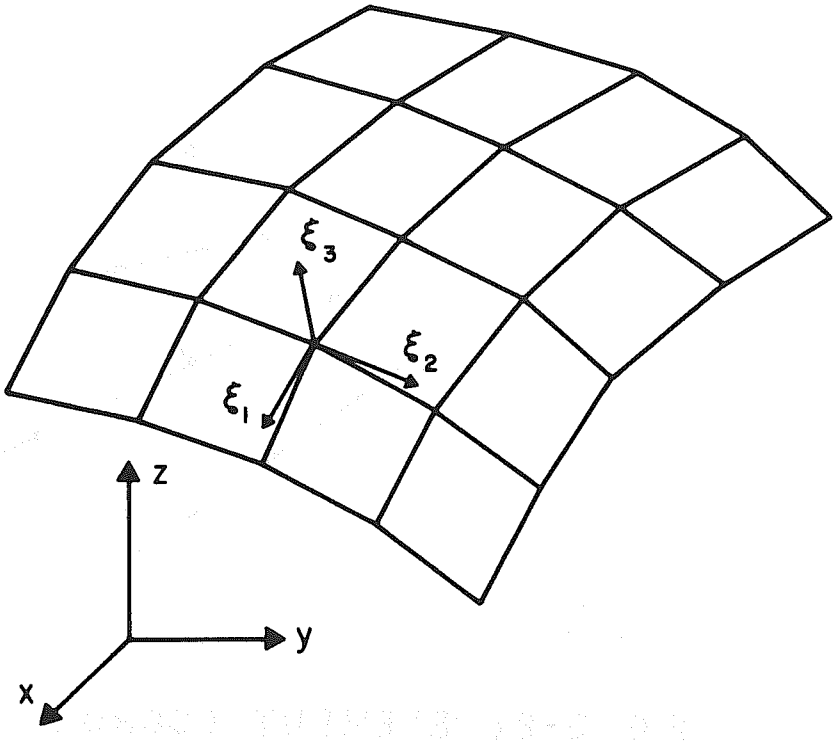

FIG. 2-1a FINITE ELEMENT IDEALIZATION OF SHELL STRUCTURE

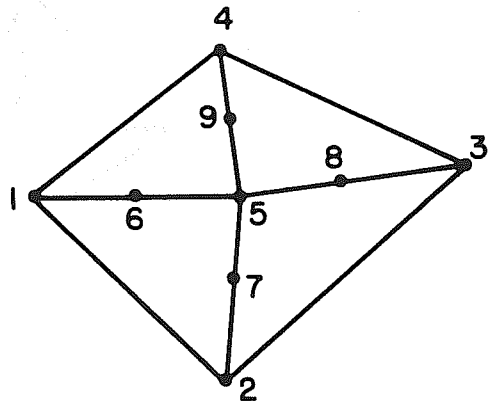

FIG. 2-1b TYPICAL QUADRILATERAL ELEMENT

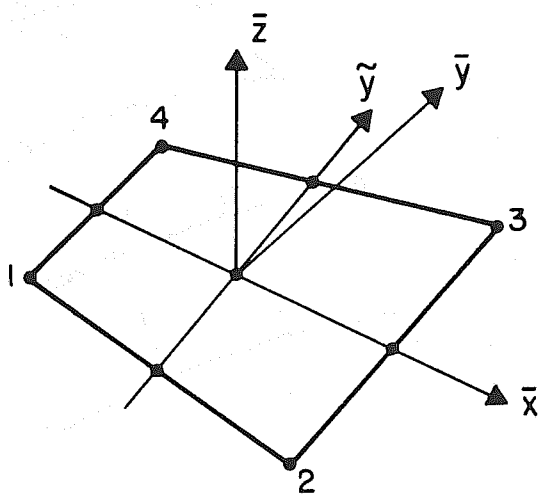

FIG. 2-2a ELEMENT COORDINATE SYSTEM

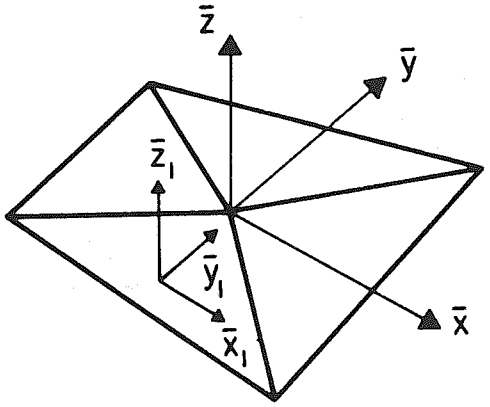

FIG. 2-2b SUBTRIANGLE COORDINATE SYSTEM

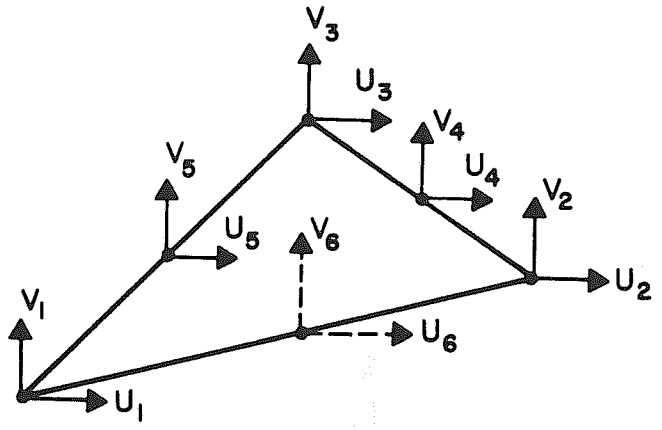

FIG. 2-3 LINEAR STRAIN TRIANGLE

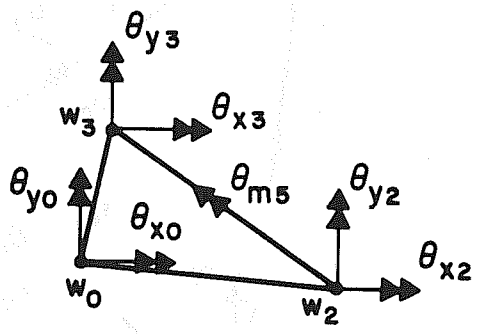

FIG. 2-4a SUBTRIANGLE OF LINEAR CURVATURE COMPATIBLE TRIANGLE

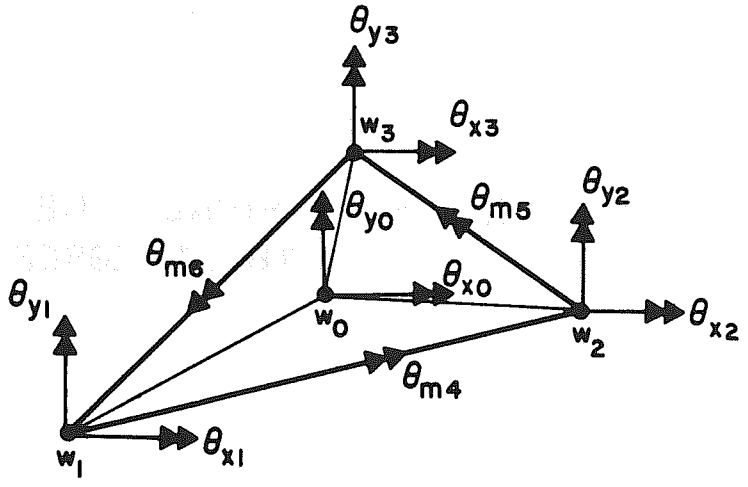

FIG. 2-4b LINEAR CURVATURE COMPATIBLE TRIANGLE

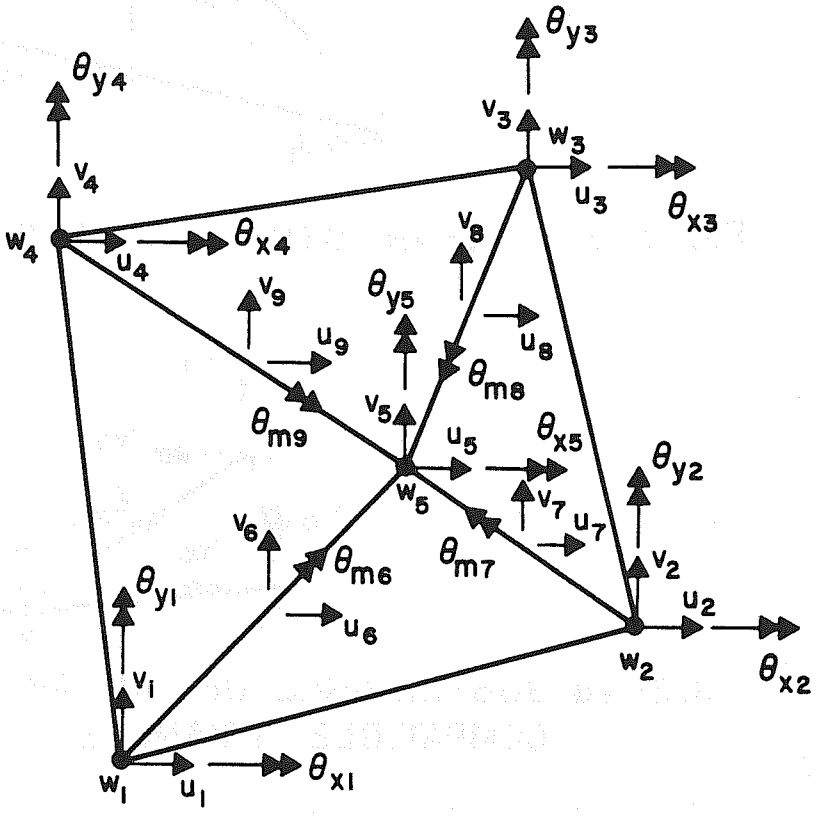

FIG. 2-5 TYPICAL SHELL ELEMENT WITH 37 DEGREES OF FREEDOM

3. THE STRUCTURAL STIFFNESS

3.1 Coordinate Systems and Their Transformations

In the direct stiffness analysis, a global coordinate system (x,y,z) is usually defined for the structure. The element stiffness matrix is then transformed into this system to form the structural stiffness matrix which is used to solve for the deflection of the structure. However for the element used in this study, only five degrees of freedom per node are defined at the element level. The resulting structural stiffness matrix which includes six degrees of freedom per nodal point in the three dimensional space, will not necessarily be positive definite (i.e. singularity may occur), because of the discrepancy between the element and global degrees of freedom. The use of a surface tangent coordinate helps to overcome this difficulty.

The surface tangent coordinate system (ξ_1, ξ_2, ξ_3) is defined for each node (Fig. 2-1a) in the global system. The ξ_3 axis is defined as normal to the shell surface. Axes ξ_1 and ξ_2 may be oriented arbitrarily as long as they both lie in the tangent surface of the shell. The external rotational degrees of freedom at the element level (two for each node) are transformed into the surface tangent coordinate and only the components of rotations around axes ξ_1 and ξ_2 are considered. The three translational degrees of freedom may be transformed into any desired coordinate system. The above transformation provides stable system with five degrees of freedom per node while the rotation about the normal ξ_3 axis (which from now on will be referred to as the sixth degree of freedom) is constrained.

It was found in previous studies that the solution is not sensitive to the accuracy with which the surface tangent coordinate is defined. Therefore, an approximate surface tangent may be used to replace the exact surface tangent. This approximation is essential in the large deflection analysis because axes normal to the surface change their directions as the structure deforms.

One method to define this approximate surface tangent at node N (Fig. 3-2) is to find the neighboring nodes I, J, K and L and take the line connecting nodes I and J as the ξ_1 axis. The line K-L will be $\bar{\xi}_2$ and ξ_3 is defined to be normal to ξ_1 and $\bar{\xi}_2$. And finally ξ_2 is taken normal to ξ_3 and ξ_1. This convention can be easily programmed for automatic computation and has proven to give satisfactory results. For nodes connected with only three other nodes, node K is assumed to share the same position as node N. And for nodes connected with only two other nodes, nodes I and K are assumed to share the same position as node N. If more than four nodes are connected with node N, nodes I, J, K and L have to be selected for it in advance.

This convention is also very convenient for defining the rotational boundary conditions because for the boundary nodes, at least one of the axes ξ_1 and ξ_2 will be approximately tangent to the boundary line.

In large deflection analysis, it is always convenient to express the translational degrees of freedom in the global coordinate system. Then the evaluation of the change of position of nodal points due to deflection is a straightforward operation.

Note that after the element stiffness matrix of the triangle is formed, those degrees of freedom corresponding to the external nodes

of the quadrilateral may be transformed directly to the global coordinate (x,y,z) or to the surface tangent coordinates (ξ_1, ξ_2, ξ_3) while the remaining degrees of freedom may be transformed to the local element coordinate ($\bar{x}$,$\bar{y}$,$\bar{z}$) and may stay in that coordinate. The computational efforts will be reduced in so doing.

3.2 Number of Degrees of Freedom Per Node

The fact that only five degrees of freedom per node instead of six are considered in this finite element shell formulation provides an immediate advantage in that both the number of simultaneous equations and the band width of the structural stiffness matrix are reduced by a factor of 6/5. Therefore the required core storage in the computer is reduced by a factor $1.2^2 = 1.44$ and the equation solving time is reduced by a factor $1.2^3 = 1.728$. However, neglecting the sixth degree of freedom is equivalent to imposing an artificial constraint on the structure; i.e. no rotation about the normal axes is allowed (Fig. 3-2). Although past experience (19) has shown that this constraint has an insignificant effect in the analysis of stiff structures, it may be important for a very flexible structure.

The sixth degree of freedom is not defined at the element level. However, for a node on the surface of a doubly curved shell, the stiffness for the sixth degree of freedom will be defined after the transformation to the global coordinate system. To be more specific, if the elements adjacent to a node do not lie in a common plane, this node will be stable, i.e., no singularity will occur. In this case, the sixth degree of freedom may be retained to form a global system having six degrees of freedom per node.

Two types of singularities do occur for some element assemblages. The first type is represented by a flat plate for which every node is singular. Columns and rows in the structural stiffness matrix corresponding to all the sixth degree of freedom are zero and there is no coupling between these degrees of freedom and the rest. The second type is best illustrated by a cylindrical shell whose surface is curved in only one direction. Singularity occurs only at nodes along the straight boundaries of the shell and the sixth degree of freedom at these singular nodes are uncoupled with the others. There is no singularity at the other nodes, and the sixth degree of freedom of these are coupled. In both cases, an artificial torsional spring has to be attached to each singular node in the direction of the normal axis to make the system mathematically stable. Since the stiffness connected with these degrees of freedom are uncoupled, the size of the spring can be arbitrary. However, for practical purposes, it is much easier to attach a spring to every node rather than to identify each singular node. In this case, the spring stiffness has to be small so as not to influence the physical behavior of the structure. If the spring stiffness is too large, the system will be constrained similar to the way the five degrees of freedom per node system is constrained. The necessary spring stiffness may be selected as the average stiffness of rotations about the ξ_1 and ξ_2 axes times a factor. In practice, it has been found that a factor equal to 10^{-6} provides satisfactory results; it is large enough to provide numerical stability but not so large as to introduce a spurious constraint. By this means a stable system with six degrees

of freedom per node may also be constructed using this element.

Two examples have been studied to examine the effect of neglecting and including the sixth degree of freedom.

a) Static Case

A cylindrical shell with one end clamped and the other end free to deflect under its own weight is shown in Fig. 3-3. This example is designed to bring out the effect of constraining the sixth degree of freedom in a static stable system. A series of cases were solved in which the length L was varied from 25 feet to 200 feet while all other dimensions were held constant. Four elements were used in the circumferential direction. The number of elements in the longitudinal direction was increased from five for L = 25 feet to ten for L = 200 feet. The resulting vertical deflection at the middle point of the free end for cases both with and without constraints (i.e. five and six degrees of freedom per node systems) are as shown in Table 3-1:

TABLE 3-1. END DEFLECTION OF CANTILEVER SHELL

LENGTH L (Ft)	DEFLECTION (FT)		DIFFERENCE (%)
	5-DOF	6-DOF	
25	0.03695	0.03696	0.03
50	0.2374	0.2375	0.04
100	1.303	1.307	0.31
160	4.501	4.509	0.18
200	8.064	8.075	0.14

It can be seen from the above table that the effect of constraining the sixth degree of freedom is very small. The fact that the percentage difference drops as the length exceeds 100 feet is because the structure becomes so flexible that the total deflection increases at a faster rate than the difference.

b) Dynamic Case

A very flexible cylinder hinged at one end and free at the other end is shown in Fig. 3-4. This cylinder is free to rotate about the x-axis, thus the frequency of its first vibrational mode (rigid body rotation) is zero. Taking advantage of the symmetric conditions, a quarter of the cylinder with five elements in the circumferential direction and seven elements in the longitudinal direction was analyzed for its vibrational modes (using inverse iteration as described in Section 4.3) considering five and six degrees of freedom per node. The resulting natural frequencies of the first three modes are:

TABLE 3-2. NATURAL FREQUENCIES OF HINGED TUBE

	FREQUENCY (rad/sec)	
Mode	5-DOF	6-DOF
1	.000274	.000001311
2	.004221	.004211
3	.004863	.004841

The effect of neglecting the sixth degree of freedom is shown in the first mode where the frequency should be zero. The non-zero quantity in the five degrees of freedom system is a result of the artificial constraints caused by neglecting the sixth degree of freedom (note that it is an order of magnitude lower than the next mode anyway).

The first mode frequency from the six degrees of freedom system is considered small enough in comparison with the second mode.

It should be noted that in this example the artificial torsional spring is attached to every node, therefore the resulting frequencies will depend upon the stiffness of the spring. If the stiffness is too large, the system will be constrained, but if too small, the roundoff error of the computer will overcome its contribution and cause the system to become unstable again. Only an adequately small spring will make the system stable and impose only negligible constraint to it. Also it may be noted that the frequencies of the second and third modes from both system have a very small difference considering how flexible the system is. This fact shows that the five degrees of freedom per node system imposes only very small constraint on the structure in a dynamic analysis, if the system is properly supported (i.e. if no rigid body displacement is allowed).

It may be concluded from the preceding examples that the five degrees of freedom per node system gives good results as long as the structure is reasonably stiff and is properly supported. This formulation will be used for the rest of this research.

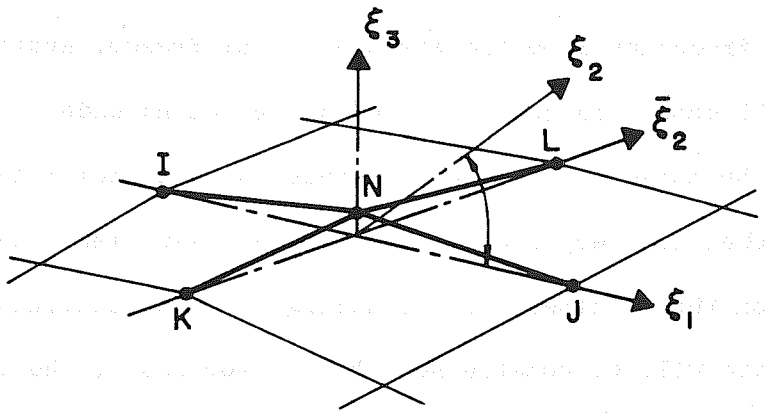

FIG. 3-1 APPROXIMATE TANGENT COORDINATE

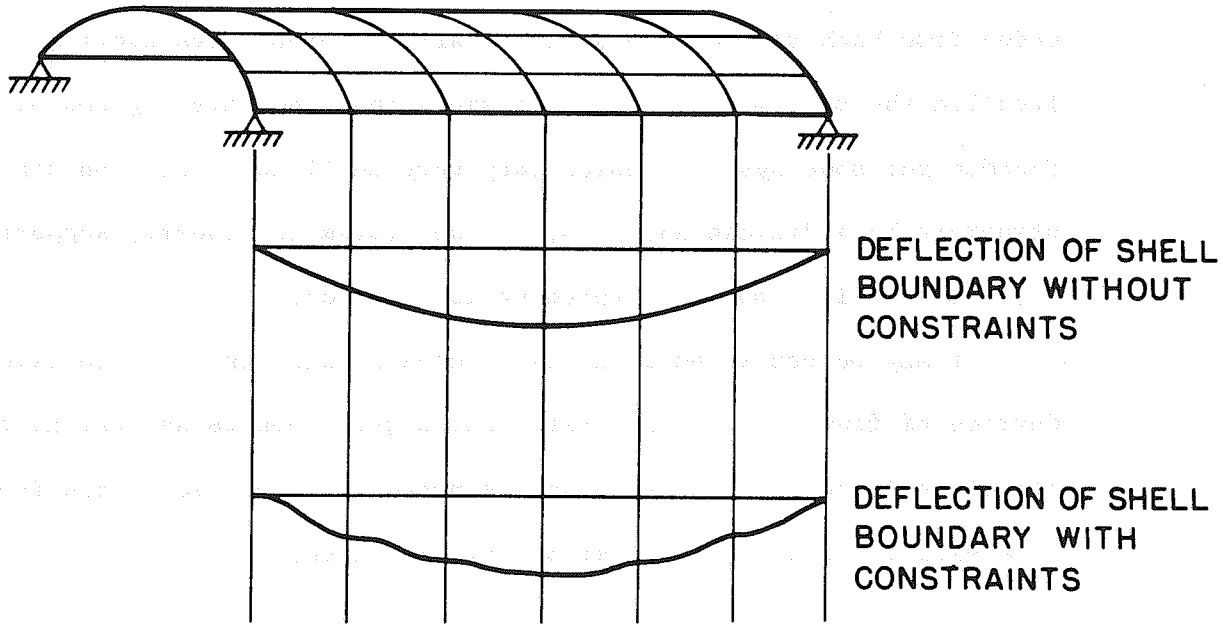

FIG. 3-2 CONSTRAINTS CAUSED BY NEGLECTING THE SIXTH DEGREE OF FREEDOM

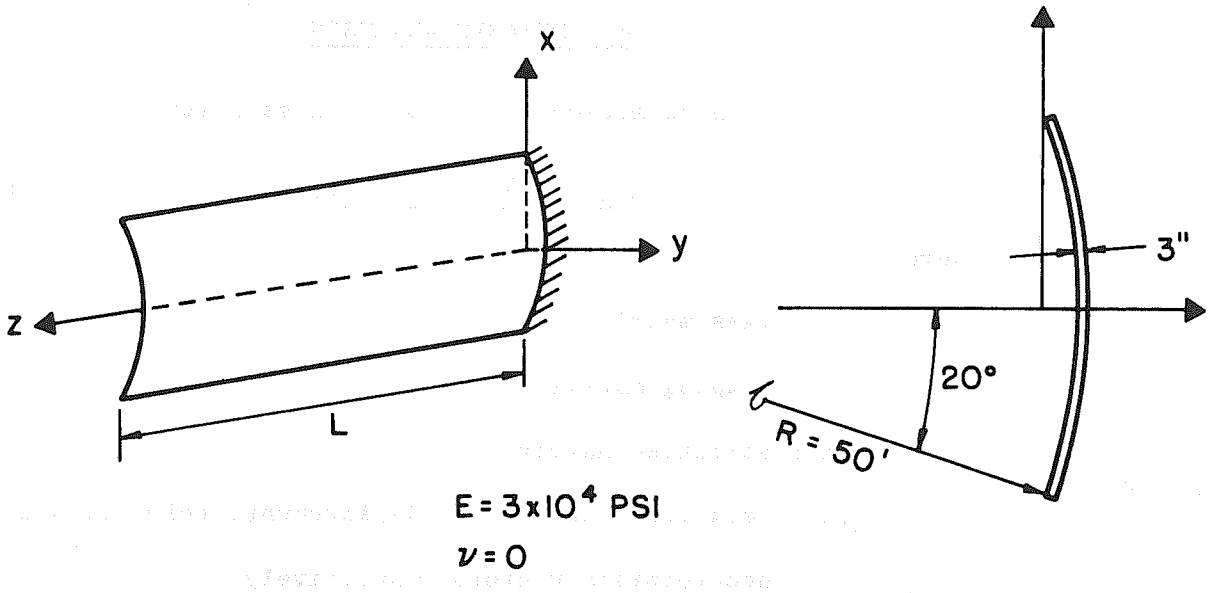

FIG. 3-3 CANTILEVER SHELL

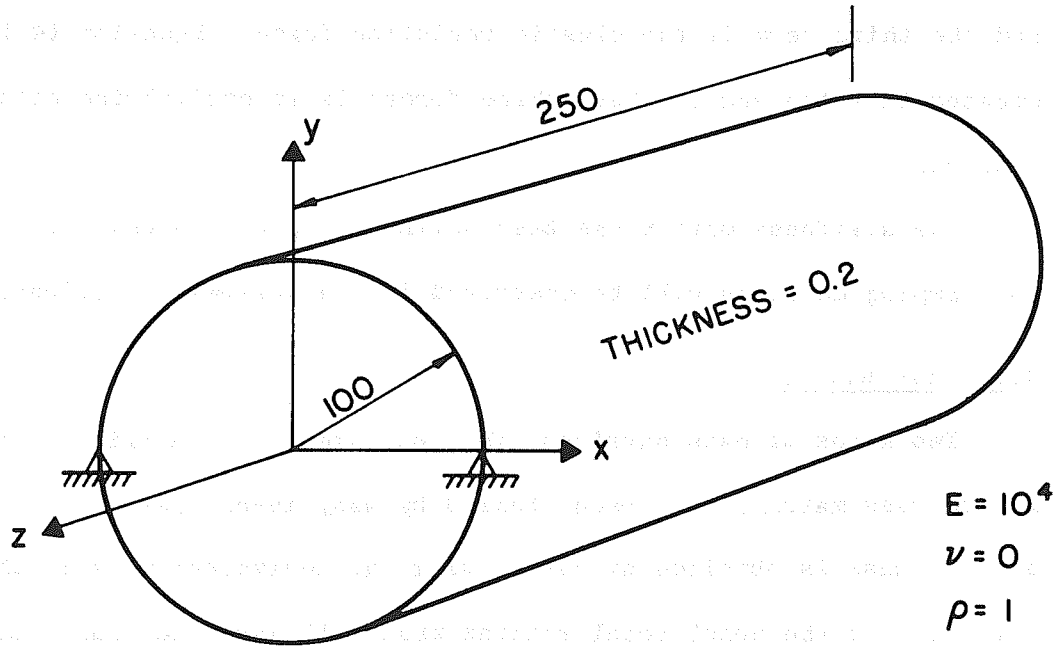

FIG. 3-4 HINGED CYLINDRICAL TUBE

4. DYNAMIC ANALYSIS

The equation of motion in dynamic analysis is:

$$\underline{M}\,\ddot{\underline{x}} + \underline{C}\,\dot{\underline{x}} + \underline{K}\,\underline{x} = \underline{P}(t) \qquad (4.1)^*$$

where

$\underline{M}$: mass matrix

$\underline{C}$: damping matrix

K : stiffness matrix

$\underline{x},\dot{\underline{x}},\ddot{\underline{x}}$: relative nodal point displacement, velocity and acceleration vectors respectively

$\underline{P}(t)$: external load vector (function of time)

The first term in the left hand side of the above equation represents the inertia force in the system, the second term is the damping force and the third term is the elastic resisting force. Equation (4.1) indicates that the sum of these three forces is in equilibrium with the external load.

The stiffness matrix has been defined in previous chapters. Mass and damping matrices will be described in the following sections.

4.1 Mass Matrix

Two kinds of mass matrices, the consistent mass matrix and the lumped mass matrix, have been studied by many investigators. The consistent mass is obtained by calculating the equivalent mass in the direction of the nodal accelerations that will have the same amount of kinetic energy as the distributed element mass due to acceleration. This can be achieved by integrating the displacement interpolation

*An underlined symbol will represent a matrix or a vector in the following.

functions of the element. The consistent mass matrix of an element is therefore defined by:

$$\underline{m} = \int_v \rho h \, \underline{\varphi}^T \underline{\varphi} \, dv \qquad (4.2)$$

where ρ is the mass density, h is the thickness of the element (may be function of position) and $\underline{\varphi}$ is the displacement interpolation function for this element. It should be noted that other mass matrices may also be constructed using this equation together with lower order interpolation functions. The computational effort is reduced in so doing, while the accuracy of the solution is still retained. This is because in the mass matrix, diagonal elements corresponding to the translational displacements do not change significantly from different interpolation functions and the solution is not sensitive to the values of the other elements of the mass matrix.

Element m_{ij} of the matrix $\underline{m}$ represents the inertia force in the direction of the i-th displacement resulted from unit acceleration in the direction of the j-th displacement. The consistent mass matrix of each element, generally, is fully populated. The element mass matrices are assembled to form the structural mass matrix $\underline{M}$ in the same way the structural stiffness matrix is formed. Matrix $\underline{M}$ has the same banded form as matrix $\underline{K}$ if it is based on a consistent element mass matrix.

The lumped mass matrix may be obtained by concentrating the mass of the structure to the nodal points. This will result in a diagonal mass matrix, in which the elements m_{ii} corresponding to the rotational degrees of freedom will be zero. Previous studies made by several investigators have shown that the lumped mass assumption leads to a

more accurate result than the consistent mass despite the fact that the latter has a better mathematical interpretation (6, 11). In addition, the lumped mass system has the advantage of yielding great savings in the computer core storage and in computational effort. The only advantage of the consistent mass formulation is that its solution gives the upper bound of the true solution if the element is fully compatible while this property does not apply to the lumped mass. However, for the quadrilateral element used in this research the displacements between element, in general, are not compatible and this advantage does not exist. Therefore the lumped mass formulation is used in this work.

The method to be used in lumping mass is more or less arbitrary, but the results of different procedures are only slightly different. In this study, a quadrilateral element is divided into four pieces by connecting the middle points of opposite sides and the mass of each piece is applied to the adjacent node. For a single triangle element, one third of the total mass is concentrated at each node.

The fact that elements m_{ii} in the mass matrix corresponding to the rotational degrees of freedom are zero causes some problem in solving the eigenvalue problem (Section 4.3). In the present work, a small quantity is assigned to these coefficients to make the lumped mass matrix positive definite. Physically speaking, this means that instead of lumping the mass to a point with zero rotational inertia, the lumped mass will have a small but finite dimension. The quantity assigned is rather arbitrary and the solution is not sensitive to its magnitude as long as it is not so large as to constrain the rotations of the nodal points. In the direct step-by-step integration (Section 4.5) the mass matrix is used to evaluate the inertia resisting force

in addition to the elastic force and a zero element in the diagonal of the lumped mass matrix will not cause numerical difficulty as in the mode superposition method.

4.2 Damping Matrix

The presence of damping forces tends to decrease the dynamic response of a structure and a solution obtained without damping gives an upper bound to the response. Damping forces do exist in actual structures but their exact form is unknown in most systems. The magnitude of the damping is usually obtained experimentally in the form of a modal damping ratio for each vibrational mode:

$$C_n = \lambda_n (C_n)_{cr} \tag{4.3}$$

where $(C_n)_{cr}$ is the critical damping of the n-th vibrational mode of the structure.

The modal damping ratio is used directly in the mode superposition analysis as will be shown later. For a step-by-step integration of the equations of motion, however, the damping matrix has to be defined. If the damping forces are proportional to the velocities of the mass points, it can be shown that the damping matrix will be proportional to the mass matrix. If the damping forces are proportional to the strain velocities the damping matrix will be proportional to the stiffness matrix. Thus if both types of damping exist, the damping matrix will have the following form:

$$\underline{C} = \alpha \underline{M} + \beta \underline{K} \tag{4.4}$$

The relationship between the above two types of damping and their properties will be discussed in the following sections.

4.3 Eigenvalue Problem Solution

The dynamic properties of structures can be studied by examining their free vibration mode shapes; i.e. considering the motion without damping and external loads. The equation of motion for free vibration is:

$$\underline{M}\,\ddot{\underline{x}} + K\,\underline{x} = \underline{0} \tag{4.5}$$

In this case the displacement is in harmonic motion and can be expressed as:

$$\underline{x} = \underline{X} \sin(\omega t) \tag{4.6a}$$

where $\underline{X}$ is the vibrational mode shape and is independent of time t and ω is the natural frequency of the structure. Then the acceleration will be:

$$\ddot{\underline{x}} = -\omega^2\,\underline{X} \sin(\omega t) = -\omega^2\,\underline{x} \tag{4.6b}$$

Substituting $\underline{x}$ and $\ddot{\underline{x}}$ into Eq. (4.5), the following equation is obtained.

$$\underline{K}\,\underline{X} = \omega^2\,\underline{M}\,\underline{X} \tag{4.7}$$

For a lumped mass assumption, matrix $\underline{M}$ is a diagonal matrix and this equation can be converted to the standard eigenvalue form by defining:

$$\underline{X} = \underline{M}^{-\frac{1}{2}}\,\underline{Y} \tag{4.8}$$

Equation (4.7) then becomes:

$$\underline{M}^{-\frac{1}{2}}\,\underline{K}\,\underline{M}^{-\frac{1}{2}}\,\underline{Y} = \omega^2\,\underline{Y} \tag{4.9a}$$

or

$$\underline{A}\,\underline{Y} = \omega^2\,\underline{Y} \tag{4.9b}$$

In order to carry out the above transformation, all the diagonal terms in the matrix $\underline{M}$ have to be greater than zero. This requires

a positive inertia term to be defined for those elements m_{ii} corresponding to the rotational degrees of freedom in the lumped mass formulation (Section 4.1). With this positive definite lumped mass matrix $\underline{M}$, the transformation is straightforward. Matrix $\underline{A}$ remains positive definite, symmetric and banded if the original $\underline{K}$ matrix is positive definite, symmetric and banded. Equation (4.9) is a standard eigenvalue problem and may be solved by many existing computer subroutines.

An alternate procedure may also be used when the lumped mass matrix is involved. Considering the fact that the masses corresponding to the rotations are zero, these degrees of freedom can be eliminated by a static condensation procedure. The matrix resulting from the condensation procedure is smaller than the original one, but this matrix is fully populated. Therefore, this procedure may not be more efficient than solving Eq. (4.7) directly.

Another procedure in which a flexibility matrix consisting of only the unconstrained translational degrees of freedom is constructed and used to solve the eigenvalue problem, also deals with a smaller but fully populated matrix. The flexibility matrix can be formed by applying unit load in the direction of each translational displacement successively. The resulting translational displacement components for each load case represent one column of the flexibility matrix. The formulation of the flexibility matrix is a very efficient procedure which takes advantage of the banded form of the original $\underline{K}$ matrix in solving for the displacements. The interested reader should refer to Ref. 3 for more details.

There are two types of method to obtain the numerical solution of the eigenvalue problems. They are the iteration method and the matrix transformation method (5, 18). Computer subroutines based on different forms of these two methods for different purposes are available to solve the eigenvalue problems. Most subroutines are restricted in their capacities due to the limitation of computer core storage. For larger systems, several forms of Rayleigh-Ritz technique have been developed to reduce the size of the matrix before solving for eigenvalues. Those who are interested should refer to other publications, e.g. Ref. 3, for more details.

In this research, an inverse iteration procedure has been used to solve the eigenvalue problem. The procedure is described below:

i) Equation (4.7) is converted to the classical form of Eq. (4.9b).

ii) The smallest eigenvalue can be obtained by inverse iteration. The iteration is carried out by estimating vector $\underline{Y}$ on the right hand side of Eq. (4.9b) and solving for $\underline{Y}$ on the left hand side, then using this $\underline{Y}$ as a new estimation and repeating this procedure. It can be shown that this procedure will converge to the lowest eigenvalue and eigenvector.

iii) After the lowest eigenvalue is obtained, matrix $\underline{A}$ is deflated by a procedure reported by Rutishauser (32) and the iteration carried on for the next lowest eigenvalue.

iv) This procedure is continued until all the required eigenvalues and eigenvectors are obtained.

A computer subroutine called BANEIG written by Felippa and based on the above procedure was used in the present study. This subroutine takes into account the symmetric and banded form of the matrix. It can handle a large system with a narrowly banded matrix efficiently if only a relatively small number of eigenvalues are needed, which is usually the case in structural analysis. The capacity of BANEIG is limited by the computer. With a 140 K (octal) machine, a matrix with 500 equations and band width around 50 can be handled.

4.4 Mode Superposition Method

The displacement vector $\underline{x}$ can be expressed as a linear combination of all the vibration mode shapes of the structure

$$\underline{x} = \underline{X}\,\underline{y} \tag{4.10}$$

where $\underline{X}$ is a square matrix. Each column of $\underline{X}$ represents one vibration mode shape of the structure and is independent of time. Vector $\underline{y}$ is the time dependent amplitude of each mode. Substituting Eq. (4.10) into Eq. (4.1), the equation of motion becomes:

$$\underline{M}\,\underline{X}\,\ddot{\underline{y}} + \underline{C}\,\underline{X}\,\dot{\underline{y}} + \underline{K}\,\underline{X}\,\underline{y} = \underline{P}(t) \tag{4.11}$$

This set of equations can be decoupled by considering the orthogonal properties of the vibration mode shapes. (It is assumed that the damping matrix satisfies the same orthogonal property as the stiffness and the mass matrices.) Pre-multiplying Eq. (4.11) by $\underline{X}_n^T$, where $\underline{X}_n$ is the n-th column of matrix $\underline{X}$ (the n-th mode shape) leads to:

$$M_n^* \ddot{y}_n + C_n^* \dot{y}_n + K_n^* y_n = P_n^*(t) \tag{4.12}$$

in which

$$M_n^* = \underline{X}_n^T \underline{M} \underline{X}_n \tag{4.13a}$$

$$C_n^* = \underline{X}_n^T \underline{C} \underline{X}_n = 2\lambda_n \omega_n M_n^* \tag{4.13b}$$

$$K_n^* = \underline{X}_n^T \underline{K} \underline{X}_n = \omega_n^2 M_n^* \tag{4.13c}$$

$$P_n^*(t) = \underline{X}_n^T \underline{P}(t) \tag{4.13d}$$

Equations (4.13) define the generalized mass, damping, stiffness and load. It should be noted that λ_n is the modal damping ratio of the n-th vibration mode. The critical damping for the n-th mode is defined by:

$$(C_n)_{cr} = 2 \omega_n M_n^* = 2 (K_n^* M_n^*)^{\frac{1}{2}} \tag{4.14}$$

The use of the orthogonal property of the damping matrix requires an assumption on the form of damping matrix $\underline{C}$. In practical analysis it is convenient to assume that $\underline{C} = \alpha\underline{M} + \beta\underline{K}$. Since the coupling caused by damping is usually small, this assumption is generally justified. The damping ratio λ_n of Eq. (4.13b) is usually found by experiements.

The generalized equation of motion (4.12) is usually solved numerically either by the Duhamel Integral (37) or by a step-by-step integration technique. After solving for amplitude $\underline{y}$, the total displacement of the structure $\underline{x}$ can be obtained using Eq. (4.10).

It should be noted that for many types of loading the higher vibration modes contribute very little to the displacement $\underline{x}$, therefore only the few lowest vibration modes will be needed to obtain an accurate result. This is an important advantage of the mode superposition method. Otherwise the computational effort involved in solving all the vibration modes of a moderate system, say 300 degrees

of freedom, will be formidable.

4.5 Step-By-Step Integration Method

Various numerical procedures have been developed to integrate the second order differential Eq. (4.1) directly. These procedures are referred to as the step-by-step integration method. Two of the most used procedures were reported by Newmark (27) and by Wilson and Clough (40). Newmark derived a general recurrent equation with a parameter β. As different values are assigned to β, the general equation will be reduced to special forms for different assumptions on the behavior of the system (linear acceleration, constant acceleration, etc.). Given initial conditions, an iterative procedure is used to calculate the response at the end of time step. Later it was pointed out by Wilson and Clough that this iteration is not necessary.

The advantages of this step-by-step procedure are:

i) It has a clear physical interpretation.

ii) In the calculation, only information at the beginning of the time step is needed to predict the response at the end of time step. (For many higher order integration techniques, information of more than one step will be needed.)

For problems in which only the first few modes contribute significantly to the dynamic response, the mode superposition method requires less computational effort. However, for structures whose natural frequencies are close together or for loadings which excite the higher vibration modes, the direction integration of the equations of motion is more reliable and efficient. It should also be noted that the step-by-step integration method is the only technique that can be applied to a non-linear dynamic problem.

The basic concept of the step-by-step procedure is to divide the time space into a sequence of time steps of length Δt. Knowing the initial conditions (i.e. displacement, velocity and acceleration at the beginning of a time step) the response at the end of the time step can be predicted with the aid of an assumption on the behavior of the motion during the time step. The results of this prediction can then be used as the initial conditions of the next time step and the calculation carried on successively. It is obvious that the accuracy of this method depends upon the size of the time step. The smaller the time step the more accurate the results will be.

The linear acceleration version of the step-by-step method is based on assuming that the acceleration of the system varies linearly during each time step. Therefore the velocity will vary quadratically and displacement cubicly (Fig. 4-1) as follows:

$$\ddot{\underline{x}} = \ddot{\underline{x}}_0 + \frac{t}{\Delta t}(\ddot{\underline{x}}_1 - \ddot{\underline{x}}_0) \tag{4.15a}$$

$$\dot{\underline{x}} = \dot{\underline{x}}_0 + t\,\ddot{\underline{x}}_0 + \frac{t^2}{2\Delta t}(\ddot{\underline{x}}_1 - \ddot{\underline{x}}_0) \tag{4.15b}$$

$$\underline{x} = \underline{x}_0 + t\,\dot{\underline{x}}_0 + \frac{t^2}{2}\,\ddot{\underline{x}}_0 + \frac{t^3}{6\Delta t}(\ddot{\underline{x}}_1 - \ddot{\underline{x}}_0) \tag{4.15c}$$

where subscripts 0 and 1 refer to quantities at the beginning and the end of the time step respectively. By expressing the acceleration and velocity at the end of the time step ($t = \Delta t$) in terms of displacement at the end of time step, the above equations become:

$$\ddot{\underline{x}}_1 = \frac{6}{\Delta t^2}\underline{x}_1 - \frac{6}{\Delta t^2}\underline{x}_0 - \frac{6}{\Delta t}\dot{\underline{x}}_0 - 2\,\ddot{\underline{x}}_0 \tag{4.16a}$$

$$\dot{\underline{x}}_1 = \frac{3}{\Delta t}\underline{x}_1 - \frac{3}{\Delta t}\underline{x}_0 - 2\,\dot{\underline{x}}_0 - \frac{\Delta t}{2}\ddot{\underline{x}}_0 \tag{4.16b}$$

$$\underline{x}_1 = \underline{x}_1 \tag{4.16c}$$

To carry out the analysis, Eqs. (4.16) are substituted in Eq. (4.1) and rearranged in a set of equivalent static equations:

$$\bar{\underline{K}}\ \underline{x}_1 = \bar{\underline{P}} \tag{4.17}$$

where

$$\bar{\underline{K}} = \underline{K} + \frac{3}{\Delta t}\underline{C} + \frac{6}{\Delta t^2}\underline{M}$$

$$\bar{\underline{P}} = \underline{P}(t=\Delta t) + \underline{C}\ \underline{A} + \underline{M}\ \underline{B}$$

$$\underline{A} = \frac{3}{\Delta t}\underline{x}_0 + 2\dot{\underline{x}}_0 + \frac{\Delta t}{2}\ddot{\underline{x}}_0$$

$$\underline{B} = \frac{6}{\Delta t^2}\underline{x}_0 + \frac{6}{\Delta t}\dot{\underline{x}}_0 + 2\ddot{\underline{x}}_0$$

Equation (4.17) can be easily solved for $\underline{x}_1$ by any standard linear equation solving technique, like Gauss Elimination. Then velocity and acceleration at the end of the time step can be recovered using Eqs. (4.16).

It is noted that the function of mass matrix $\underline{M}$ is to add to the stiffness matrix. If the lumped mass matrix is used, a quantity of $\frac{6}{\Delta t^2} m_{ii}$ (≥ 0) is added to the diagonal terms of the stiffness matrix. Therefore a zero rotational inertia term will not cause any numerical difficulty.

This method is straightforward and can be programmed easily for automatic calculation. It can also be used to solve the uncoupled Eq. (4.12). The only disadvantage is that the solution may sometimes become unstable. Instability may be observed as the solution starts to oscillate violently and blows up within a few more steps. It is found that in order to obtain a stable solution, a small time step has to be used; if Δt is smaller than one fourth of the highest natural

period of the system the solution will be stable. However, the highest period of a system is frequently so small that it is impractical or even impossible to solve the problem in this way (see example in Section 4.6).

In order to obtain a stable solution with a large time step, a similar method employing a constant acceleration assumption is introduced. It is assumed that the acceleration within each time step remains constant as the average of the accelerations at the beginning and the end of the time step. Therefore the velocity varies linearly and displacement quadratically (Fig. 4-2). The constant acceleration version of the step-by-step method is always stable regardless of the size of the time step (27). One drawback of this procedure is that artificial damping is introduced to the system when the time step becomes too large (see Section 4.6). However in order to get a realistic solution the time step has to be reasonably small anyway (say smaller than a fraction of the natural period of the highest <u>significant</u> mode). Therefore this will not be an important restriction.

The main advantage of the step-by-step integration technique is that it can be applied to the non-linear problem. In this case it is convenient to express the equation of motion (4.1) in an incremental form:

$$\underline{M}\Delta\ddot{\underline{x}} + \underline{C}\Delta\dot{\underline{x}} + \underline{K}\Delta\underline{x} = \Delta\underline{P}(t) \qquad (4.18)$$

The equations corresponding to Eqs. (4.18) in incremental form and with constant acceleration assumption will be:

$$\Delta\ddot{\underline{x}} = \frac{4}{\Delta t^2}\underline{x} - \left(\frac{4}{\Delta t}\dot{\underline{x}}_0 + 2\ddot{\underline{x}}_0\right) \qquad (4.19a)$$

$$\Delta\dot{\underline{x}} = \frac{2}{\Delta t}\,\underline{x} - 2\,\dot{\underline{x}}_0 \tag{4.19b}$$

$$\Delta\underline{x} = \Delta\underline{x} \tag{4.19c}$$

The solution is then obtained by substituting Eqs. (4.19) into Eq. (4.18) to form an equivalent static problem and solving for the incremental displacement $\Delta\underline{x}$. The incremental velocity and acceleration can be obtained using Eq. (4.19). The total displacement, velocity and acceleration at the end of the time step are obtained by adding the incremental quantities to the initial quantities.

For a step-by-step integration method, the damping matrix is frequently defined by Eq. (4.4). The relationship between the modal damping ratio λ_n and the constants α and β may be derived as follows:

Pre- and post-multiplying Eq. (4.4) by a mode shape vector $\underline{X}_n$, it becomes:

$$\begin{aligned} 2\,\lambda_n\,\omega_n\,M_n^* = C_n^* &= \alpha\,M_n^* + \beta\,K_n^* \\ &= \alpha\,M_n^* + \beta\,\omega_n^2\,M_n^* \end{aligned} \tag{4.20a}$$

or

$$\lambda_n = \frac{\alpha}{2\omega_n} + \frac{\beta\omega_n}{2} = \frac{\alpha T_n}{4\pi} + \frac{\beta\pi}{T_n} \tag{4.20b}$$

where T_n is the natural period of the n-th vibration mode. This equation may be used to determine how much damping, in terms of modal damping ratio λ_n, is actually introduced by the damping matrix defined by Eq. (4.4). It is noted from Eq. (4.20b) that the constant α tends to damp out the lower modes while the constant β tends to damp out the higher modes. For the derivation of damping matrix $\underline{C}$ from the modal damping ratio λ_n, the interested reader should refer to Ref. 5.

The use of this step-by-step integration technique on a large system is possible only with the aid of a high speed computer. In the analysis, the stiffness matrix occupies most of the computer core storage. It is noted that if the damping matrix is defined by Eq. (4.4), the stiffness matrix $\underline{K}$ will appear on both sides of Eq. (4.17). This means that twice the storage will be needed to store the information. However, this problem can be avoided by a little algebraic operation. Assume that the damping matrix has the form of Eq. (4.4) and substitute Eqs. (4.19) into Eq. (4.18). Retain all the terms which contain matrix $\underline{K}$ on the left hand side of the equation and after some manipulations, the equation of motion becomes:

$$\bar{\underline{K}}\Delta\bar{\underline{x}} = \Delta\bar{\underline{P}} \tag{4.21}$$

where

$$\bar{\underline{K}} = \frac{C_1}{C_2}\underline{M} + \underline{K}$$

$$\Delta\bar{\underline{x}} = C_2\,\Delta\underline{x} - \beta\underline{B}$$

$$\Delta\bar{\underline{P}} = \Delta\underline{P} + \underline{M}\left(\underline{A} + \left(\alpha - \beta\frac{C_1}{C_2}\right)\underline{B}\right)$$

$$C_1 = \frac{4}{\Delta t^2} + \alpha\frac{2}{\Delta t}$$

$$C_2 = 1 + \beta\frac{2}{\Delta t}$$

$$\underline{A} = \frac{4}{\Delta t}\dot{\underline{x}}_0 + 2\ddot{\underline{x}}_0$$

$$B = 2\dot{\underline{x}}_0$$

After solving for $\Delta\bar{\underline{x}}$ from Eq. (4.21), the incremental displacement, velocity and acceleration may be calculated using the following equations

$$\Delta\underline{x} = \frac{1}{C_2}\left(\Delta\bar{\underline{x}} + \beta\underline{B}\right) \tag{4.22a}$$

$$\Delta\dot{\underline{x}} = \frac{2}{\Delta t}\Delta\underline{x} - \underline{B} \qquad (4.22b)$$

$$\Delta\ddot{\underline{x}} = \frac{4}{\Delta t^2}\Delta\underline{x} - \underline{A} \qquad (4.22c)$$

This procedure was developed by Professor Powell at the University of California at Berkeley and can be programmed very easily.

It should be noted that the static analysis can be regarded as a special case whose inertia and damping forces are zero, of the above procedure. Therefore a computer program for dynamic analysis may also be applied to static problems simply by setting the mass and damping of the system to zero. This characteristic does not apply for the mode superposition method. It should be noted, however, that this is not a very efficient static analysis procedure, because many unnecessary operations have to be carried out to take care of the mass and damping terms.

4.6 Illustrative Example

An example has been selected to investigate the various aspects of the dynamic analysis procedure described in the previous sections. The numerical results are checked against closed form analytic solutions to check their accuracy.

A rectangular plate simply supported along all four sides is shown in Fig. 4-3a. Dimensions and material properties of the plate are:

Thickness	h = 1.0 inch
Length in x-direction	a = 100 inches
Length in y-direction	b = 35 inches
Young's Modulus	E = 3000 ksi

Poisson's Ratio $\nu = 0.30$

Mass Density $\rho = 0.00001$ k-sec^2/in^4

The natural frequencies of this plate and its dynamic response under certain types of loadings can be obtained using a series approach. These results are checked against the finite element solution as described below:

i) Natural Frequencies

Considering bending deformation only, the analytic solution for the natural frequencies of the plate is:

$$\omega_{mn} = \pi^2 \sqrt{\frac{D}{h\rho}} \left[\frac{m^2}{a^2} + \frac{n^2}{b^2}\right] \qquad (4.23)$$

where $D = \frac{Eh^3}{12(1-\nu^2)}$, and m and n are the number of half waves of the free vibration mode in the x- and y-direction respectively.

A quarter of the plate (Fig. 4-3a) was analyzed for its natural frequencies using the finite element approach. Assuming doubly symmetric conditions along the two center lines, only vibration modes for which both m and n are odd were included. The lumped mass formulation and the inverse iteration procedure were used.

Several different quantities were used for the rotational inertia term (m_{ii}) in the lumped mass matrix. The resulting natural frequencies of the first four modes, compared with the results of Eq. (4.23), are as follows:

TABLE 4-1. NATURAL FREQUENCIES (RAD/SEC) OF S.S. PLATE

	m_{ii} (k-in-sec^2)	ω_1 m=1,n=1	ω_2 m=3,n=1	ω_3 m=5,n=1	ω_4 m=7,n=1
Finite Element Solution 4X5 Mesh	10	8.132	10.86	14.82	18.19
	10^{-3}	46.75	88.48	169.7	277.3
	3×10^{-5}	47.46	91.07	178.3	293.2
	10^{-6}-10^{-9}	47.48	91.15	178.6	293.7
Exact soln. Eq. (4.23)		47.40	88.79	171.6	295.7

It can be seen from the above table that the finite element approach predicts very good results, and that the solutions are not sensitive to the magnitude of the rotational inertia, m_{ii}, as long as it is not so large as to constrain the system. In this example the rotational inertias of a typical element about the x- and y-axis are 6.96×10^{-4} and 3.65×10^{-3} (k-in-sec^2) respectively. In general, a quantity smaller than the actual rotational inertia of a typical element is recommended for m_{ii}.

ii) Dynamic Response

Assume that the transverse load on the plate is defined by:

$$P(x,y,t) = q_0 \sin(\Omega t) \tag{4.24}$$

It can be shown that for a simply supported plate the transverse displacement may be expressed by:

$$w(x,y,t) = \sum_{m=1}^{\infty} \sum_{n=1}^{\infty} w_{mn}(t) \sin \frac{m\pi x}{a} \sin \frac{n\pi y}{b} \tag{4.25}$$

where

$$w_{mn}(t) = \frac{16q_o}{mn\pi^2 h\rho}\left(\frac{1}{\omega_{mn}^2 - \Omega^2}\right)\left(\sin \Omega t - \frac{\Omega}{\omega_{mn}} \sin \omega_{mn} t\right)$$

In this example it is assumed that $q_0 = 1.0$ lb/in^2 and $\Omega = 10\pi$. An analytic solution was calculated using Eq. (4.25) with 25 terms (i.e. m=1-5, n=1-5). This solution is used for comparison against the finite element results below.

a) Linear Acceleration Assumption

A quarter of the plate was analyzed with the same 4X5 mesh. The mode superposition method was used and the decoupled equations of motion were solved by the step-by-step integration method assuming linear acceleration. Four different cases were analyzed, considering 2,3,4 and 5 modes respectively. The results indicate that only the first four modes are significant, the differences between the cases which include four and five modes being very small. The natural period of the fourth mode is $T_4 = 0.0215$ second, which is 4.3 times the time step used in this study ($\Delta t = 0.005$ second). Figure 4-3a shows excellent agreement between the analytic and the finite element solutions. In general a time step smaller or equal to $\frac{1}{4}$ of the highest significant mode period is recommended.

The same problem was analyzed again with a direct step-by-step integration assuming linear acceleration with the same time step (0.005 sec.). In this case, all vibration modes were included and the solution becomes unstable numerically (Fig. 4-3a) because of the inclusion of the higher modes.

Clearly, the linear acceleration assumption can be used in the mode superposition method to integrate the decoupled equations, because

the time step can be properly selected according to the natural period of the highest mode included. However the method should be avoided in the direct step-by-step integration.

b) Constant Acceleration Assumption

The same problem has also been analyzed by direct step-by-step integration assuming constant acceleration. Two different time steps, 0.005 and 0.01 second, were used, and the results are shown in Fig. 4-3b. It can be seen that the constant acceleration assumption gives stable solutions. However, artificial damping is introduced. The damping in the case of $\Delta t = 0.005$ second is negligible but the damping introduced by the larger time step (0.01 second which is almost equal to $\frac{1}{2}T_4$) reduces the maximum displacement by approximately 2.7%. In general, good results may be expected if the time step is smaller or equal to $\frac{1}{4}$ of the natural period of the highest mode which contributes significantly to the response.

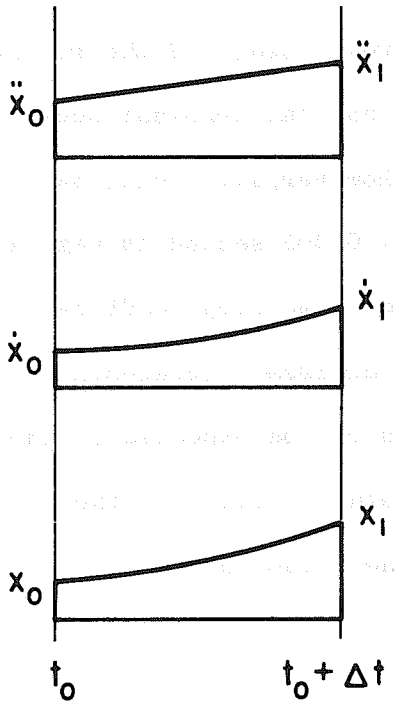

FIG. 4-1

LINEAR ACCELERATION

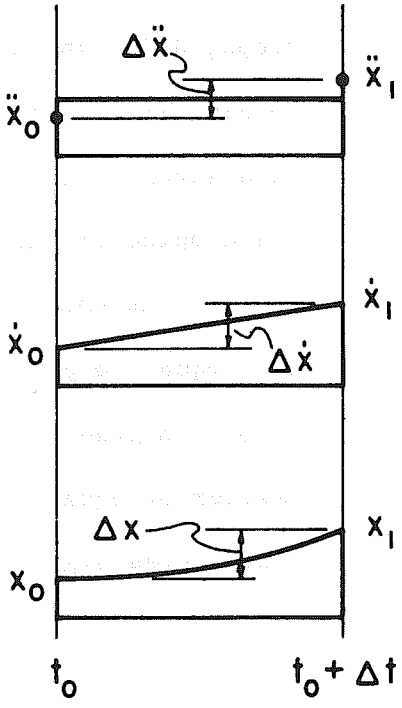

FIG. 4-2

CONSTANT ACCELERATION

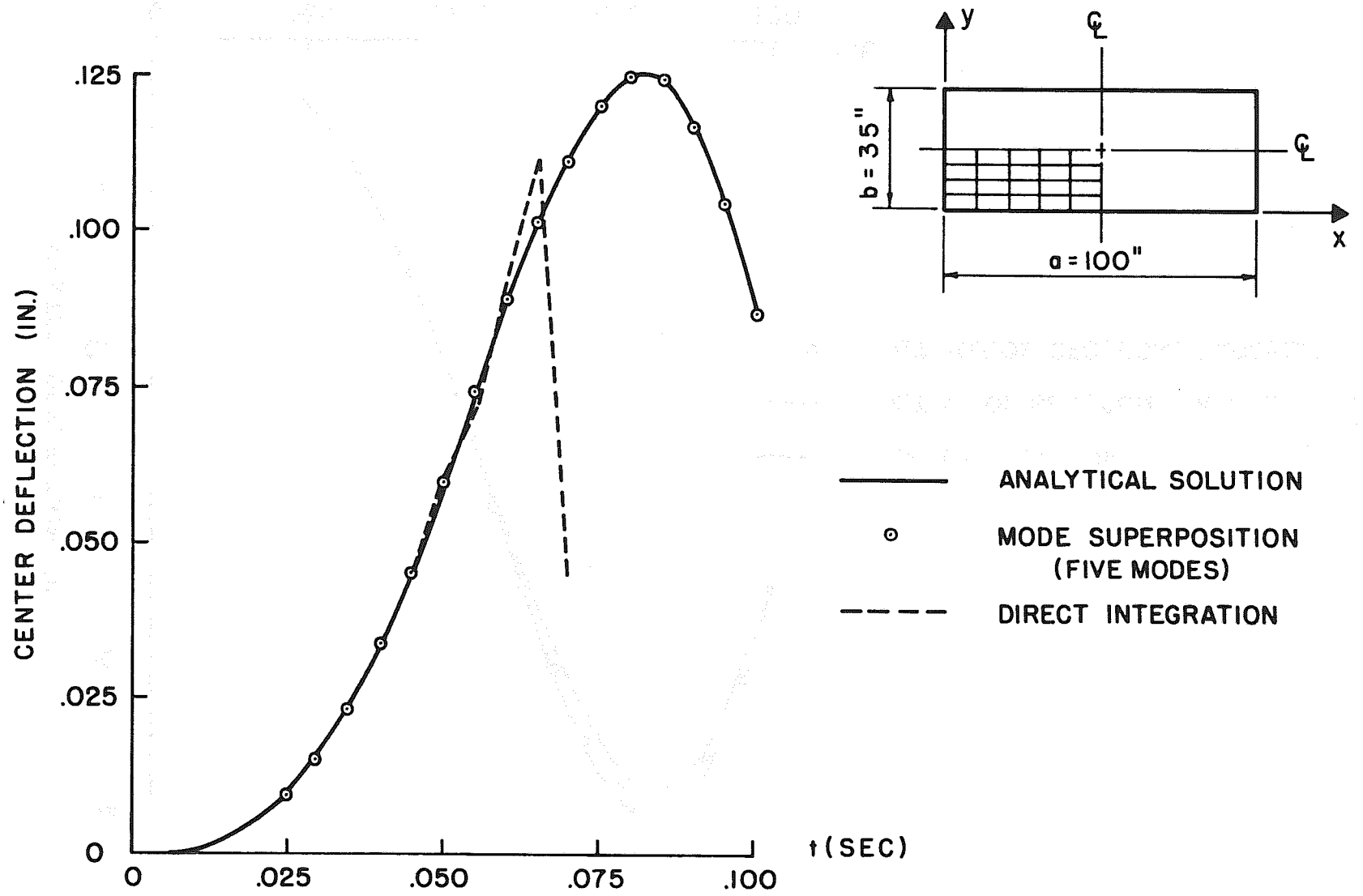

FIG. 4-3a SIMPLY SUPPORTED PLATE AND RESULTS OF LINEAR ACCELERATION ASSUMPTION

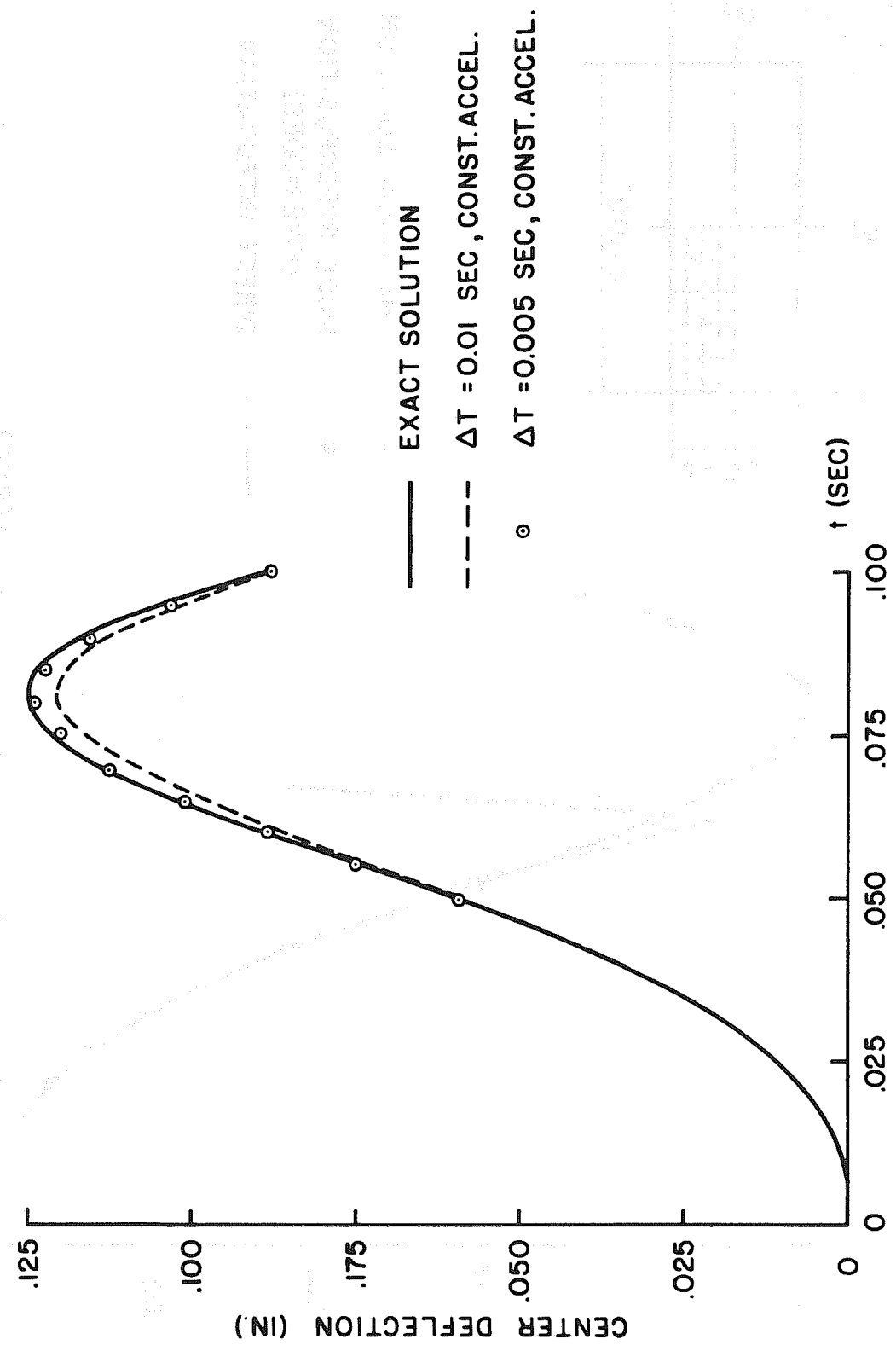

FIG. 4-3 b DAMPING IN CONSTANT ACCELERATION ASSUMPTION

5. NON-LINEAR ANALYSIS

5.1 Definition of the Problem

There are two types of non-linearities in structural analysis, namely geometric non-linearity, associated with finite geometric change of the structure, and material non-linearity, associated with change of material properties. It is assumed in this study that the material properties remain constant throughout the analysis. Therefore, only geometric non-linearity will be considered.

All of the discussions in the previous chapters apply to linear system only. The stiffness discussed in chapters 2 and 3 represents the elastic stiffness of the structure. In a more general consideration, the structural stiffness matrix $\underline{K}$ is contributed from both the elastic stiffness matrix $\underline{K}_e$ (referred to as $\underline{K}$ before) and the geometric stiffness matrix $\underline{K}_g$ (to be discussed later), i.e.,

$$\underline{K} = \underline{K}_e + \underline{K}_g \tag{5.1}$$

In a linear analysis, the deformation of the structure is assumed to be so small that the deformed geometry of the structure may be considered identical to the undeformed one. In this case, if the effect of the geometric stiffness is not considered, or if the geometric stiffness matrix is constant, the behavior of the structure is unchanged during the process of loading because the structural elastic stiffness matrix, which is a function of the geometry of the structure, remains constant. (A non-linear problem has to be solved if the geometric stiffness matrix is not constant.) For a large deflection analysis, the structural deformation becomes finite in comparison with the dimensions of the structure. In this case, both the elastic

and the geometric stiffnesses are no longer constant and the problem becomes a non-linear one.

Figure 5-1 shows a generalized load (P) vs displacement (δ) curve for a structure. The slope of the tangent line at the origin represents the initial stiffness of the structure for linear analysis. This may be termed the initial tangent stiffness. It should be emphasized that this is only a symbolic representation in which a multi-degrees of freedom system is represented by a single degree of freedom curve. In an actual case, the curve in Fig. 5-1 becomes a curved hypersurface in a multi-dimensional space and the tangent line becomes a tangent hyperplane. If a load P_0 is applied to the structure, displacement δ_1 is determined by a linear analysis.

It sometimes may be possible, for certain simple structures, to formulate explicitly a set of non-linear equations which describe the deflection behavior; that is, it may be possible to find the stiffness matrix $\underline{K}(\underline{x})$ as a function of the displacement vector $\underline{x}$, and to solve directly the following equations:

$$[\underline{K}(\underline{x})]\,\underline{x} = \underline{P} \qquad (5.2)$$

The matrix $\underline{K}(\underline{x})$ is a function of $\underline{x}$, and therefore also a function of $\underline{P}$. For the load P_0 in Fig. 5-1, this stiffness is represented by the slope of the secant line between the origin and the point "A" on the curve, and may be termed the secant stiffness. The displacement δ_0 can be obtained by solving Eq. (5.2).

This is the classical approach to the solution of a non-linear problem, but it can be carried out only for very simple structures.

5.2 Linearized Approach to the Non-linear Problem

In addition to the difficulties in solving Eq. (5.2), it is practically impossible for many structures to set up the non-linear equations in the first place. Therefore, various methods using a series of linear analyses, have been developed to solve the non-linear problems.

There are three main methods of this type, namely the Iteration Method, the Incremental Method and the combination of these two methods. Each method has its own advantages and limitations and can be applied to different classes of problems. The properties and ranges of application of the methods are discussed in the following sections.

a) Iteration Method

In one very efficient form of the iteration method, the deflection of the structure due to applied load is estimated by a linear analysis using the initial tangent stiffness of the structure. The internal resisting force of the structure caused by this deflection is calculated, and subtracted from the total applied load to obtain the out-of-balance force. A new tangent stiffness is then defined, based on the deformed geometry of the structure, and the out-of-balance force is applied to get an additional deflection. This procedure is repeated until equilibrium is achieved, i.e. until the out-of-balance force vanishes. This method is sometimes referred to as Newton's method and can be expressed graphically as in Fig. 5-2a. The slopes of the tangent lines in the diagram represent the tangent stiffness for different deformed geometries of the structure. The tangent stiffness changes for the following reasons:

i) The geometry of the structure changes because of finite deformations.

ii) Changes in membrane forces lead to changes of the geometric stiffness (Section 5.3).

It is also possible to calculate the additional deflection based on the original tangent stiffness instead of redefining the stiffness for each iteration. The procedure is shown in Fig. 5-2b in which all tangent lines are parallel to the one at the origin. In this case, the convergence can be expected to be slower; however, the computational effort saved in not forming the stiffness again may compensate this disadvantage.

The iteration method is usually used in static analysis only. It is a widely used method in cases where:

i) The solution is unique.

ii) Only the final equilibrium position is of interest, i.e. the history of deflection is not important.

iii) The internal resisting force can be accurately calculated for a known finite deformation. Note that if the exact form of the resisting force, as a function of finite structural deformation $\underline{x}$, is known, its derivative with respect to $\underline{x}$ yields the secant stiffness.

In this study, the exact value of the internal resisting force of the quadrilateral element due to a given finite deformation is not easily definable; in addition the iteration method cannot be applied to dynamic problems. Therefore, it will not be discussed further.

b) Incremental Method

The incremental method is also called the step-by-step method, although it should be distinguished from the step-by-step method discussed in Section 4.5, which involved stepping through time.

In the incremental method, the total load is applied to the structure in steps. For each load increment (step), a linear analysis is carried out with the tangent stiffness based on the current deformed geometry and the current geometric stiffness of the structure. This method is graphically represented in Fig. 5-3. The advantages of this method are:

i) It can be carried out for any kind of structures without special restriction.

ii) It will predict the complete load-deflection curve and can be used for dynamic response calculation.

The major disadvantage of the incremental method is that its solution may tend to diverge from the true solution. Mathematically, this method is equivalent to the forward difference method in the numerical solution of initial value problems. Its error (amount of divergence from the true solution) is proportional to the size of the load increment.

Several techniques have been developed to reduce the error caused by this method. The following two have been found by the author to be most useful and easy to apply.

i) If the internal resisting force due to a known deflection of the structure can be determined accurately, or even approximately, the out-of-balance force developed in one step may be

calculated and added to the next load increment. The solution thus obtained will be represented by the broken lines in Fig. 5-3. The improvement of the solution is obvious, yet the additional computational effort is small.

ii) The results would be improved if a chord stiffness instead of the tangent stiffness could be defined for each load increment. (The chord stiffness is represented by the slope of the chord line between two points on the load-deflection curve as shown in Fig. 5-4. The difference between the chord stiffness and the secant stiffness is that the former does not start from the origin.) Generally, the exact chord stiffness can only be obtained by using an iteration procedure. However, an approximate chord stiffness may be estimated and used to improve the solution. This estimation can be made by estimating the structural deflection for the load increment and using the tangent stiffness based on the geometry of the structure at the middle point of the load increment. If the estimation of the displacement were exact, the procedure would be equivalent to the centered difference method in the numerical solution of initial value problems, and the error would be proportional to the square of the size of the load increment (18). Generally, the estimated chord stiffness approach will give an improvement over the plain incremental method with very little additional computational effort and computer core storage.

c) Combined Method

There are two types of combinations of the above two methods:

i) Iteration may be performed until equilibrium is obtained within each load increment.

ii) An increment analysis may be carried out for the nearly linear portions of the problem and iteration can be employed whenever a strong non-linearity shows up.

These methods should give the most accurate results for a given number of load steps, and can also be used to predict the complete load-deflection curve. However, a large amount of computational effort is involved in the process, and therefore, the methods are not necessarily the best for practical computation. They have not been used in the research described here, because it is very difficult to carry out the iteration steps in dynamic analysis.

5.3 Analytic Procedure Selected for This Study

In addition to the assumption that the material remains elastic throughout the analysis, it is also assumed that the structure may be subject to large rigid body displacements and rotations, but that the strains remain small. As a result of these assumptions, the constitutive equations will be unchanged during the response analysis.

An incremental analysis is used to calculate the non-linear dynamic response. A series of linear analyses is carried out with the load applied in steps. The equation of motion is expressed in incremental form shown by Eq. (4.18). It is assumed in this study that the mass matrix $\underline{M}$ remains constant and the damping matrix is expressed by Eq. (4.4). Therefore, only the change of the stiffness matrix $\underline{K}$ has to be determined. The stiffness matrix changes from step to step

because of:

i) Change of geometry due to finite deflection.

ii) The effect of the inclusion of the geometric stiffness.

In addition, an equilibrium (out-of-balance force) correction is also considered in the procedure. These three effects are discussed as follows:

a) Change of Geometry Due to Deflection

In a large deflection analysis, the structural deformation is finite as compared with the dimensions of the structure. The following two effects have to be considered in the analysis:

i) Non-linear terms are introduced in the strain-displacement relationship.

ii) Equilibrium has to be expressed in the deformed geometry of the structure.

In an incremental analysis, if the load increment is small, the strain-displacement relationship may be assumed to be linear for each load increment. By constructing the tangent stiffness for each increment based on the current geometry, and by considering the out-of-balance force correction, violation of equilibrium will be small. The solution thus obtained will converge to the true solution as the load increment decreases.

In the incremental analysis described in Section 5.2, a series of linear analyses is carried out and at the end of each load increment, the deformed position of each nodal point is obtained simply by adding the increase in nodal point displacements, $\Delta\underline{x}$, to the nodal point coordinates. A new tangent stiffness may then be formed based on the new geometry of the structure. This new tangent stiffness is used to

calculate the incremental displacement for the next load increment. Thus, a complete linear analysis has to be carried out for each increment.

Under the assumption that the displacements will be only moderately large, i.e. that the deformed structure will not be completely different from the undeformed structure, it is possible to neglect the change of shape and dimension of each element. Therefore, the triangular element elastic stiffness in its local coordinate $(\bar{x}_m, \bar{y}_m, \bar{z}_m)$ may be assumed to remain constant throughout the analysis. The change of geometry due to deformation will be expressed only by the change in the displacement transformation matrices from the local coordinate to the global coordinate. From a study of the first example to be described in Chapter 6, it has been found that this assumption causes approximately a one percent of error in the solution, while reducing the computer time by approximately fifteen percent. However, it should be noted that these figures may be different for other problems.

It was mentioned in Section 5.2 that the solution would be improved if a chord stiffness could be determined to replace the tangent stiffness for each step; and if the load increment is small, an approximate chord stiffness may be obtained by estimating the incremental displacement. The simplest way to estimate the incremental displacement is to assume that it will be the same as the previous step. By adding $1\frac{1}{2}\ \Delta\underline{x}$ to the nodal point coordinates, an estimated middle point geometry for the next step can be obtained; a tangent stiffness based on this geometry can be formulated and used as an approximate chord stiffness for the next step. The solution thus obtained will be

improved over the plain incremental analysis, while the additional computational effort is very small.

This method is approximately equivalent to the centered difference method in the numerical solution of differential equations and the error is approximately proportional to the square of the size of the load increment. The plain incremental analysis is equivalent to the forward difference method and its error is proportional to the size of the load increment.

An example has been chosen to test this estimated chord stiffness approach and the plain incremental analysis. A simply supported cylindrical shell subjected to uniform pressure, whose time history was a sinusoidal impulse, was analyzed. (This is the same problem as the second dynamic example presented in Chapter 6; the reader should refer to it for more detail.) A static analysis was carried out with a quarter of the shell represented by a 2 X 2 mesh. Although there is no other solution to compare with, physically, it can be seen that the displacement time history under this load should have a similar shape of the load time history, and there will be no displacement when the load is removed after time t = 1.0 second. Therefore a residual deflection resulted from the divergent character of the increment analysis would indicate the amount of error caused by this method. Both the estimated chord stiffness method and the plain incremental method were tested with 10 and 20 load increments from t = 0 to t = 1.0 second. The maximum deflection at the center of the free edge is approximately 0.37 foot and the residual deflection for each case is shown in the table below.

TABLE 5-1. ERROR IN THE INCREMENTAL ANALYSIS

	RESIDUAL DISPLACEMENT AT THE CENTER OF THE FREE EDGE (FT)	
	10 Steps	20 Steps
Plain Incremental Method	0.04345	0.02193
Estimated Chord Stiffness Method	0.01095	0.00277

It can be seen that this estimated chord stiffness method yields better solution and also converges faster than the plain incremental method. It is of interest to note that the estimated chord stiffness approach yields a result even better than that of the plain incremental analysis with twice as many steps.

Another way to estimate the incremental displacement is to actually calculate it with the tangent stiffness at the beginning of the step, and then to construct the "middle point" tangent stiffness and use it to approximate the chord stiffness for the same step. This is usually referred to as the predictor-corrector method. In the predictor-corrector method, the first incremental displacement is obtained by calculation, therefore it should yield better results than the estimated chord stiffness method just discussed. However, it requires twice as much computational effort as the plain incremental method because the incremental displacement is calculated twice for each step. Therefore, it is is not used in this study.

b) Geometric Stiffness Matrix

The geometric stiffness matrix K_g (10), which is also called the initial stress matrix, is a function of the stresses in the element (mainly the in-plane stresses) and may be interpreted as the influence

of the existing stresses on the behavior of the structure. The geometric stiffness matrix is combined with the elastic stiffness $\underline{K}_e$ to give a better representation of both the tangent and secant (chord) stiffnesses as indicated by Eq. (5.1).

The element geometric stiffness matrix for the plate bending element is defined (6) by:

$$\underline{k}_g = \int_A \begin{bmatrix} \underline{\varphi}^T_{,x} & \underline{\varphi}^T_{,y} \end{bmatrix} \begin{bmatrix} N_x & N_{xy} \\ N_{xy} & N_y \end{bmatrix} \begin{bmatrix} \underline{\varphi}_{,x} \\ \underline{\varphi}_{,y} \end{bmatrix} da \qquad (5.3)$$

where $\underline{\varphi}_{,x}$ and $\underline{\varphi}_{,y}$ are the derivatives of the transverse displacement interpolation function of the element with respect to the $\bar{x}_m$ and $\bar{y}_m$ coordinates, respectively. N_x, N_y and N_{xy} are the in-plane stress resultant components in the element. Matrix $\underline{k}_g$ is transformed to the global coordinate system and assembled to form the structural geometric stiffness matrix $\underline{K}_g$ similar to the elastic stiffness matrix.

It should be noted that the interpolation function $\underline{\varphi}$ used here does not have to be consistent with that used for the elastic stiffness derivation. The use of lower order interpolation functions gives approximations of the geometric stiffness matrix. It has been found (6) that a single cubic expansion (43) gives a result as good as a fully compatible cubic expansion used for the elastic stiffness derivation, but much less computational effort is needed. Therefore, it has been used in this research.

In linear static systems, the geometric stiffness is proportional to the external load, and is used in bifurcation buckling analysis. The object of the bifurcation analysis is to find the critical load, P_{cr}, under which the structure is in a state of neutral

equilibrium (35). Mathematically the critical load is represented by the non-trivial solution of the following equations:

$$(\underline{K}_e + \underline{K}_g)\ \underline{x} = \underline{0} \tag{5.4a}$$

or

$$\underline{K}_e\ \underline{x} = -\lambda\ \overline{\underline{K}}_g\ \underline{x} \tag{5.4b}$$

where

$$\underline{K}_g = \lambda\ \overline{\underline{K}}_g$$

λ is referred to as the load factor

$\overline{\underline{K}}_g$ is the geometric stiffness matrix for certain reference load state.

If the deflection is small, both $\underline{K}_e$ and $\overline{\underline{K}}_g$ are constant. Equation (5.4b) is an eigenvalue problem. Each eigenvalue represents a critical load for a different buckling mode. But usually only the lowest one is of interest, and it can be found by an inverse iteration technique similar to the one discussed in section 4.3.

The eigenvalue problem yields only the critical buckling load, P_{cr}, and does not predict the post buckling behavior, which is different for different structures. For example, a plate structure usually becomes stiffer as it deflects, a shell will become more flexible, and the strength of a column will remain constant if the deflection is not too large (Fig. 5-5a).

For large deflection analysis, both $\underline{K}_e$ and $\underline{K}_g$ are functions of the displacement $\underline{x}$, and the buckling problem may be solved by an asymptotic analysis. In this case, the external load is applied in an incremental form and the critical load is approached asymptotically (Fig. 5-5b). The process may be carried on for the post buckling

behavior analysis.

In this research, the tangent stiffness is defined by Eq. (5.1) based on the current geometry and internal stresses for each step. It should be noted that in this case, the elastic and geometric stiffnesses may be combined at the element level, and the transformation to global coordinates has to be performed only once.

In cases where the estimated chord stiffness is used, it is also possible to estimate the internal stresses at the middle point of each load increment. Assuming that the stress increment at one load increment is the same as that of the previous load increment, then the geometric stiffness matrix (5.3) may be constructed using the estimated middle point stresses in order to be consistent with the elastic stiffness.

The geometric stiffness has little influence on the structure when the stresses are small. Its importance increases as the load approaches the critical load, i.e. as the structure tends to buckle. A shell structure is more likely to buckle normal to its surface than within its surface, i.e. the critical loads for in-plane buckling modes are much higher than those of the out-of-plane buckling modes. Therefore, only the geometric stiffness matrix for the plate bending element (geometric stiffness normal to the surface) is considered in this research, as is shown in Eq. (5.3).

c) Equilibrium Correction

In the incremental analysis, after the deflection of the structure has been calculated, an equilibrium correction may be performed in the following way:

i) The global displacement is transformed to the local system to find the element strains which, in turn, are used to calculate the element stresses.

ii) Element stresses are transformed back to the global system, based on the deformed geometry, to get the resisting forces.

iii) The resisting forces are subtracted from the total applied loads to get the out-of-balance force which is then added to the next load increment.

This is an efficient procedure especially for dynamic analysis for which iteration is difficult. It has also been used by other investigators (e.g. Ref. 9).

Although in an incremental analysis, the out-of-balance force for each load increment may be neglected if the load increment is small, the internal stresses developed in the early stage of loading may not always be in equilibrium with the load which caused these stresses, as the structure continues to deform under additional loads. Consider the structure in Fig. 5-6, assuming that at position 1 the internal stress $\underline{S}_1$ is in equilibrium with the load $\underline{P}_1$, i.e.

$$\underline{A}_1^T \underline{S}_1 = \underline{P}_1 \qquad (5.5)$$

where $\underline{A}_1$ is the displacement transformation matrix from the local element coordinates to the global coordinates for the geometry of position 1. In the next load increment, $\Delta\underline{P}$ is added to the structure which in turn deforms to position 2 with additional internal stresses ΔS. In general, the total stress $\underline{S}_1 + \Delta\underline{S}$ at position 2 will not be in equilibrium with the total load $\underline{P}_1 + \Delta\underline{P}$ because stress $\underline{S}_1$ has changed its direction due to deformation. Load $\underline{P}_1$ may or may not change its

direction depending upon the type of load (e.g. dead weight of the structure may be assumed to remain in the same direction and normal pressure may change its direction due to deformation). Assuming that the direction of the load $\underline{P}_1$ remains unchanged, the out-of-balance force may be expressed by:

$$\Delta\underline{F} = (\underline{A}_2^T - \underline{A}_1^T)\ \underline{S}_1 \tag{5.6}$$

where $\underline{A}_2$ is the displacement transformation matrix at position 2. This force is small if the incremental displacement is small, but its effect is cumulative. If the load $\underline{P}_1$ also changes its direction (in which case this is a non-conservative system) this effect becomes even more important.

In order to take this effect into account, the equilibrium correction, described previously, is used. In actual computer calculation, assuming that the load increment is small and the displacement-strain relationship is a linear one within each step, the equilibrium correction may be carried out as follows.

At the end of n-th step, the incremental displacement $\Delta\underline{x}$ is calculated and the incremental "stresses" $\Delta\underline{S}$ may be obtained by transforming $\Delta\underline{x}$ to the local coordinate $(\bar{x}_m, \bar{y}_m, \bar{z}_m)$ using the displacement transformation matrix $\underline{A}_{n-1}$ and pre-multiplying it by the element stiffness matrix:

$$\Delta\underline{q} = \underline{A}_{n-1}\ \Delta\underline{x} \tag{5.7a}$$

$$\Delta\underline{S} = \underline{k}_e\ \Delta\underline{q} \tag{5.7b}$$

where $\underline{k}_e$ is the element elastic stiffness matrix in the local coordinates, and subscript n-1 refers to the quantity at the end of the (n-1)-th step (same definition applies to superscripts n and n + 1

below).

The total "stresses" are obtained by accumulating the incremental stresses from each step:

$$\underline{S}_n = \underline{S}_{n-1} + \Delta\underline{S} \tag{5.7c}$$

The total "stresses" $\underline{S}_n$ are then transformed to the global coordinates, based on the geometry at the end of the n-th step, and subtracted from the total applied load at the end of the (n+1)-th step to get the load increment for the next step:

$$\Delta\underline{P} = \underline{P}(t_{n+1}) - \underline{A}_n^T \underline{S}_n \tag{5.8}$$

The $\Delta\underline{P}$ thus obtained will be used in Eq. (4.20).

If an estimated chord stiffness matrix is used, the transformation matrix will be formed based on the estimated "middle point" geometry.

This is a simple operation and only very small amount of computational effort will be needed.

As a final remark, the step-by-step integration (Section 4.5) is combined with the incremental method (Section 5.2b) to calculate the non-linear dynamic response. The equation of motion is expressed by Eq. (4.18) in which the stiffness matrix is defined by Eq. (5.1) to form an estimated chord stiffness, the lumped mass matrix $\underline{M}$ is assumed to remain constant, the damping matrix is defined by Eq. (4.4) and the load increment is derived from Eq. (5.8).

This procedure yields good results if the load increment is reasonably small. The results will converge to the exact solution as the load increment decreases.

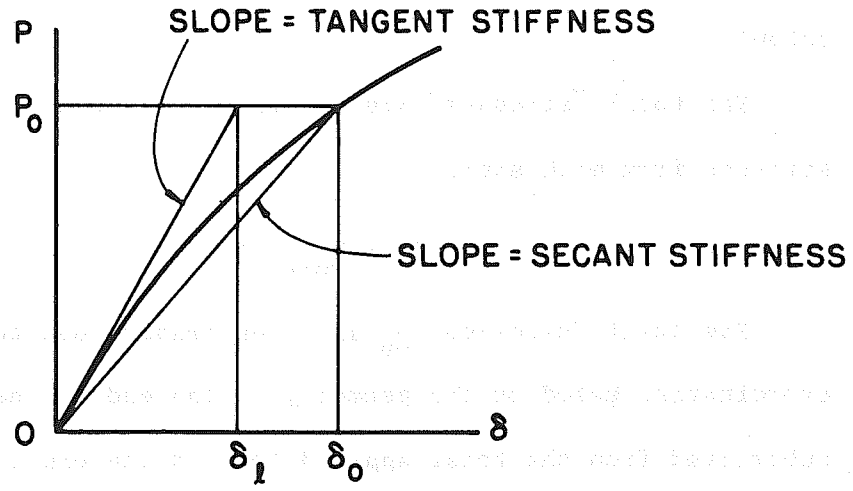

FIG. 5-1 TANGENT AND SECANT STIFFNESS

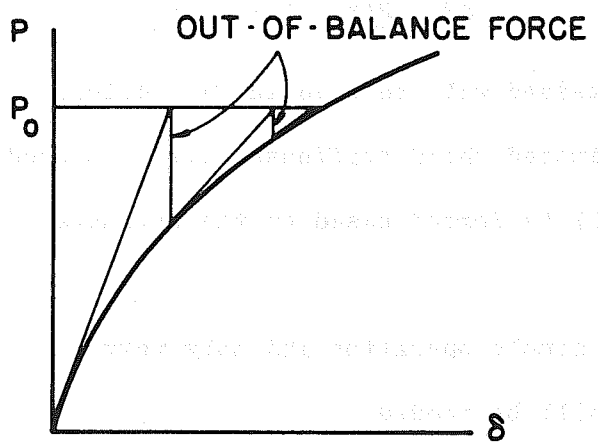

FIG. 5-2a ITERATION METHOD, CHANGING STIFFNESS

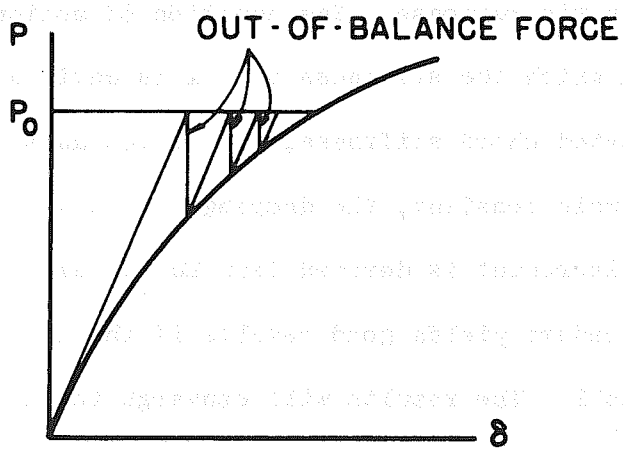

FIG. 5-2b ITERATION METHOD, CONSTANT STIFFNESS

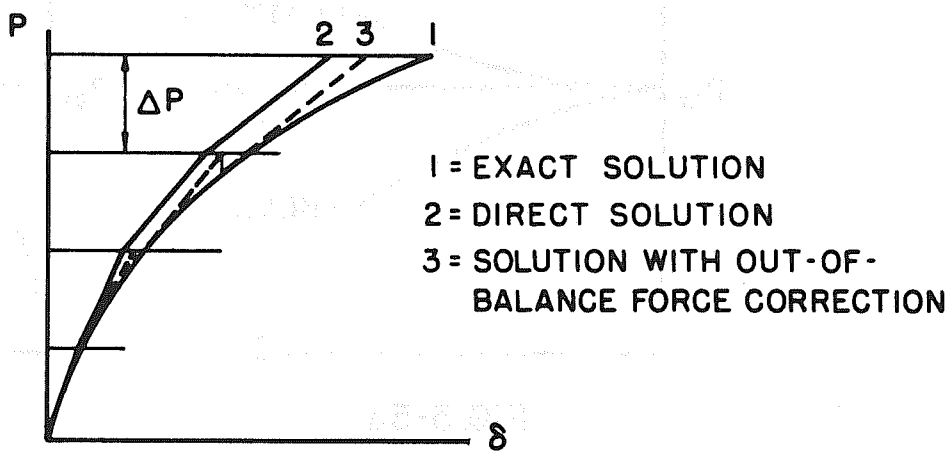

FIG. 5-3 INCREMENTAL METHOD

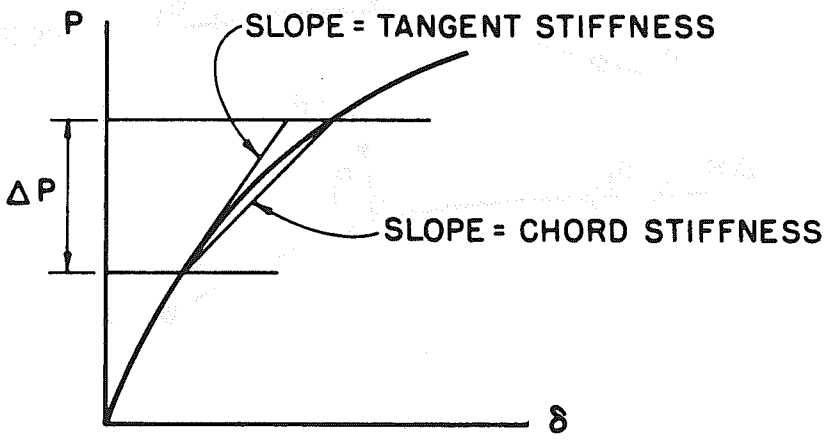

FIG. 5-4 TANGENT AND CHORD STIFFNESS IN AN INCREMENTAL ANALYSIS

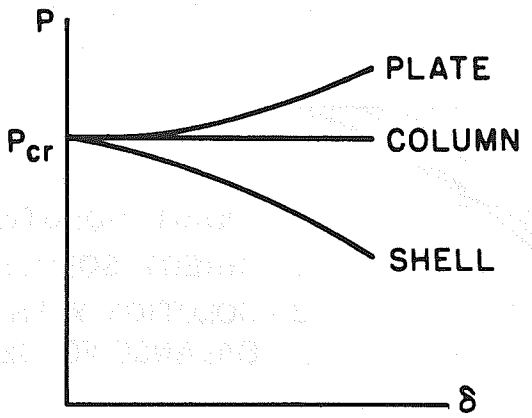

FIG. 5-5a

BIFURCATION ANALYSIS

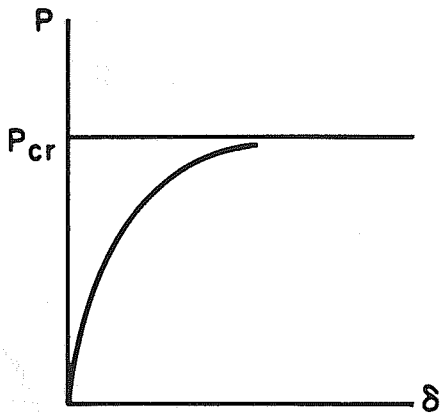

FIG. 5-5 b

ASYMPTOTIC ANALYSIS

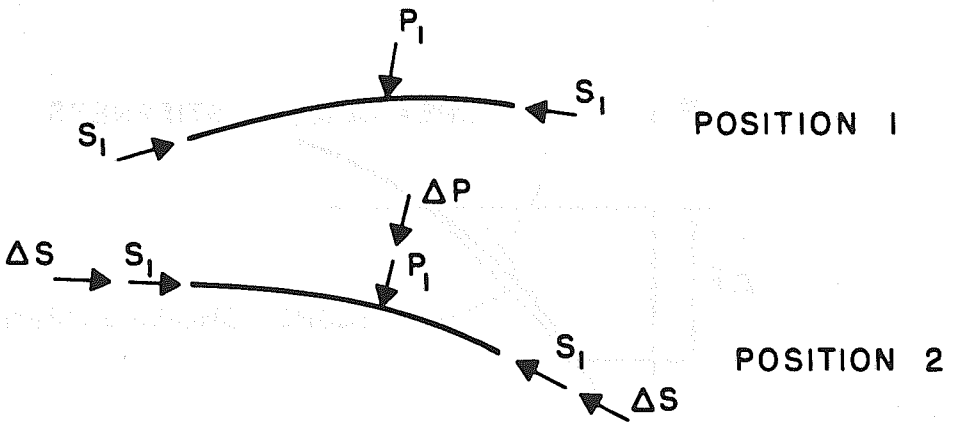

FIG. 5-6 CHANGE OF DIRECTION OF INTERNAL STRESS

6. EXAMPLES AND DISCUSSION

Computer programs have been written to carry out the non-linear dynamic response calculations discussed in the previous chapters. Their results are checked against existing solutions. Because not many problems have been solved in the field of large deflection dynamic analysis of thin shells and because a static solution can be regarded as a special case in this non-linear dynamic analysis procedure for which the inertial and damping forces are zero, three non-linear static problems, two plates and one axisymmetric shell, are chosen to check the accuracy of the non-linear aspects of this procedure. (The plate can be regarded as a special form of shell; it becomes a shell once the large deflection starts.)

Dynamic aspects of the programs are checked by calculating the natural frequencies of a shell structure whose natural frequencies are known. Finally, two structures, a simply supported cylindrical shell roof and a doubly curved cooling tower, subjected to time varying loads are analyzed.

In computer programming, the time steps are usually held constant for each problem. For static analysis, different load increments can be employed by having different rates of change of load in different time periods.

In the following sections, results of this research will be referred to as the QTSHEL solutions (for quadrilateral shell element).

6.1 Static Cases

a) Simply Supported Plate

A plate, infinitely long in one direction, is simply supported along its edges and subjected to uniform pressure. Span of the plate

is 20 inches. This problem has been solved by Timoshenko (36) and has been checked by several other investigators (26, 41). The structure exhibits a strong geometric non-linearity because as soon as it starts to deflect, the membrane strength and stiffness begin to act to resist the normal pressure. Therefore it is considered as a good example to check a procedure for non-linear analysis.

Since the behavior does not vary in the infinitely long direction, only a strip of the plate has to be considered in the analysis. Taking advantage of the symmetric condition the finite element assemblage representing half of the strip is shown in Fig. 6-1a. Other properties of the plate are:

Thickness	$h = 0.5$ inch
Young's Modulus	$E = 30000$ ksi
Poisson's Ratio	$\nu = 0.3$

The solution plotted against Timoshenko's results for loading up to 625 psi is shown in Fig. 6-1b. It can be seen that the finite element procedure yields very accurate results.

It should be noted that the stiffness of this structure increases rapidly once it starts to deflect. Therefore small load increments are used for the first few steps and larger increments are used for the later steps. In general, several test cases with successively reduced load increments have to be carried out to determine an adequate size of the load increments. The first step with relatively large, evenly distributed load increments yields the approximate behavior of the structure. The relative sizes of the load increments may then be adjusted, if necessary, according to the result of this first test. A load increment is considered as adequate if further

reduction does not introduce significant changes in the solution.

b) Plate Buckling

A simply supported plate subjected to uniaxial compression is shown in Fig. 6-2a. This example was chosen to demonstrate the asymptotic analysis. Since the in-plane stress is nearly constant within the structure, a relatively coarse finite element mesh may be used.

Considering symmetric conditions, a quarter of the plate was analyzed with a 2X2 mesh (Fig. 6-2a). Dimensions and material properties of the plate are:

$$a = 100 \text{ inches}$$

$$h = 1 \text{ inch}$$

$$E = 30000 \text{ ksi}$$

$$\nu = 0$$

The buckling stress of the plate is given by:

$$\sigma_{cr} = 4 \frac{\pi^2 D}{a^2 h} \qquad (6.1)$$

where

$$D = \frac{Eh^3}{12(1-\nu)}$$

In order to carry out the asymptotic analysis, a small non-zero disturbing force f has to be applied to the structure. The magnitude of the force f can be arbitrary and the resulting buckling stress will be independent of this value. In this example, force f is taken equal to one percent of the total in-plane force and is applied normal to the surface at the center of the plate.

It should be noted that the critical stress given by Eq. (6.1) is based on consideration of the bending stiffness only. The inclusion

of the membrane stiffness in the shell analysis tends to stiffen the structure. Therefore the asymptotic analysis will not find the plate bending buckling stress. In order to obtain the buckling stress given by Eq. (6.1) using a shell analysis, the membrane stiffness of this structure is artificially reduced to one percent of its actual stiffness (further reduction will make the in-plane displacement too large to be realistic).

The resulting stress-deflection curve is shown in Fig. 6-2b. Even with such coarse mesh, the finite element solution shows excellent agreement with the analytical result. The fact that the stress deflection curve crosses the critical stress (9.87 ksi) is caused by the inclusion of the membrane stiffness in the analysis.

c) Shallow Spherical Shell

Both of the previous examples involve plates. The third case is a shallow spherical shell with clamped edge. The load on the structure is a uniform pressure normal to its surface (Fig. 6-3a). The analytical solution of a symmetric snap through of this structure is presented in Ref. 21. One reason for selecting this particular structure as an example is that its structural stiffness matrix is always positive definite throughout the analysis. Otherwise special control, which has not been included in the existing program, would have to be used to take care of the negative stiffness.

The shallowness of the shell is defined by:

$$K = \frac{a^2}{hR} \qquad (6.2)$$

where:

a is the horizontal distance between the crown and the edge of the shell

h is the shell thickness

R is the radius of the shell

In this example, K is set equal to 3.0 and with

$$R = 100 \text{ inches}$$

$$h = 0.5 \text{ inch}$$

the half angle of the shell θ is approximately 7.1°. Material properties of the shell are:

$$E = 30000 \text{ ksi}$$

$$\nu = 0.3$$

A quarter of the shell was analyzed with a mesh as shown in Fig. 6-3b. The resulting normalized load $\left[\left(\frac{a}{n}\right)^4 \left(\frac{p}{E}\right)\right]$ vs normalized displacement $\left(\frac{w_o}{n}\right)$ curve comparing against Kornishin's power series solution (21) is shown in Fig. 6-3c. It is noted that in the area close to $\frac{w_o}{n} = 1.5$ i.e. where the shell snaps through, the structural stiffness is nearly zero. Therefore small load increments have to be used in this area in order to get good results. Also noted is the fact that the QTSHEL solution tends to diverge from the true solution in this region. However, the inclusion of equilibrium correction brings back the QTSHEL solution to the true solution as the load increases beyond this area (Fig. 6-3c).

It can be seen from the above three examples that the finite element procedure yields very good results as compared with existing solutions. Although only simple structures such as plates and an

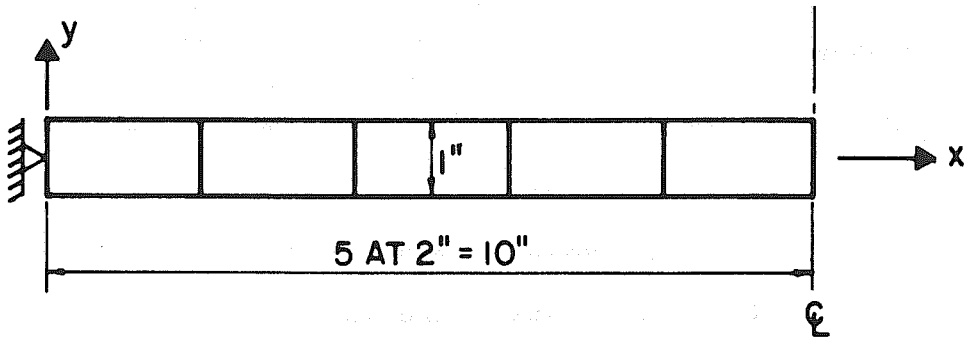

FIG. 6-1a FINITE ELEMENT MESH FOR A STRIP OF INFINITELY LONG PLATE

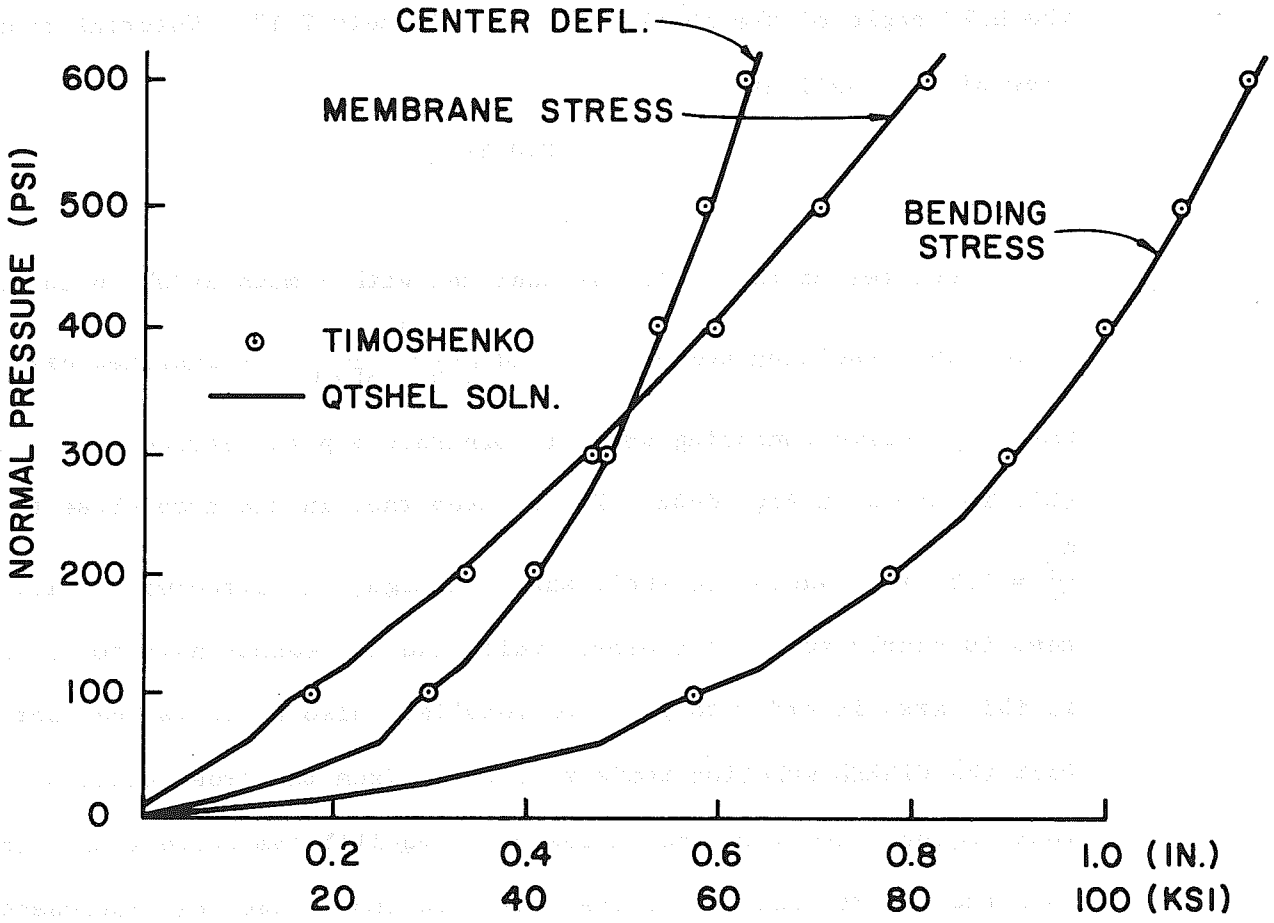

FIG. 6-1b NON-LINEAR SOLUTION OF INFINITELY LONG PLATE

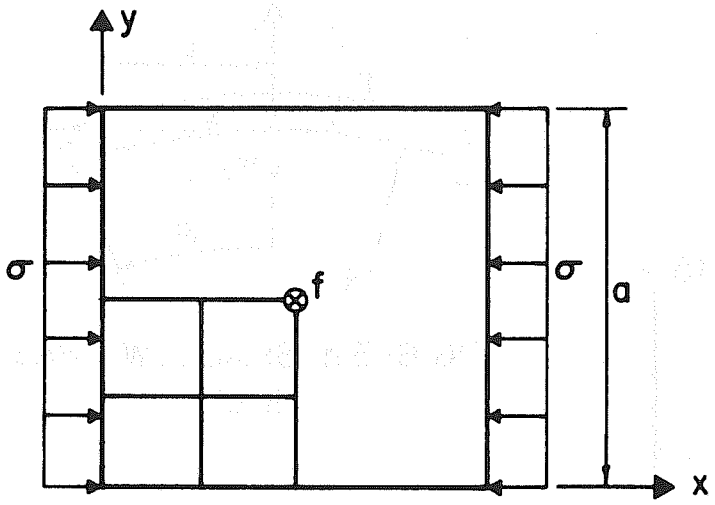

FIG. 6-2a SQUARE PLATE AND IT'S FINITE ELEMENT MESH

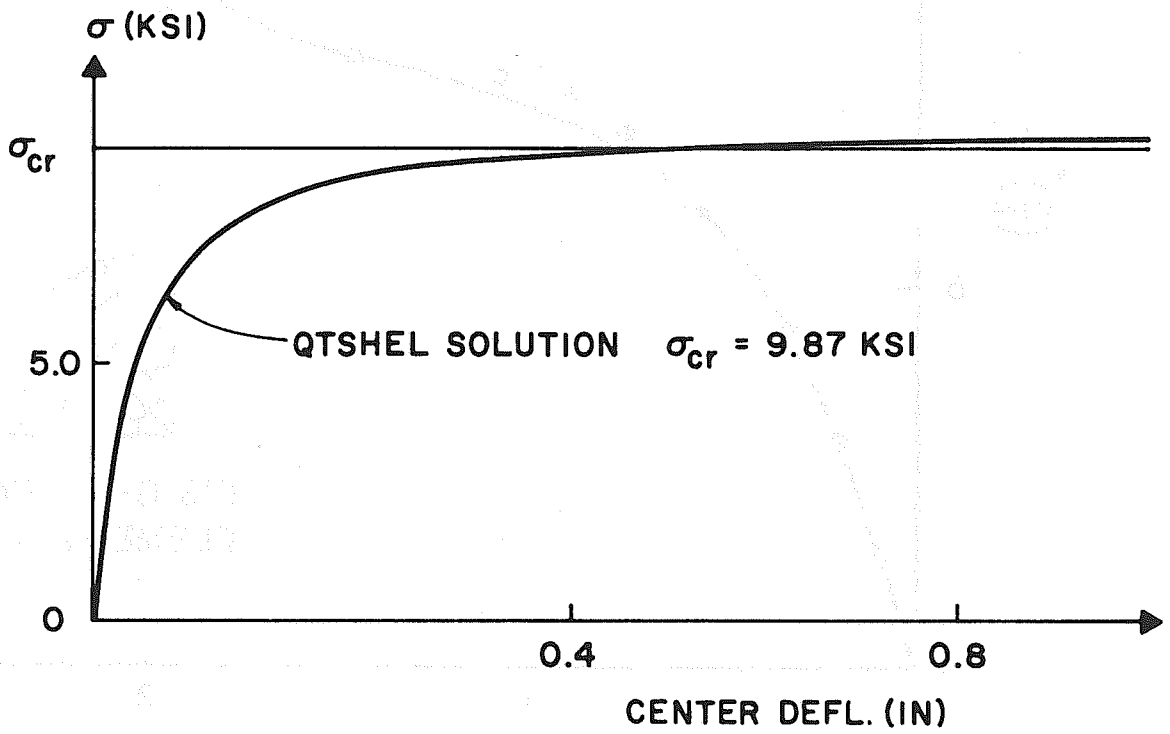

FIG. 6-2b ASYMPTOTIC SOLUTION OF SQUARE PLATE BUCKLING

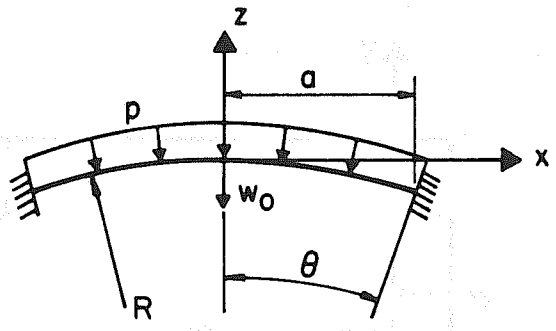

FIG. 6-3 a SHALLOW SPHERICAL SHELL

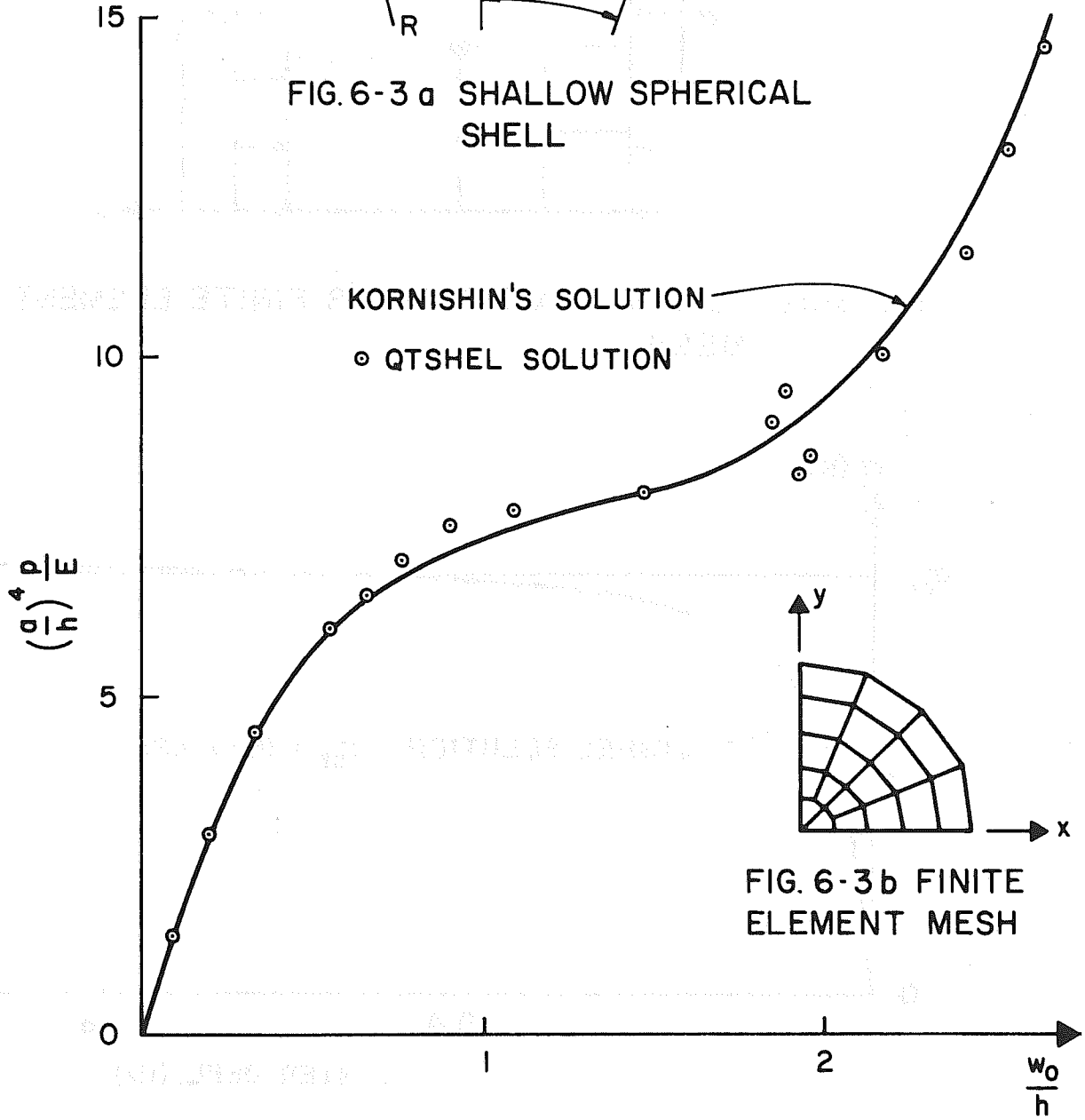

FIG. 6-3 b FINITE ELEMENT MESH

FIG. 6-3c NORMALIZED LOAD VS. DEFLECTION CURVE

axisymmetric shell are analyzed, it should be emphasized that this finite element procedure is developed to treat all shell structures indiscriminately. Therefore it may be concluded that this procedure can predict non-linear shell behavior accurately as long as the structural stiffness matrix remains positive definite and the strain is small.

6.2 Dynamic Cases

a) Cylindrical Tube

A cylindrical tube supported on diaphragms at both ends is shown in Fig. 6-4a. The diaphragms are assumed to be infinitely rigid in their own planes and infinitely flexible normal to their planes. The natural frequencies of this tube have been studied by several investigators. Therefore, this example has been selected to check the dynamic aspect of this finite element procedure.

One group of the tube's natural frequencies may be obtained by considering one eighth of the tube with symmetric boundary conditions along the three center lines. By assuming these boundary conditions, only vibrations whose number of half waves in the longitudinal direction "m" is odd and the number of complete cyles around the circumferential direction "n" is even, will be included. The mesh layout for one eighth of the tube is shown in Fig. 6-4b. This example was studied by Carr (3) using a complete compatible element. The same finite element mesh was used in Carr's analysis as presented in this study except Carr used two triangles to represent each quadrilateral used in this study.

Dimensions and material properties of the tube are:

Length $L = 500$ inches

Radius $R = 100$ inches

$h = 0.2$ inch

$E = 10000$ psi

$\nu = 0$

Mass Density $\rho = 1.0$ lb-sec^2/in^4

The material properties are artificially chosen such that:

$$\omega_0 = [\rho a^2(1-\nu^2)/E]^{-\frac{1}{2}} = 1.0$$

for simplicity. Resulting natural frequencies for the first three vibrational modes (using the lumped mass matrix and inverse iteration technique) comparing with results from Carr (3) and Forsberg (12) are presented in Table 6-1 following:

TABLE 6-1. NATURAL FREQUENCIES (RAD/SEC) OF CYLINDRICAL TUBE

m	n	QTSHEL	Carr		Forsberg
			Direct Soln.	Rayleigh-Ritz	
6	1	0.0267	0.0280	0.0274	0.0224
8	1	0.0340	0.0464	0.0372	0.0363
4	1	0.0662	0.0788	-	0.0616

It can be seen from the above table that the QTSHEL solution shows reasonable agreement as against Forsberg's solution which was obtained by numerical evaluation of several versions of classical cylindrical shell theory according to Donnell and Flügge. It should be noted that the finite element mesh used in this example is a very coarse one - each element spans 18° in the circumferential direction. Improved

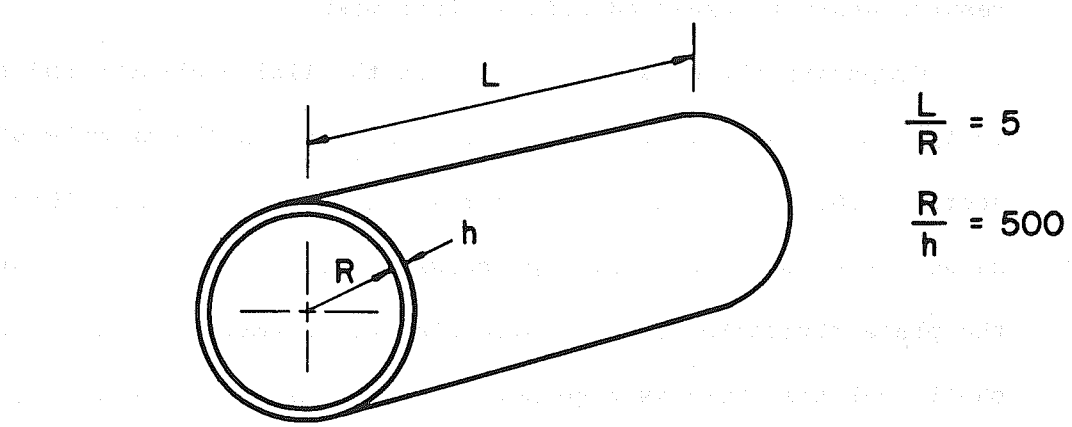

FIG. 6-4a CYLINDRICAL TUBE

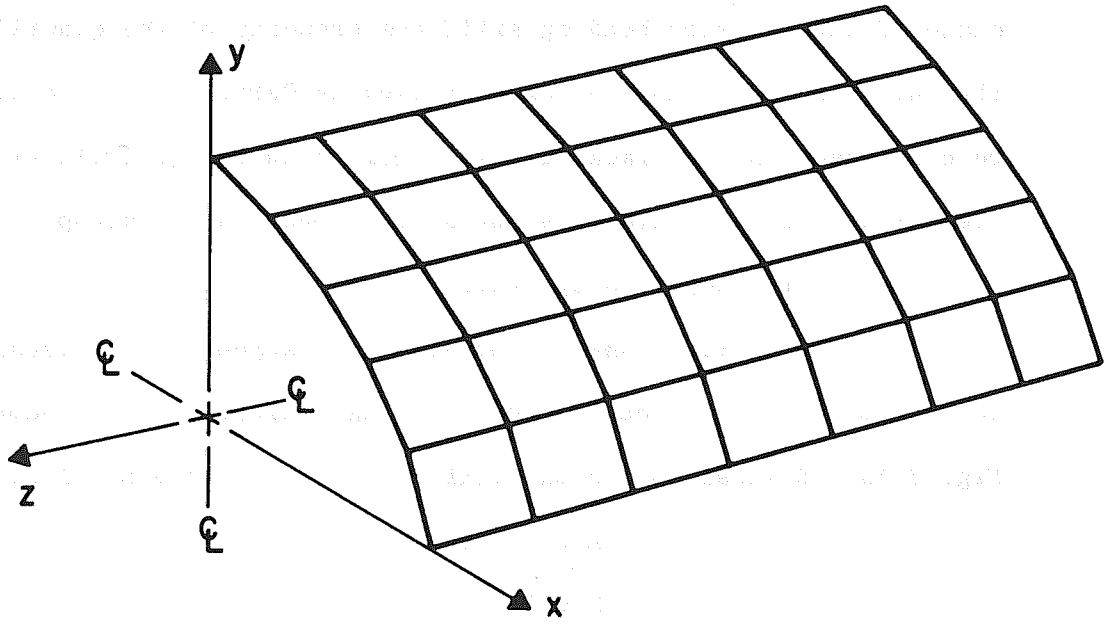

FIG. 6-4b MESH LAYOUT FOR ONE EIGTH OF THE TUBE

results would be expected with a finer mesh.

Comparing the consistency between the finite element and the analytical solutions in this example and that in the example of section 4.6, it can be seen that the latter is superior. This is because there is no geometric approximation involved in representing the plate structure by the finite element assemblage while in this shell analysis there is a geometric approximation. Therefore, the closeness between the finite element system and the real structure is a very important factor in the analysis.

Comparing the two finite element solutions, the QTSHEL solution is as good as, if not superior to, Carr's, despite the fact that the latter used a complete compatible shell element. This is mainly because of the superior bending stiffness property of the quadrilateral element over the triangular element used by Carr. Therefore it may be concluded that the lack of compatibility in the quadrilateral shell element used in this study is not a very important handicap.

b) Simply Supported Cylindrical Shell

A cylindrical shell roof structure supported on diaphragms at both ends and free to move along the longitudinal edges is shown in Fig. 6-5a. Dimensions and material properties of the shell are:

$$L = 50 \text{ feet}$$

$$R = 50 \text{ feet}$$

$$h = 3 \text{ inches}$$

$$\theta = 20°$$

$$E = 3 \times 10^6 \text{ psi}$$

$$\nu = 0$$

$$\text{Weight of shell wt} = 90 \text{ lb/ft}^2$$

The static behavior convergence of solution with respect to mesh refinement of this structure was discussed in Ref. 19. The dynamic behavior of this shell will be presented here. One reason for selecting this particular structure is that its geometry is simple. Therefore, it is relatively easier to carry out analyses for successively refined meshes. However, the same analyses can be carried out for any shell structure with this procedure at the expense of more computer time being spent. This example is considered as appropriate for the demonstration of dynamic analysis.

i) Natural Frequencies

Assuming doubly symmetric conditions, only a quarter of the shell was analyzed. A typical 4X4 mesh is shown in Fig. 6-5b. Natural frequencies, obtained by inverse iteration, for the first six vibration modes with successively refined mesh are presented in Table 6-2 below.

TABLE 6-2. NATURAL FREQUENCIES OF SHELL ROOF (RAD/SEC)

MESH	ω_1	ω_2	ω_3	ω_4	ω_5	ω_6	TIME (SECOND)
2X2	8.614	22.52	-	-	-	-	-
4X4	9.643	24.49	33.88	42.81	64.20	68.95	6
6X6	9.765	24.24	34.17	44.99	68.99	70.31	10
8X8	9.777	24.09	34.08	45.95	69.73	70.93	50

The term "Time" in the table refers to the average central processor time required to calculate one eigenvalue in a CDC 6400 machine. It can be seen that the natural frequencies converge as the mesh size is reduced. Note that in modes 2 and 3, the frequencies increase as the

mesh is refined up to 4X4 and 6X6 respectively and decrease as the mesh refinement continues. The increase is caused by the better geometric approximation of the structure by the flat finite element assemblage for these two modes; and the decrease is caused by the better representation of the structural deformation by the displacement interpolation functions assumed for each element. Similar behavior is expected for other modes as the mesh refinement continues beyond 8X8.

ii) Linear Dynamic Response to Time Varying Loading

The load on the structure is a uniform pressure of 90 lb/ft^2 whose time history is a sinusoidal impulse (Fig. 6-5c). It is assumed that there is no damping for the system.

The convergence with respect to the mesh refinement is further demonstrated by calculating the linear dynamic response to this load. The mode superposition method was used for the analysis and six modes were included. The decoupled equations were solved by a step-by-step integration method assuming constant acceleration with a time step $\Delta t = 0.025$ second.

In Fig. 6-6 through 6-10, Fig. "a" refers to the vertical deflection at the middle point of the free edge and Fig. "b" refers to the vertical deflection at the center of the shell.

Figure 6-6 shows the comparison between the linear dynamic response for a 4X4 mesh and a 6X6 mesh. Figure 6-7 shows the comparison between a 6X6 mesh and a 8X8 mesh. It can be seen that the difference shown in Fig. 6-6 is small and there is practically no difference in Fig. 6-7. Therefore, for practical purposes a 4X4 mesh is probably good enough in this structure.

iii) Effects of the Sizes of Time Steps on the Solutions

For a 4X4 mesh, a time step $\Delta t = 0.025$ second which is adequate for this problem and $\Delta t = 0.10$ second which is too large, were used. Figure 6-8 shows the comparison of linear dynamic solution for these two time steps and Fig. 6-9 shows the comparison between the non-linear dynamic solutions. It can be seen that about the same amount of discrepancy shows up in both diagrams due to inadequate time step. It can be further noted that in Fig. 6-8a, the larger time step (0.10 second) gives essentially the first mode response as expected (because the natural period of the second mode is only 2.5 times the time step). Therefore, although the constant acceleration assumption is always stable regardless of the size of the time step, excessively large time steps tend to damp out the higher mode contributions and give inferior results.

iv) Non-linear Dynamic Response

Finally a comparison between the linear and non-linear solution is made for the 4X4 mesh and $\Delta t = 0.025$ second. It can be seen in Fig. 6-10a that the structure is stiffened and higher modes are excited by the deflection of the structure. Figure 6-10b shows that the natural period is shortened because of deflection.

The fact that the linear solution was obtained by the mode superposition method considering only six modes while the non-linear solution was obtained by a direct step-by-step integration technique which, "theoretically," included all modes, may have some contribution to the difference between the results shown in Fig. 6-10. However, since the natural period of the sixth mode is only 0.091 second which is already less than four times the time step (0.025 second) used, the higher

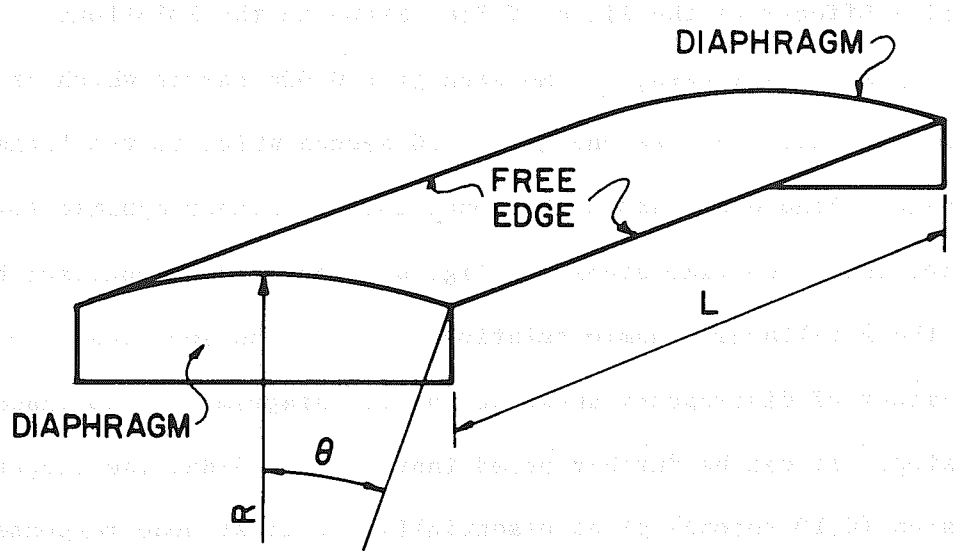

FIG. 6-5a CYLINDRICAL SHELL

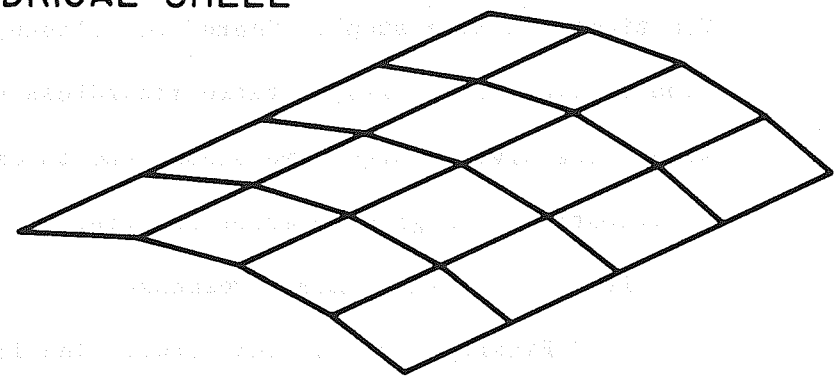

FIG. 6-5b 4x4 MESH LAYOUT FOR ONE QUARTER OF THE SHELL

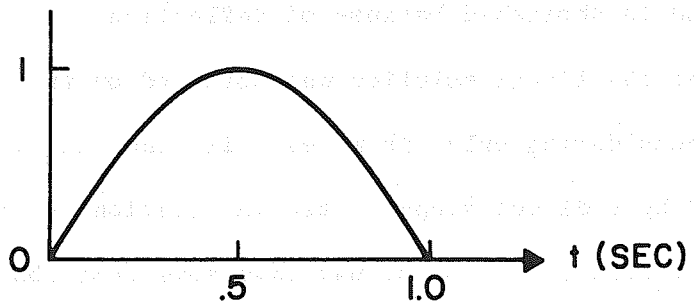

FIG. 6-5c LOAD - TIME HISTORY

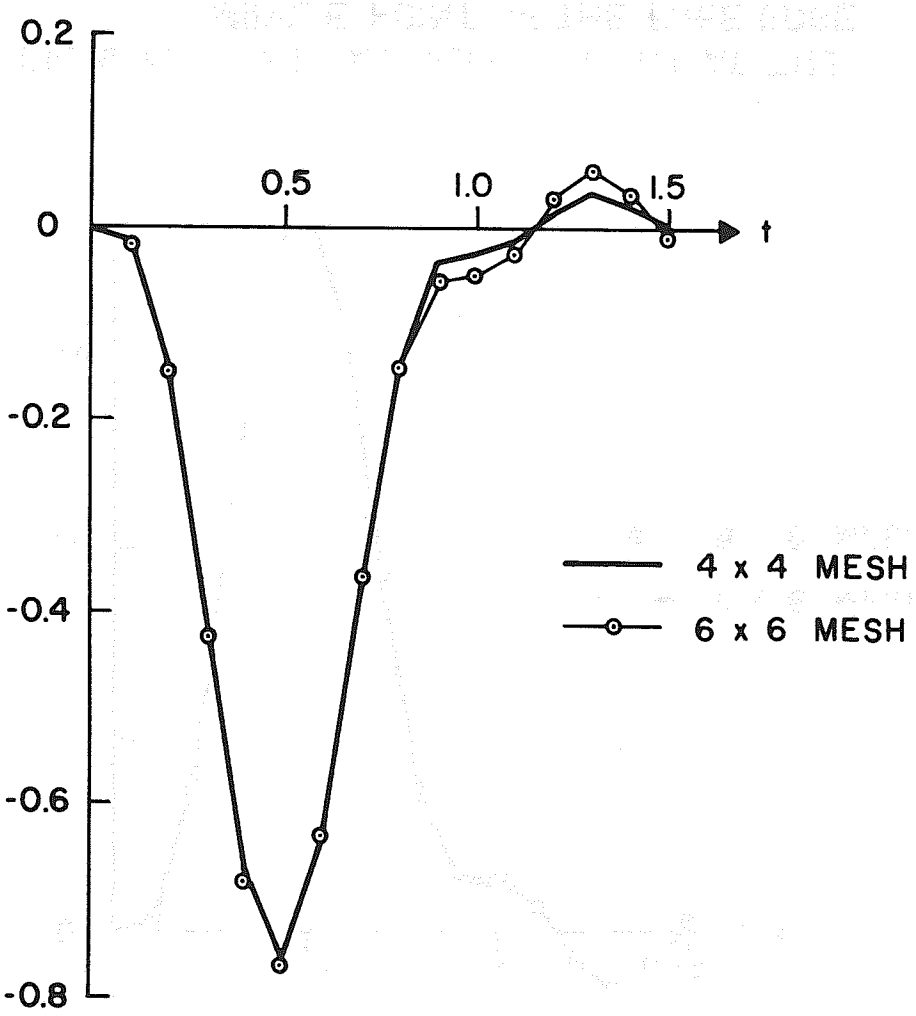

FIG. 6-6a VERTICAL DISPLACEMENT AT THE MIDDLE POINT OF THE FREE EDGE

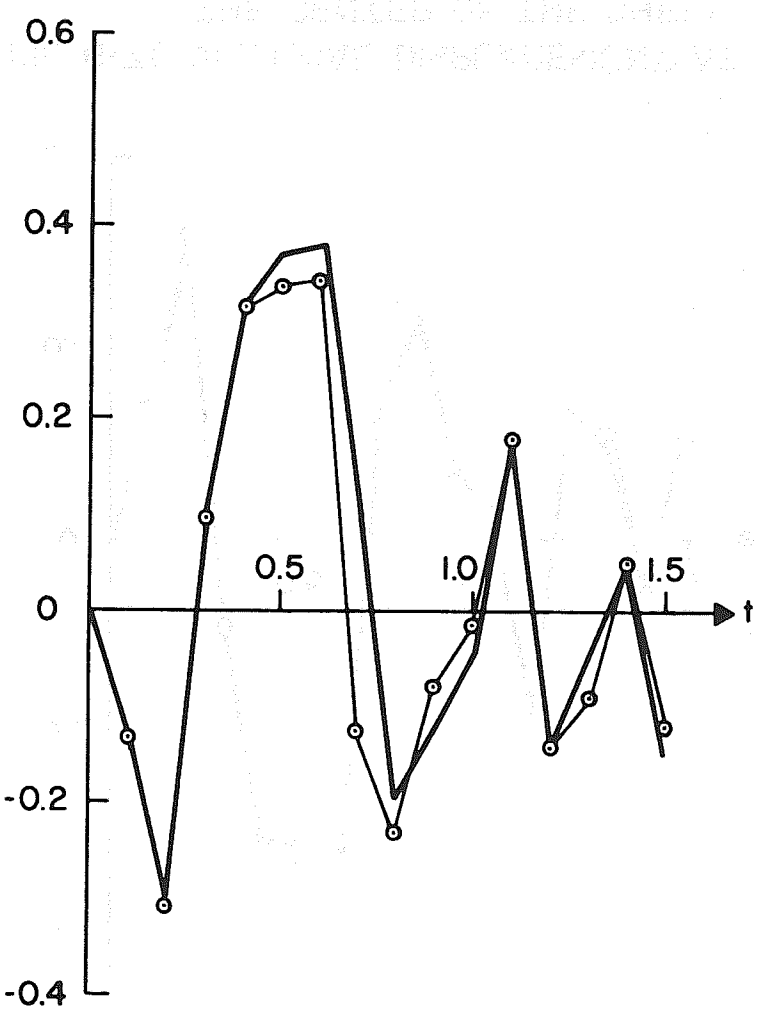

FIG. 6-6b VERTICAL DISPLACEMENT AT THE CENTER OF THE SHELL

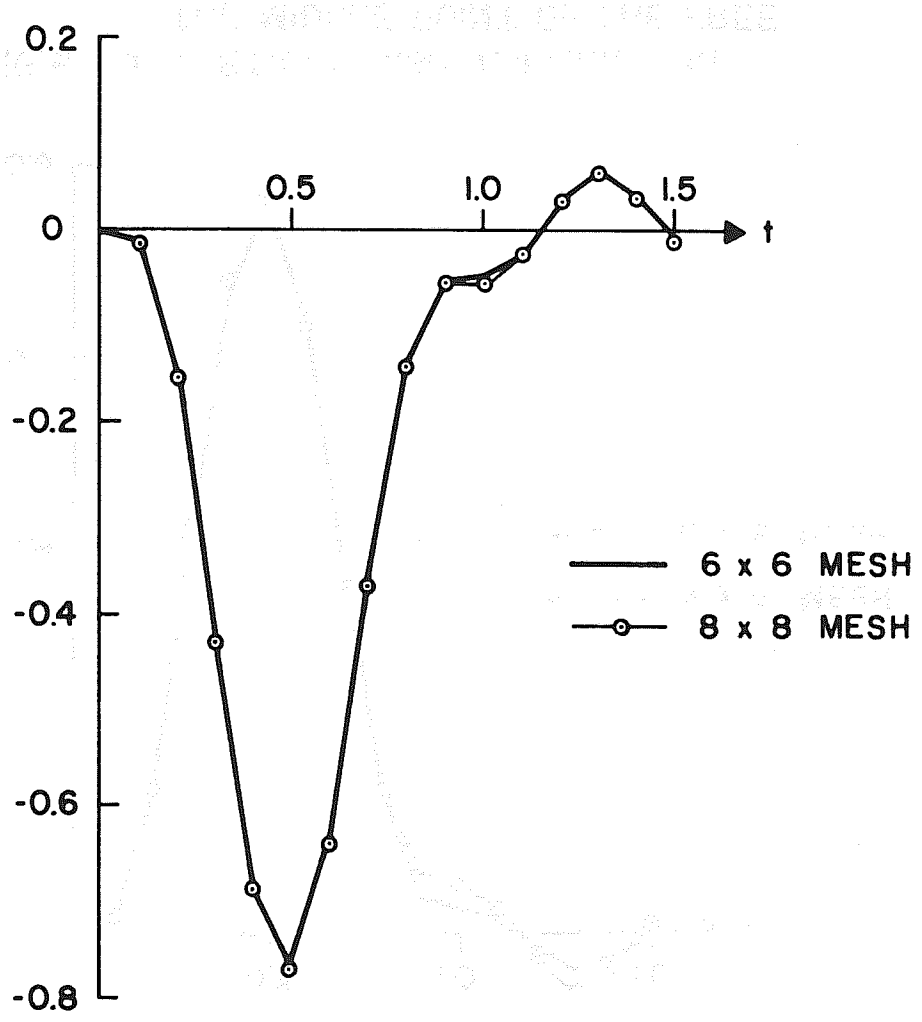

FIG. 6-7a VERTICAL DISPLACEMENT AT THE MIDDLE POINT OF THE FREE EDGE

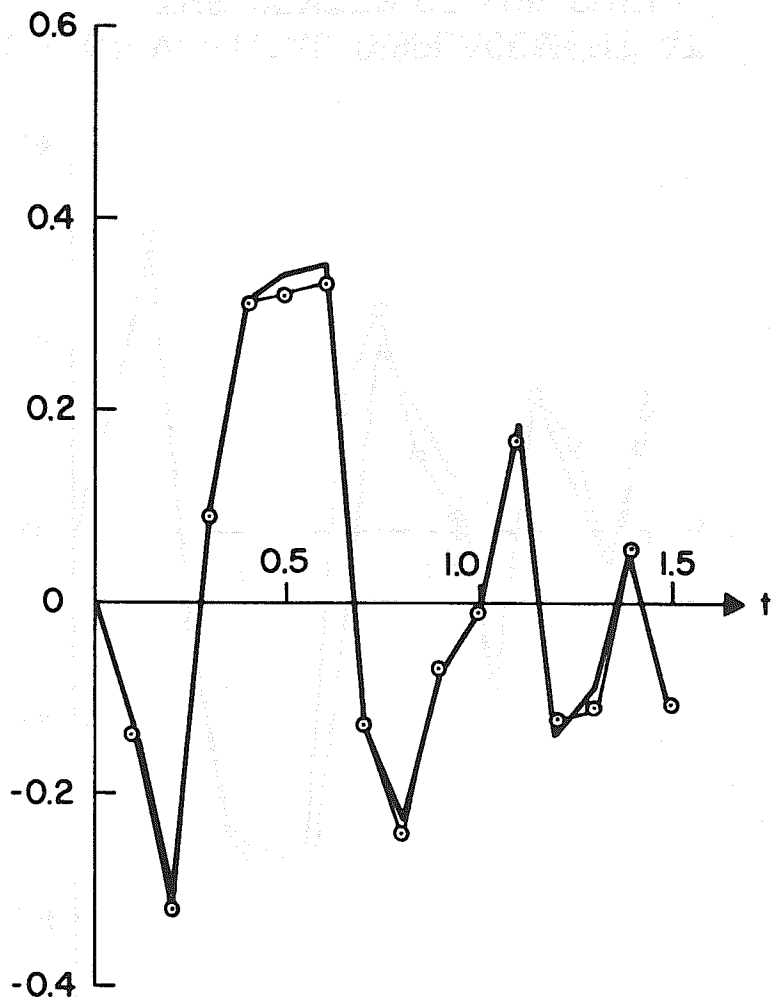

FIG. 6-7b VERTICAL DISPLACEMENT AT THE CENTER OF THE SHELL

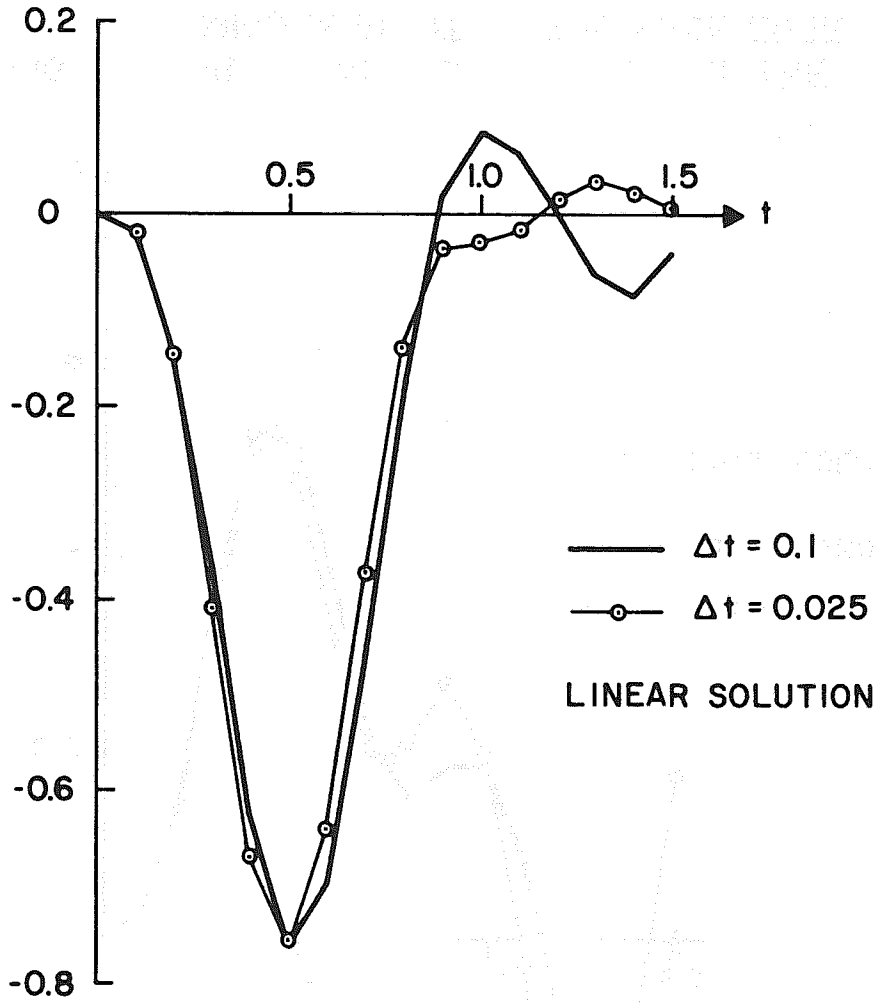

FIG. 6-8a VERTICAL DISPLACEMENT AT THE MIDDLE POINT OF THE FREE EDGE

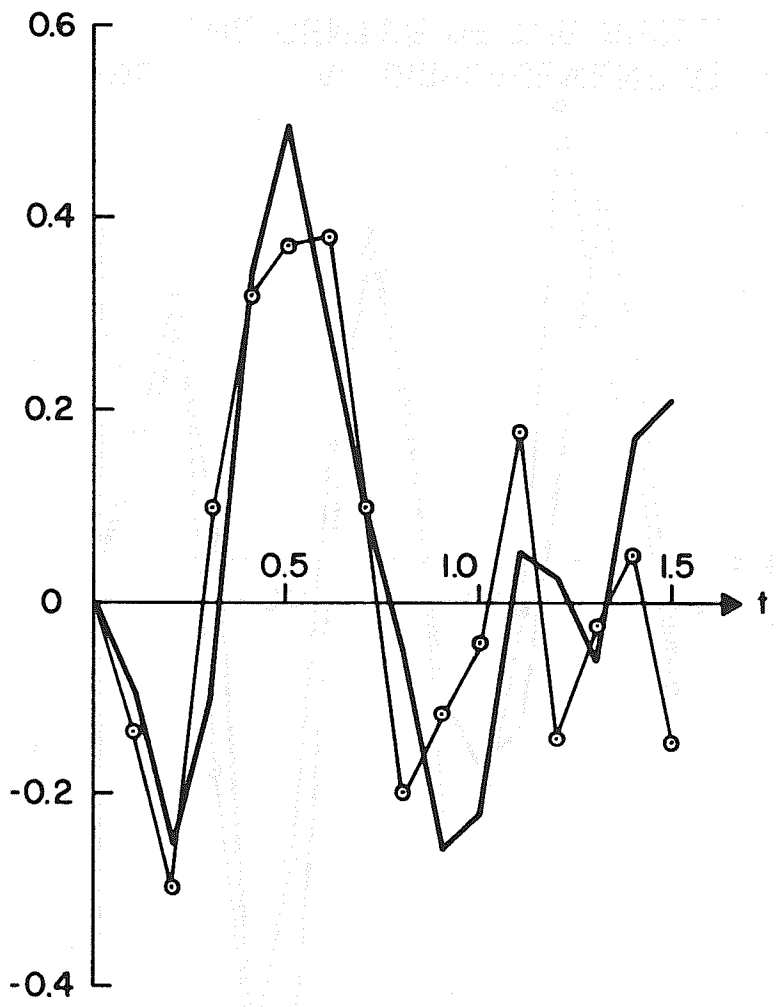

FIG. 6-8b VERTICAL DISPLACEMENT AT THE CENTER OF THE SHELL

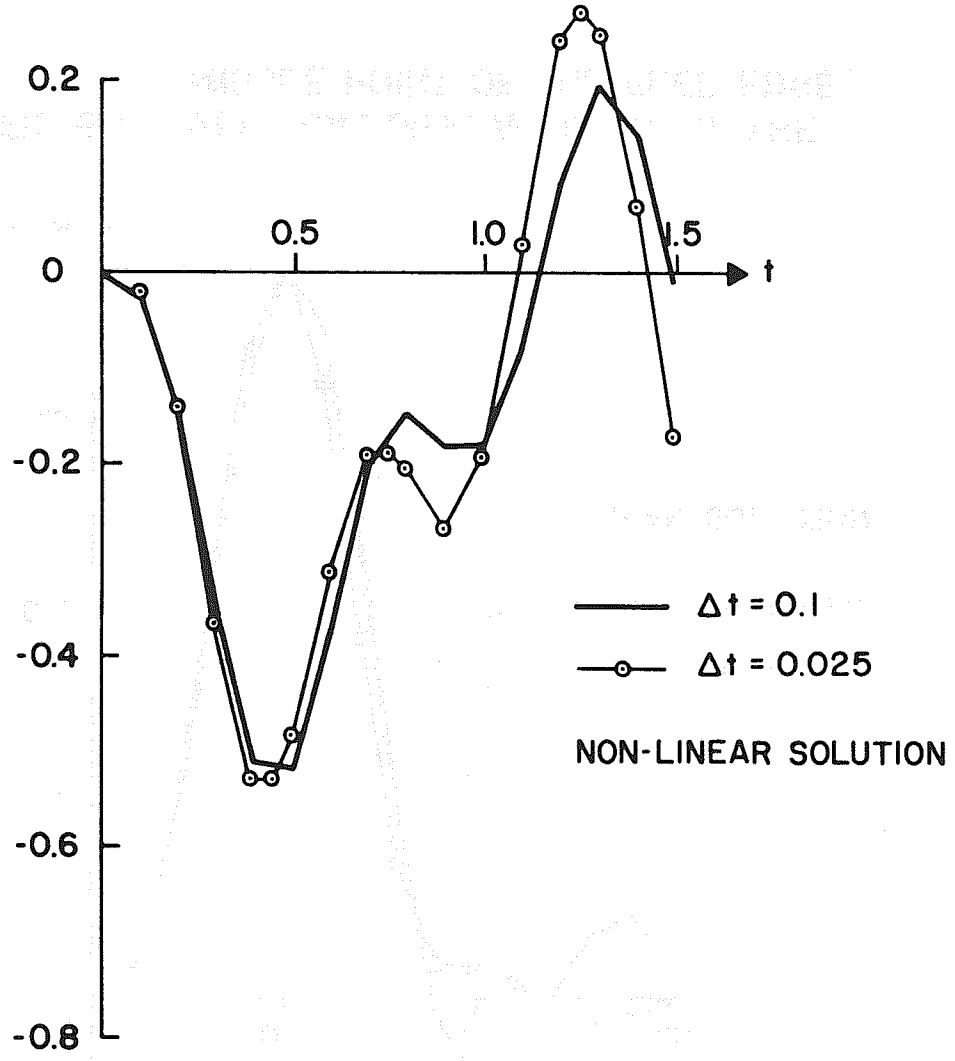

FIG. 6-9a VERTICAL DISPLACEMENT AT THE MIDDLE POINT OF THE FREE EDGE

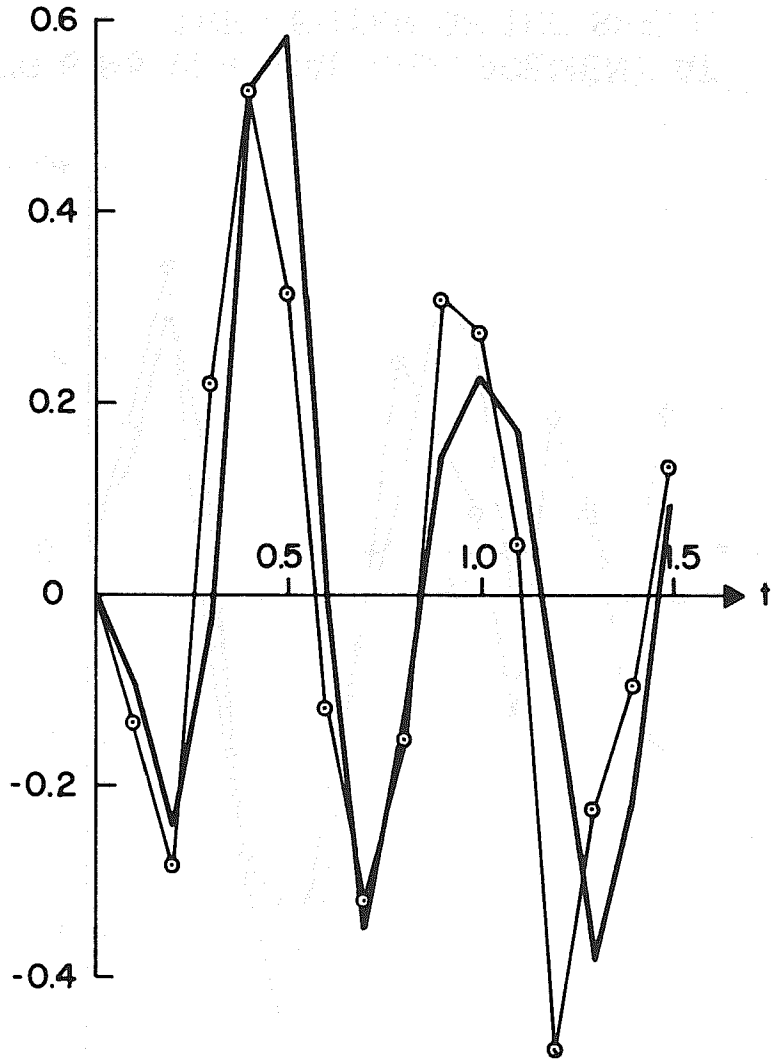

FIG. 6-9b VERTICAL DISPLACEMENT AT THE CENTER OF THE SHELL

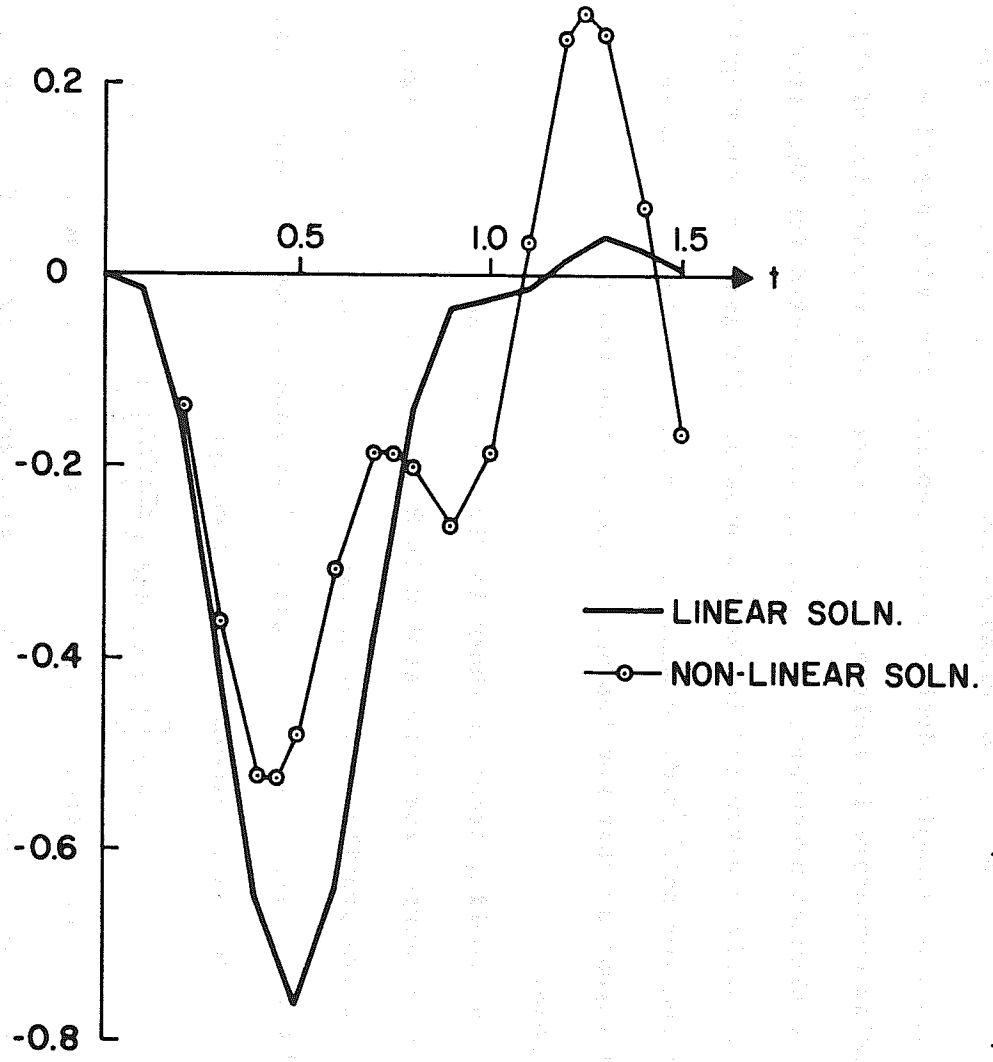

FIG. 6-10a VERTICAL DISPLACEMENT AT THE MIDDLE POINT OF THE FREE EDGE

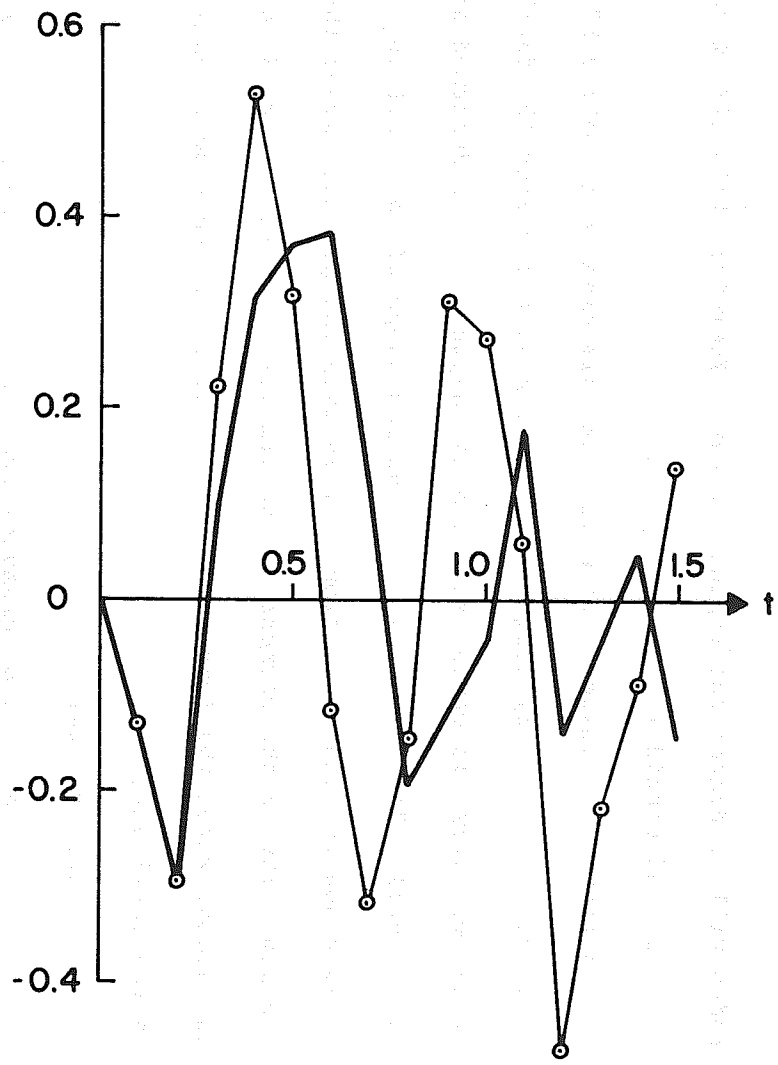

FIG. 6-10b VERTICAL DISPLACEMENT AT THE CENTER OF THE SHELL

modes will be damped out rapidly anyway. Therefore this effect should be small and considered as negligible.

Although the maximum deflection in this example is only 0.533 foot which is not very large in comparison with the span (50 feet), it is very large in comparison with the depth of the undeformed shell (3.01 feet). The change of cross section shape of the shell is drastic due to this deflection. It is this change that causes the non-linearity in the response. The difference shown in Fig. 6-10 has demonstrated the importance of including the non-linear behavior in the shell analysis.

c) Cooling Tower

All the previous examples are relatively simple structures. In this last example a doubly curved cooling tower with negative Gaussian curvature is analyzed to demonstrate the versatility of this finite element procedure. The cooling tower selected for this study was actually constructed in Czechoslovakia. Its geometry was slightly modified for this study to make it suitable for relatively coarse mesh layout so that not too much computer time would be spent for the analysis.

The cooling tower is shown in Fig. 6-11a. The shell structure above the supporting truss system is 312.5 feet (3750 inches) high. Half of its profile is shown in Fig. 6-11b. The smallest radius "a" (= 905.5 inches) is at the height of 3024 inches from the base of the shell. The radius elsewhere is defined by:

$$R = a\left[1 + 0.1405\left(\frac{z-3024}{a}\right)^2\right]^{\frac{1}{2}} \qquad (6.3)$$

where z is the vertical distance (in inches) between the radius and the base of the shell. The top stiffening ring is 145 inches high

and has a constant thickness of 19.2 inches. The bottom ring is 624 inches high. Its thickness is 18 inches at the bottom and varies linearly to 5.12 inches at the height of 624 inches. The shell thickness is constant (5.12 inches) between these two rings.

The shell structure is supported by a series of inclined columns along its base (Fig. 6-11a). For the purpose of this analysis, it was assumed that the base of the shell is free to move in the radial direction and free to rotate about the surface tangent coordinates ξ_1 and ξ_2, but is constrained against vertical and tangential displacements.

The shell is made of concrete with material properties:

$$E = 4.3 \times 10^6 \text{ psi}$$

$$\nu = 0.15$$

$$wt = 150 \text{ lb/ft}^3$$

The dynamic behavior of this shell structure is described in the following sections:

i) Natural Frequencies

A quarter of the tower was analyzed for its natural frequencies. Assuming doubly symmetric conditions, only vibrations whose number of complete cycles in the circumferential direction "n" is even, will be included. Two different meshes were used in the vertical direction. One has seven elements from top to bottom and the other has ten. The mesh sizes are plotted qualitatively in Fig. 6-11b. Also two different meshes were used in the circumferential direction with six and eight elements evenly distributed for a quarter of the circle respectively. A 6X7 mesh is shown in Fig. 6-12.

The natural frequencies of the first five vibrational modes based on three different meshes are as shown in Table 6-3 below:

TABLE 6-3. NATURAL FREQUENCIES OF COOLING TOWER (RAD/SEC)

MESH	ω_1 (n=4)	ω_2 (n=6)	ω_3 (n=2)	ω_4 (n=4)	ω_5 (n=8)	TIME (SECOND)
6X7	10.03	10.07	11.84	12.19	12.48	41
8X7	10.18	10.38	11.87	12.33	13.25	56
6X10	10.08	10.31	11.88	12.10	12.28	52

The term "Time" in the table refers to the average central processor time required to calculate one eigenvalue with a CDC 6400 machine. It is noted from the above table that the 6X7 mesh gives very good results for the first four modes (i.e. the results have only little changes with a finer mesh in both vertical and circumferential directions). The frequency of the fifth mode increases approximately six percent as the number of elements in the circumferential direction increases from six to eight (mesh 6X7 and 8X7). This change results from the fact that this mode has eight complete cycles in the circumferential direction (n=8) and six elements cannot approximate this vibrational behavior closely. However, the 6X7 mesh was used for the response analysis described later because its results are considered to be reasonably good, as well as because of the restriction imposed on available computer core storage ($140{,}000_8$ for the CDC 6400 machine used at the Computer Center at Berkeley).

It is further noted that:

A) The natural frequencies of this structure are not widely separated. Therefore it is hard to decide how many modes

will contribute significantly to the dynamic response. In this case, it is much more reliable to use a direct step-by-step integration technique to evaluate the linear dynamic response than to use the mode superposition method.

B) Considering the size of the structure and the magnitude of its first mode frequency, this is a very stiff structure. Therefore the large deflection effects may be not so pronounced as in the previous examples.

ii) Dynamic Response to Wind Load

Load on the structure is assumed to be a wind blowing from the positive x-direction. The wind pressure on the structure in the circumferential direction is defined by:

$$0° \leq \theta < 72°, \quad P(\theta) = -\cos \frac{180}{72}\theta \tag{6.4a}$$

$$72° \leq \theta < 105°, \quad P(\theta) = -0.225 \cos \frac{180}{33}(\theta-72) + 0.775 \tag{6.4b}$$

$$105° \leq \theta \leq 180°, \quad P(\theta) = 0.550 \tag{6.4c}$$

where θ is the angle from the positive x-axis. In the vertical direction, it is assumed to remain constant. Wind pressure at each node is calculated using Eq. (6.4) and a linear variation is assumed within each element (Fig. 6-13a). The time history of the wind is shown in Fig. 6-13b. The maximum wind pressure on the structure during the process is 0.4 psi (57.6 lb/ft^2). Damping in the system is assumed to be $\beta = 0.01$ which is equivalent to five percent of critical damping for the first mode.

Half of the structure has been considered in the analysis (Fig. 6-14a) taking account of symmetry. A 12X7 mesh was used to represent the half shell. The mesh is plotted symbolically in Fig. 6-14b.

Figure 6-15 shows the radial displacements of three nodes along the top ring as a function of time and Fig. 6-15b shows another three nodes along the throat of the shell. Figure 6-16 a and b show the deformed shapes of the top ring and the throat respectively at the time t = 1.15 second which corresponds to the maximum deflection in the process. Figure 6-17 shows the deformed shape of the profile of the tower at the time t = 1.15 second. Displacements in all these three figures are exaggerated one hundred times to make the diagrams clear. It should be noted that the displacements are so small that the solution is almost equivalent to a linear one.

The computer central processor time required for this non-linear dynamic analysis was approximately 90 second/step with a CDC 6400 machine.

iii) Tower Collapses at Larger Load

A second case was studied with all data unchanged except that the wind pressure was increased by a factor of five. It was found that the tower collapses under this load. The collapse is caused by a local buckling which starts from the most highly compressed part of the shell and propagates to other parts. The structure finally collapses at the time t = 0.60 second.

Letting the resulting deformation of the tower from the above two loads $\underline{P}^1$ and $\underline{P}^2$ be represented by:

$$\underline{x}^1 = \underline{x}^1(t) \qquad (6.5a)$$

$$\underline{x}^2 = \underline{x}^2(t) \qquad (6.5b)$$

A normalized deformation vector will be defined by:

$$\underline{r}^i(t) = \underline{x}^i(t)/p^i_{max} \quad , \quad i=1,2 \qquad (6.6)$$

where

$$p^i_{max} = mxa\ [(\underline{P}^i(t)]\ .$$

Figure 6-18 shows the comparison of $\underline{r}^1$ and $\underline{r}^2$ at three nodes along the front edge of the shell. It can be seen that $\underline{r}^2$ starts to diverge from $\underline{r}^1$ at node 7 and propagates to node 6 and then node 5. This divergence exhibits the non-linear property due to larger deformation. Figure 6-19 shows the plot of the quantity $(r^2_j - r^1_j)/r^1_j$ for the same three nodes, where r^i_j is the j-th component of vector $\underline{r}^i(t)$. The propagation of divergence of $\underline{r}^2$ from $\underline{r}^1$ is more clearly demonstrated. Figure 6-20 shows the profile of the deformed tower just before collapse at the time t = 0.6 second.

It should be noted that a linear dynamic analysis will give a solution close to that presented in ii), but it can never predict this collapse.

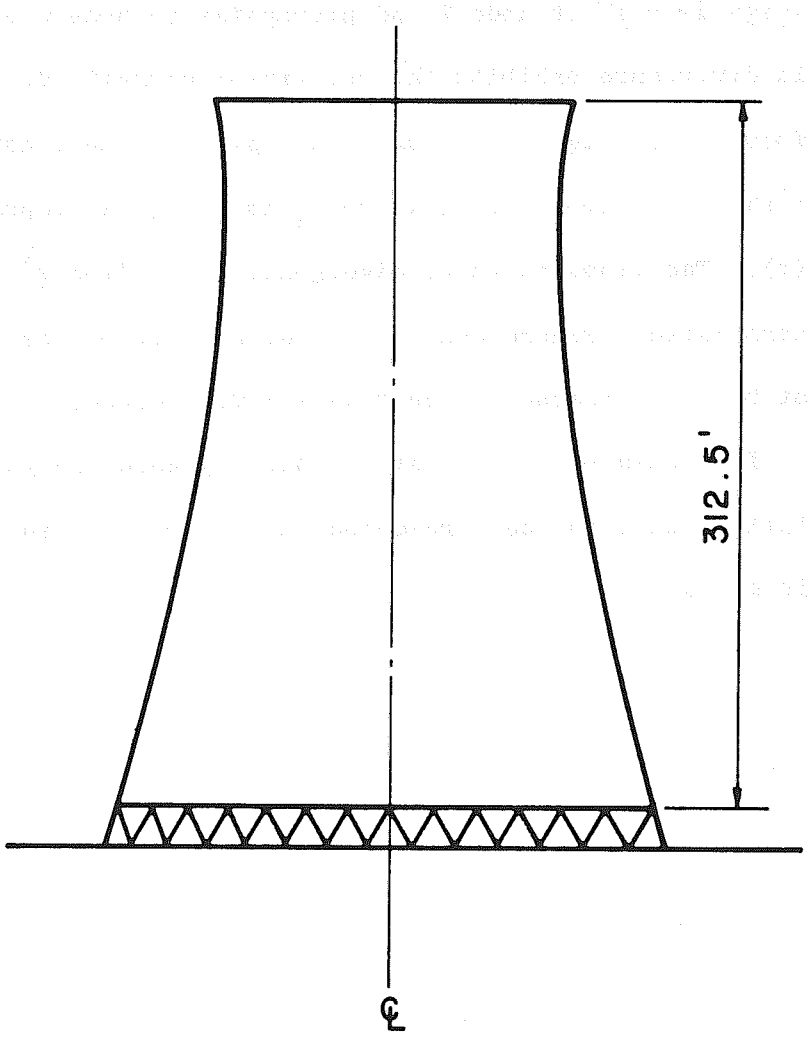

FIG. 6-11a COOLING TOWER

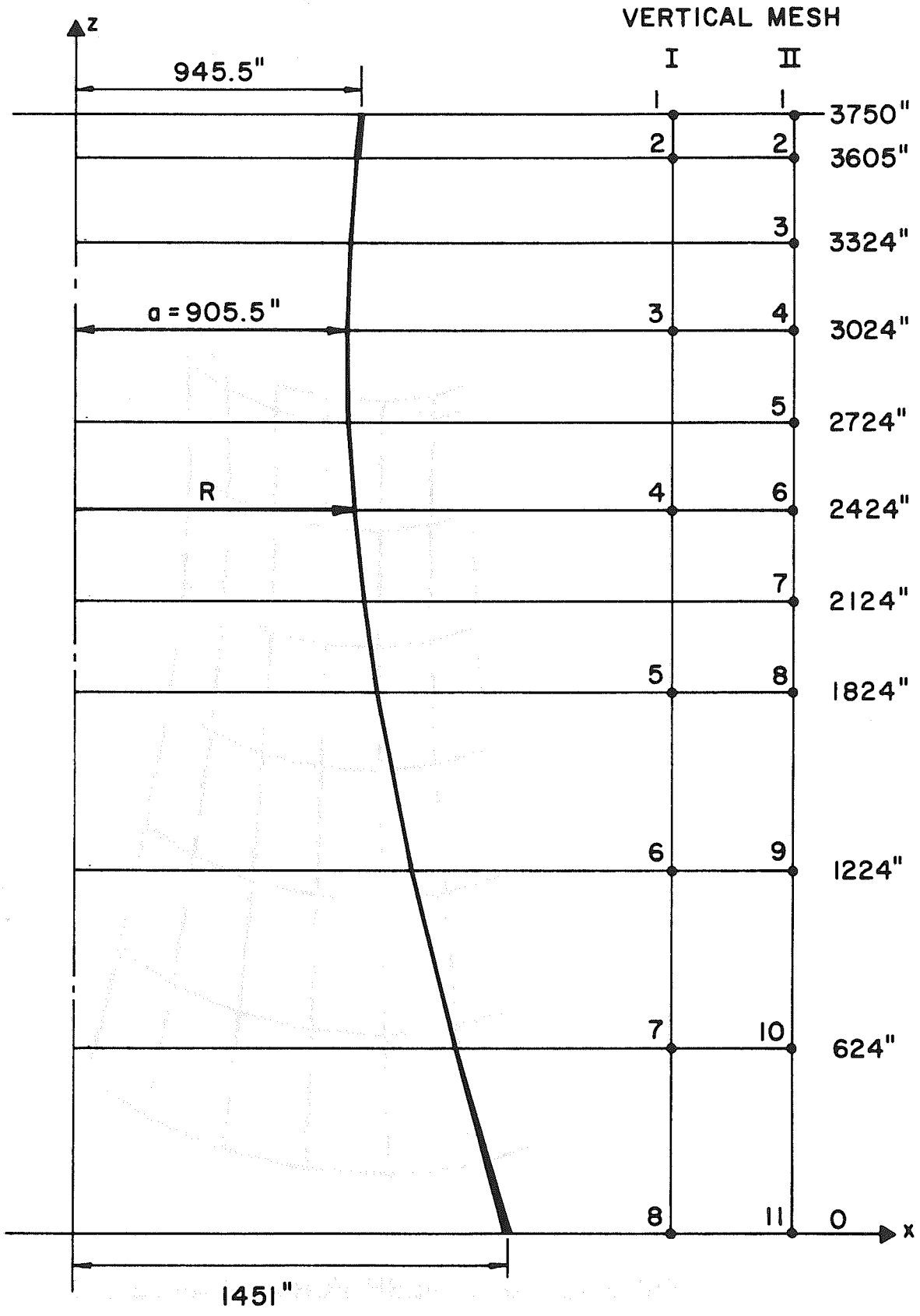

FIG. 6-11b COOLING TOWER PROFILE AND VERTICAL MESH LAYOUT

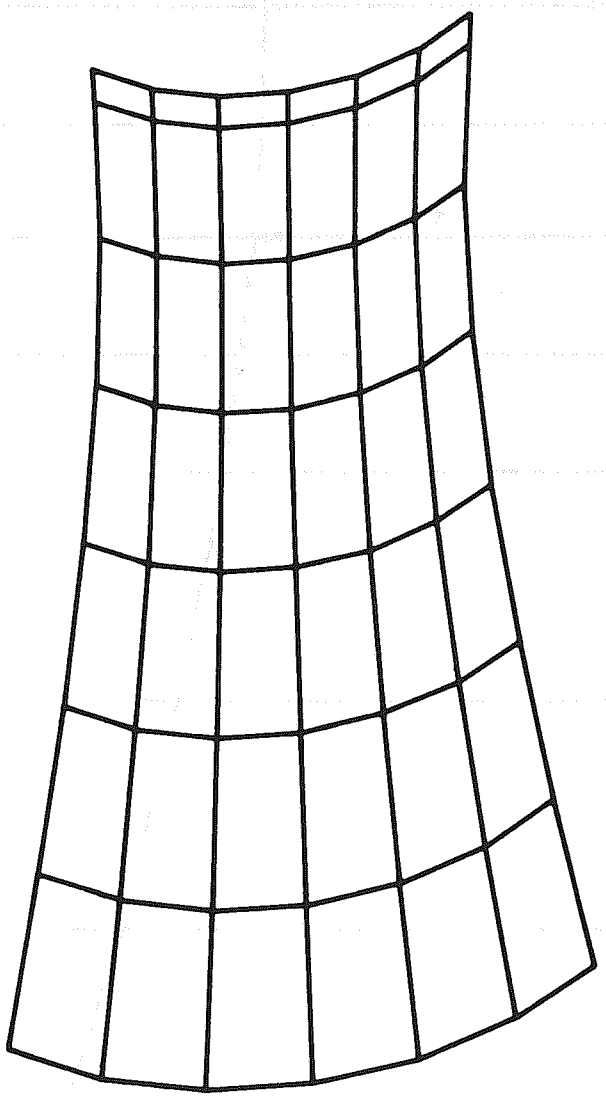

FIG. 6-12 6x7 MESH FOR A QUARTER OF THE STRUCTURE

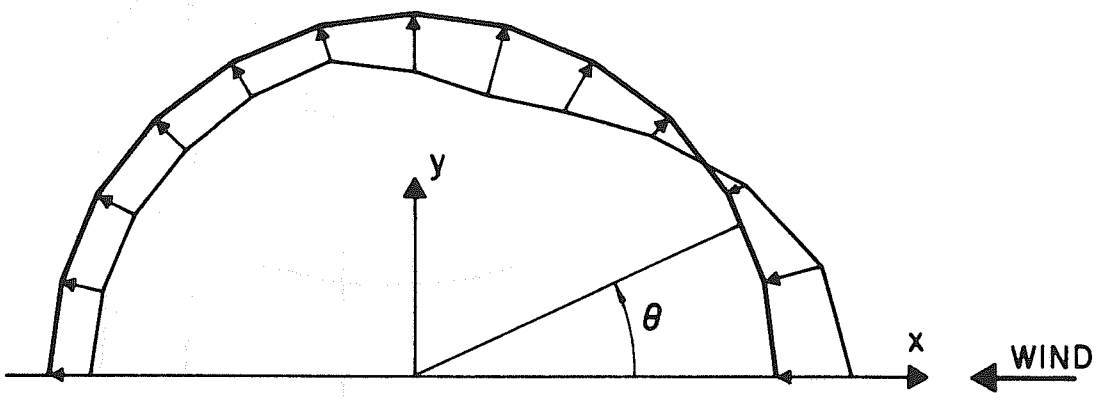

FIG. 6-13a WIND PRESSURE

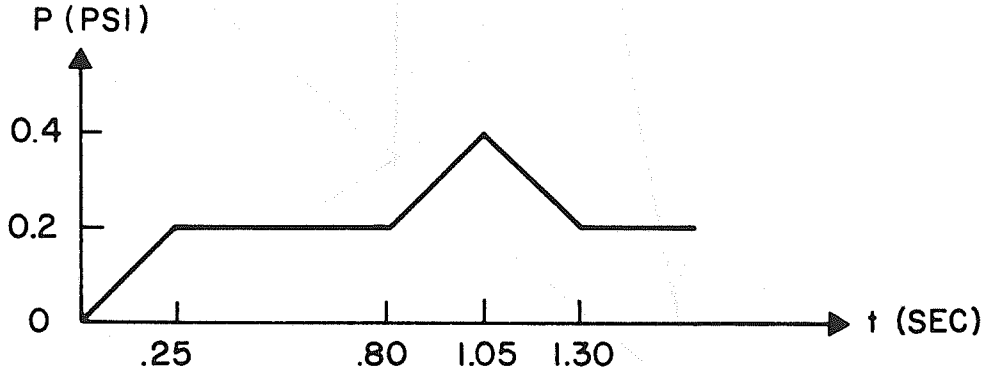

FIG. 6-13b WIND TIME HISTORY

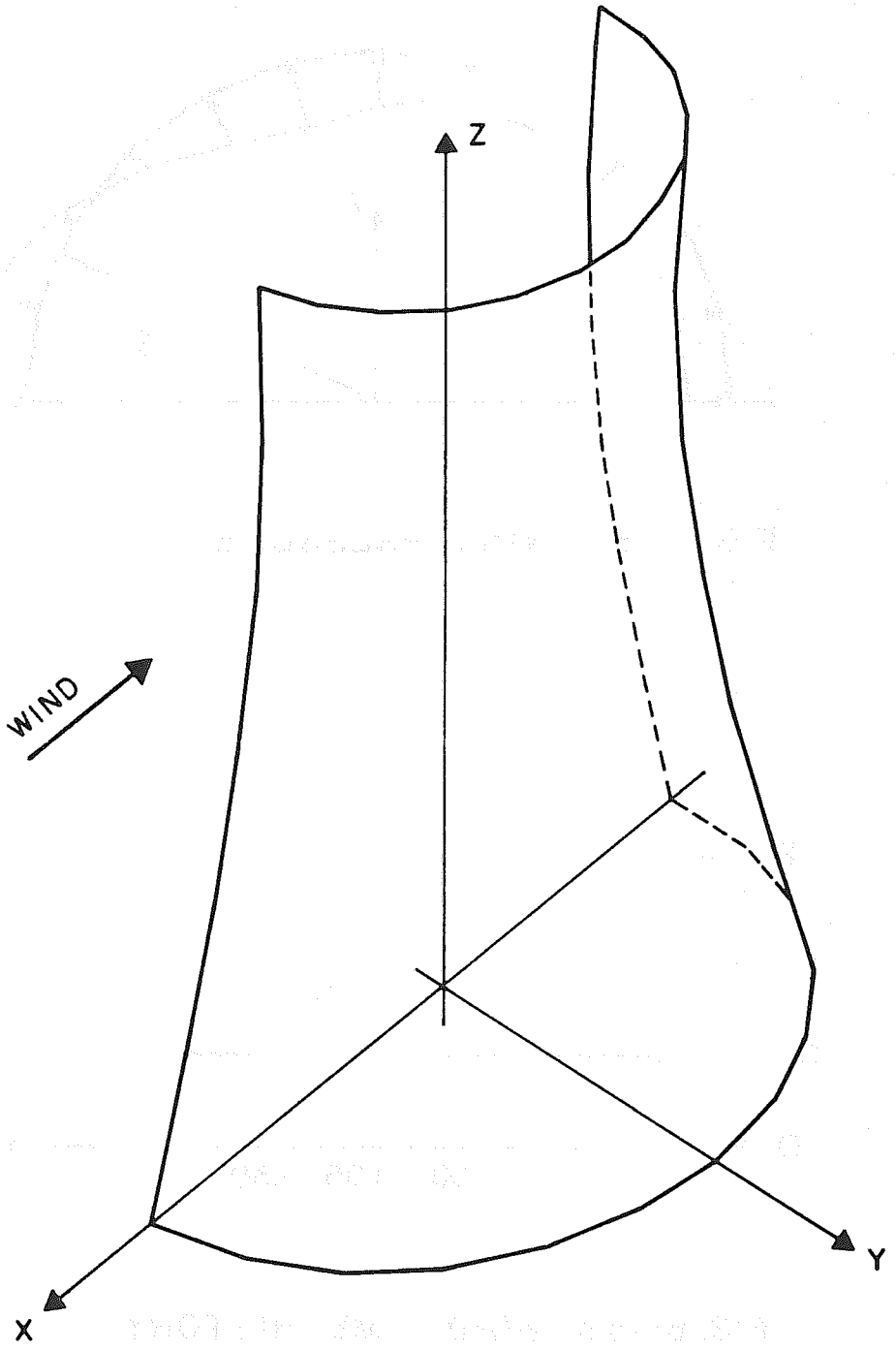

FIG. 6-14 a HALF OF THE COOLING TOWER

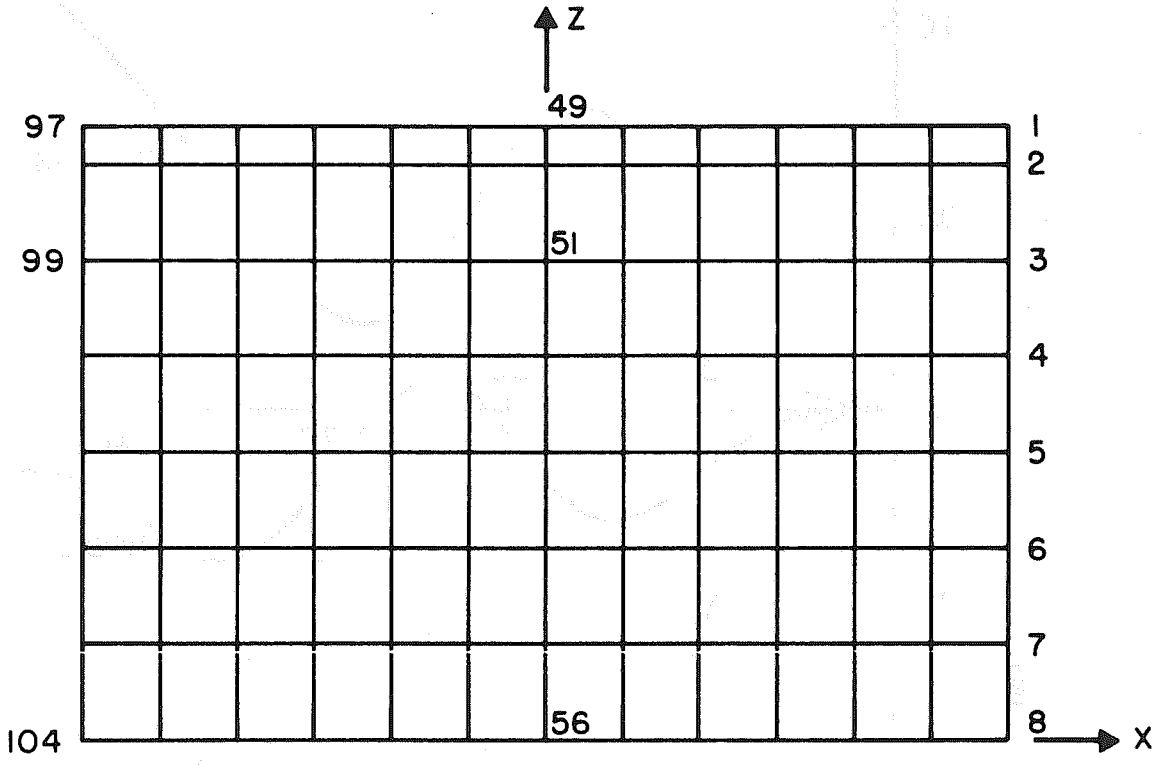

FIG. 6-14 b ELEMENT LAYOUT FOR HALF OF THE TOWER

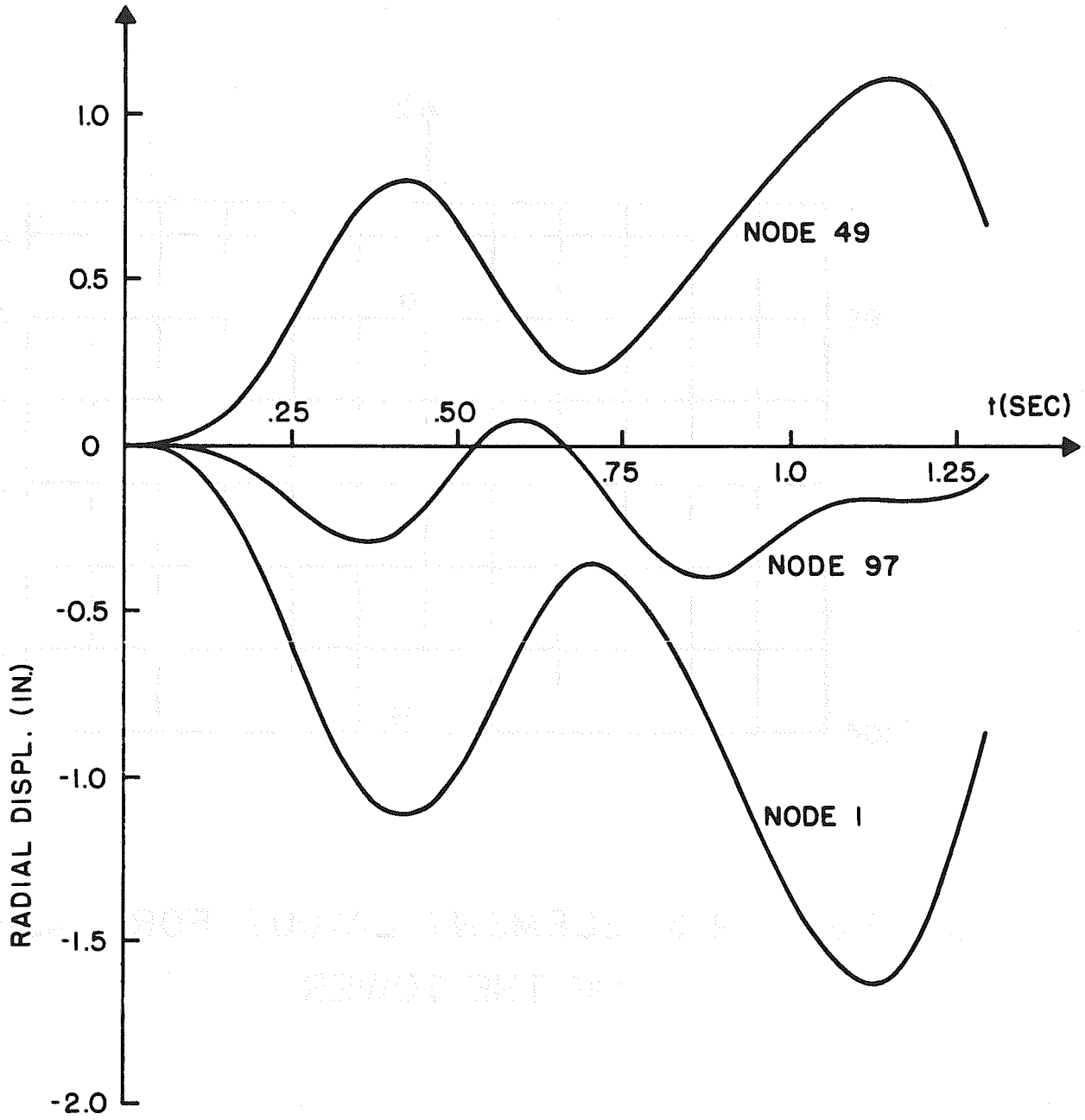

FIG. 6-15 a TOP RING DISPLACEMENTS

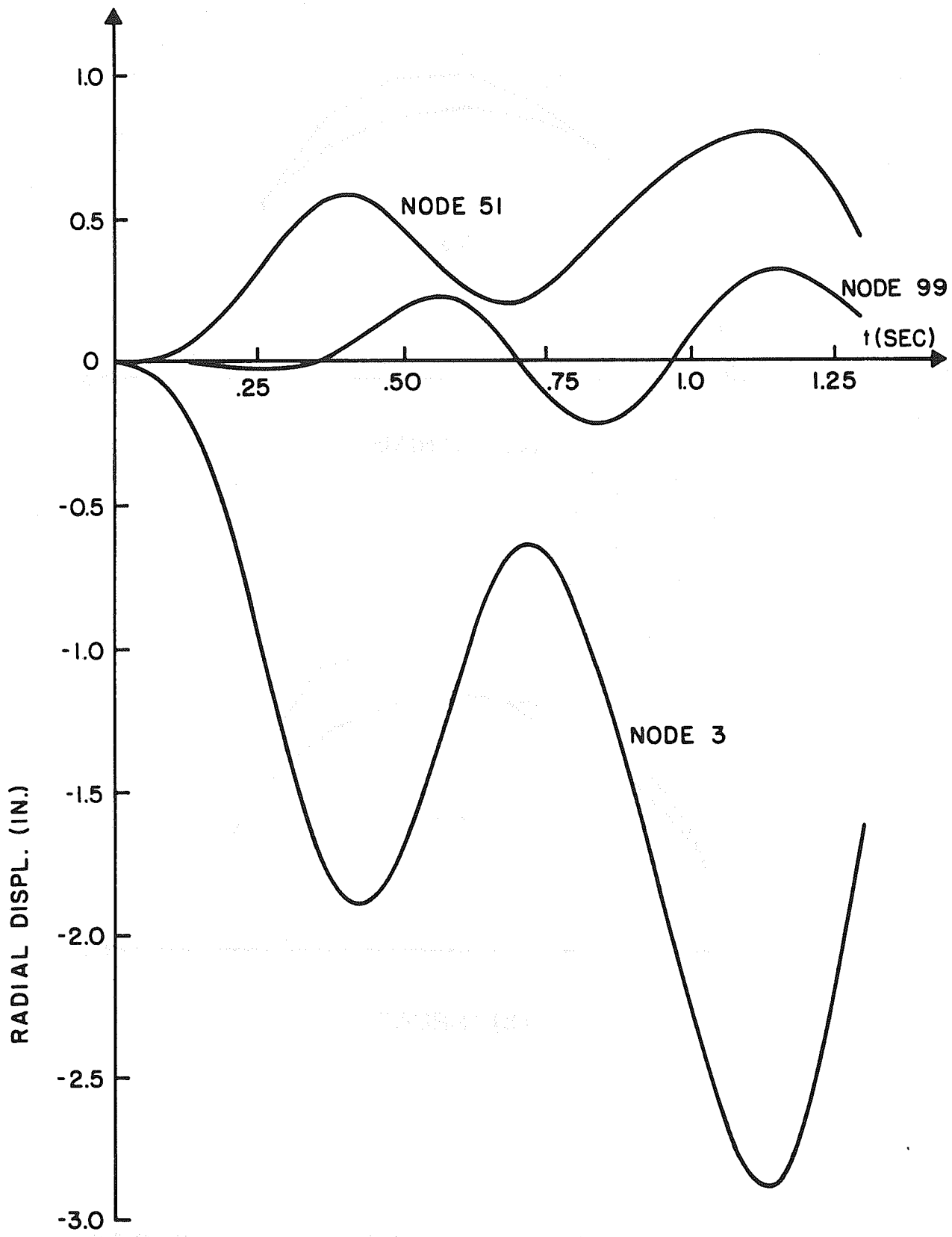

FIG.6-15 b THROAT DISPLACEMENTS

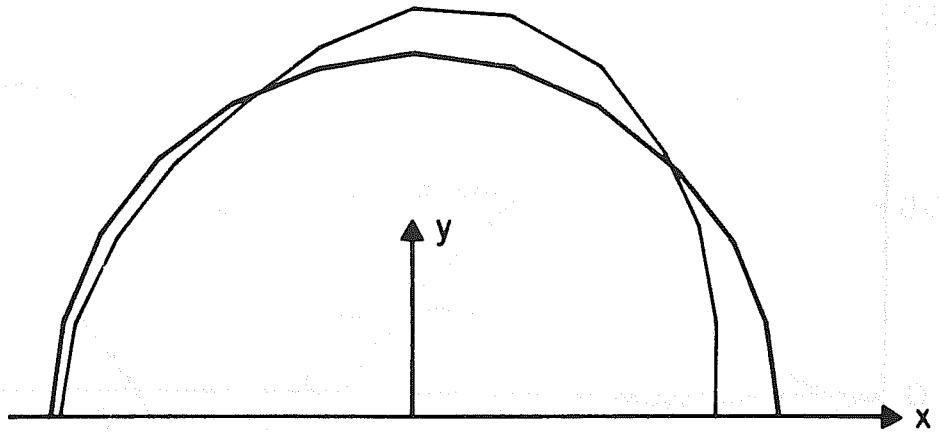

(a) TOP RING

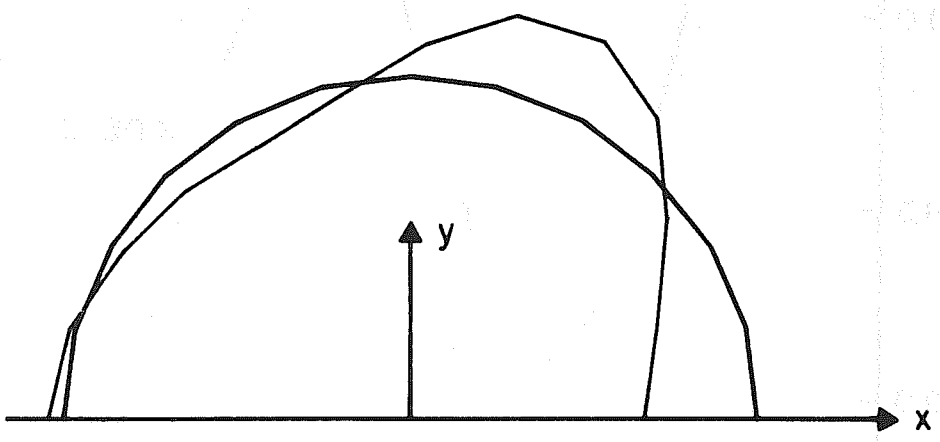

(b) THROAT

FIG. 6-16 DISPLACEMENT AT t = 1.15 SEC.
(magnified 100 times)

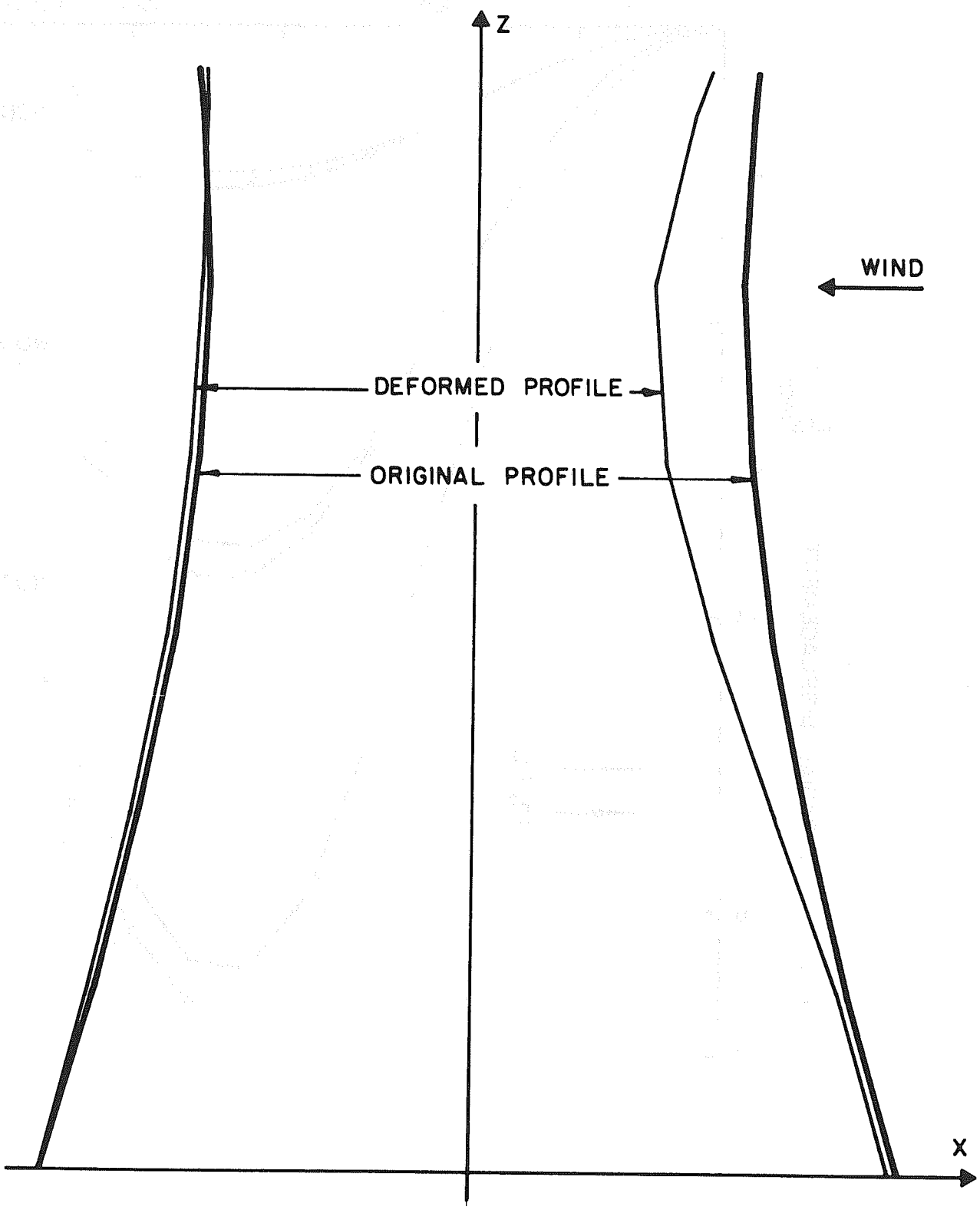

FIG. 6-17 DISPLACEMENT AT t = 1.15 SEC
(magnified 100 times)

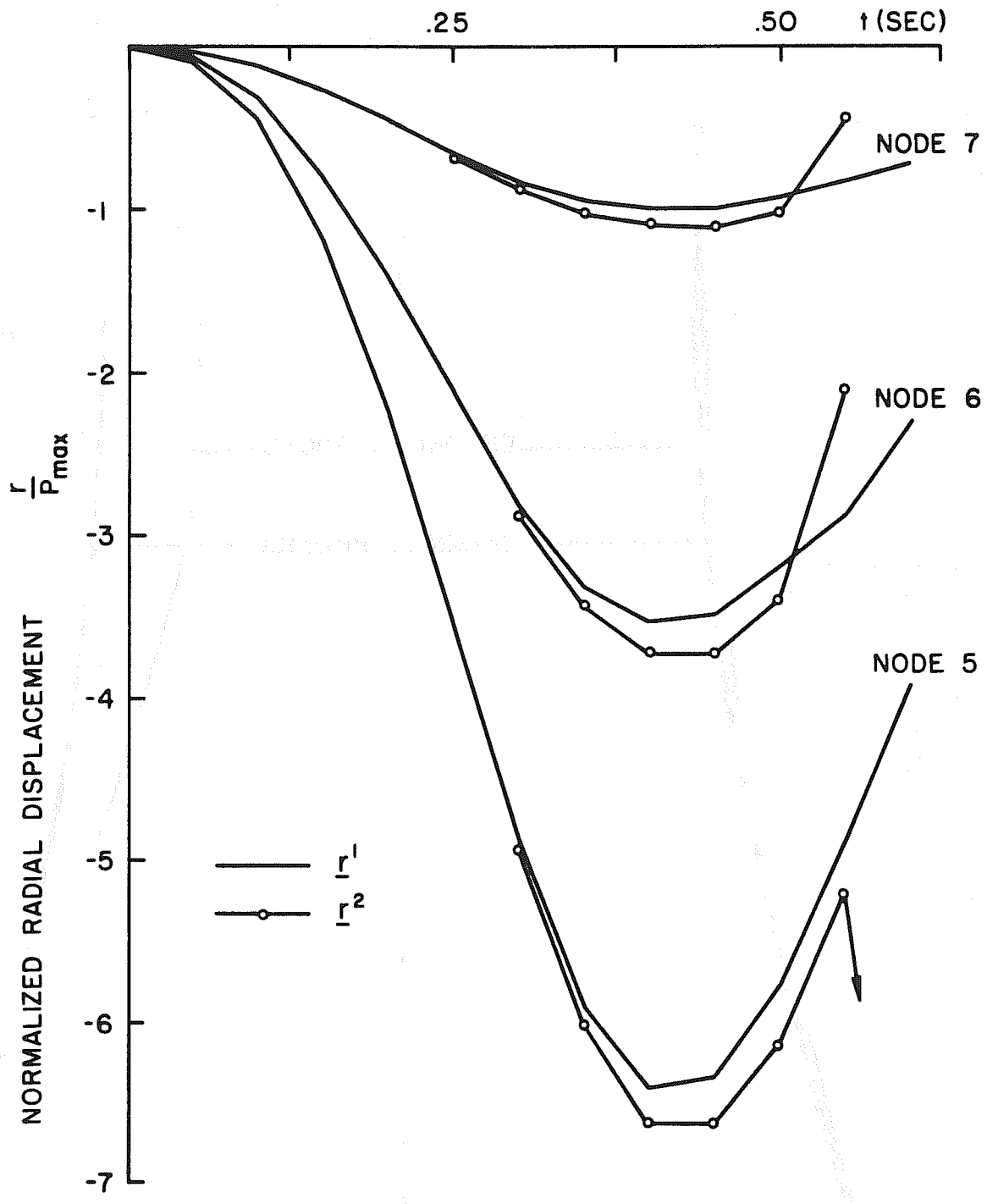

FIG. 6-18 DIVERGENCE OF NON-LINEAR SOLUTION (I)

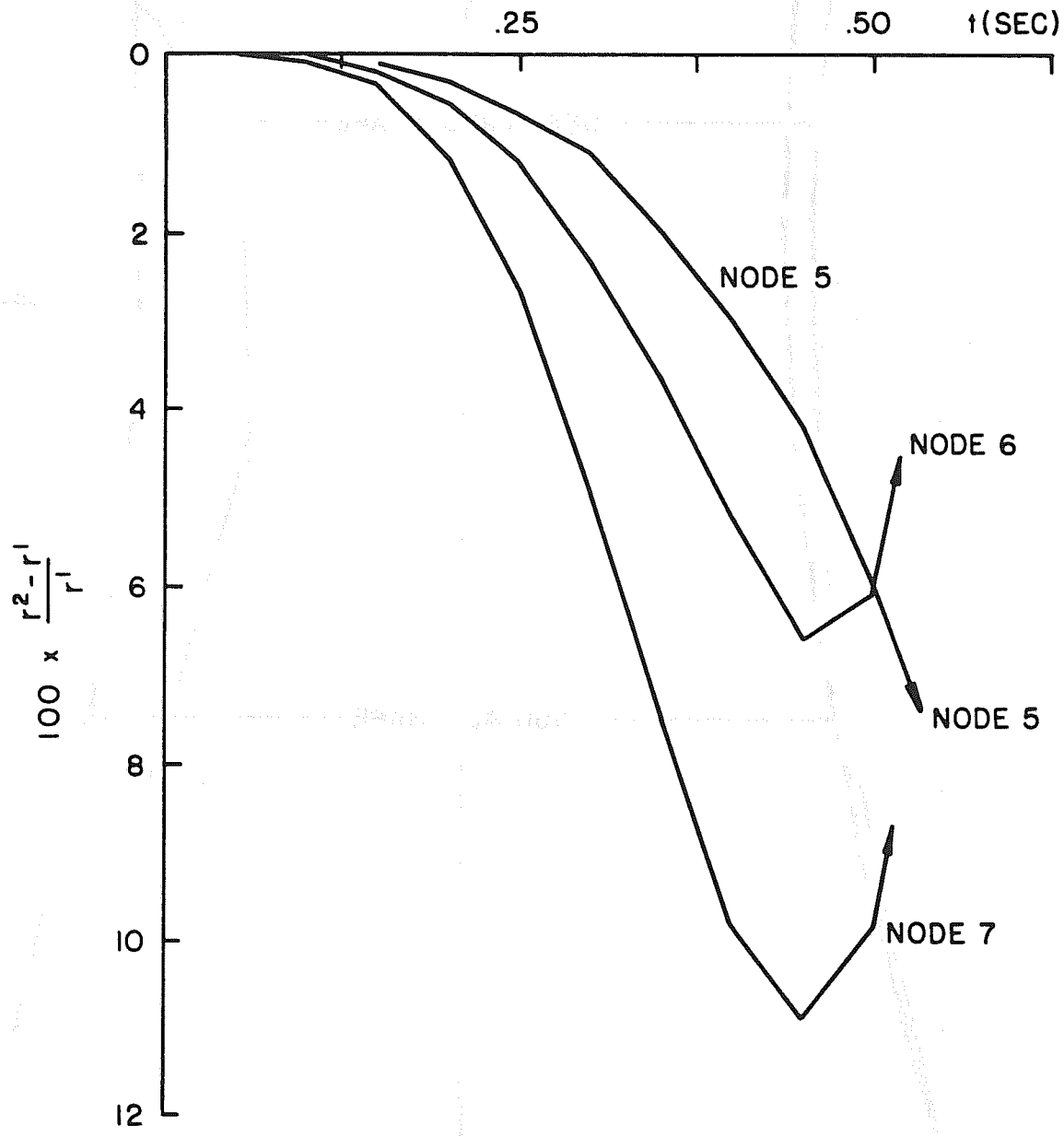

FIG. 6-19 DIVERGENCE OF NON-LINEAR SOLUTION (II)

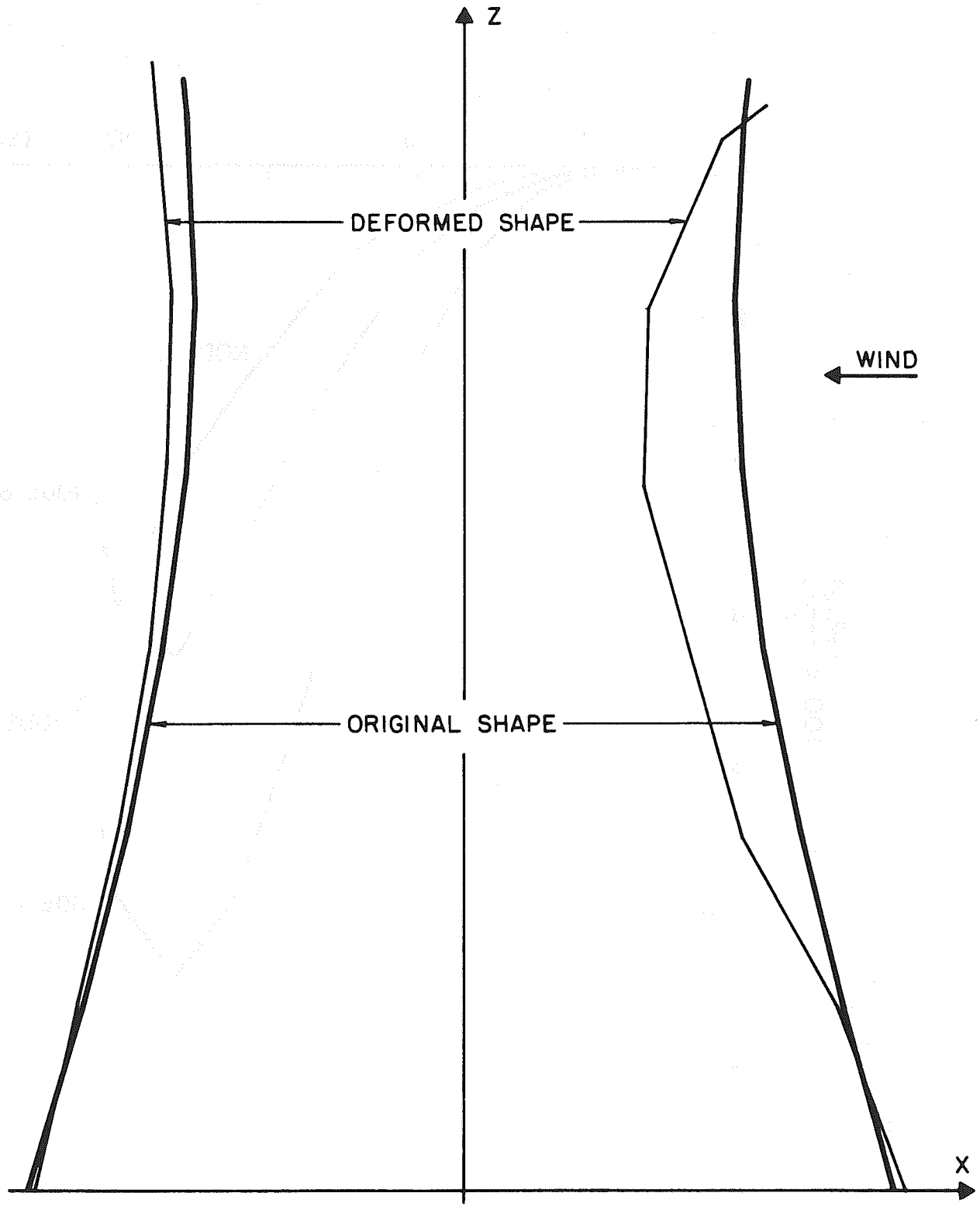

FIG. 6-20 DEFORMED TOWER BEFORE COLLAPSE
t=0.6 SEC (magnified 20 times)

7. CONCLUSIONS

A general procedure has been developed in this investigation for the determination of the nonlinear dynamic response of shell structures. This procedure is direct and simple and can be applied to structures of virtually any type if the element stiffness matrices of these structures can be properly defined.

The examples presented in Chapter 6 have demonstrated how this procedure can be applied to solve a variety of static and dynamic shell problems involving geometric nonlinearities. The three static examples indictate that the nonlinear behavior of a shell structure undergoing finite deformation can be correctly predicted. In the dynamic analyses, the convergence of the computed natural frequencies with successively refined mesh sizes demonstrates that the Finite Element Method may be used to study the dynamic behavior of shell structures. Therefore, it may be concluded that with a reasonably fine mesh and small time step, the proposed procedure should predict the nonlinear dynamic response of thin shell structures with sufficient accuracy for practical purpose.

Although only shells with relatively simple geometry and loading have been studied, it should be emphasized that a shell with any shape and boundary conditions, subjected to arbitrary loadings, can be analyzed by this procedure.

There are some restrictions on this procedure. First, a structure whose stiffness matrix becomes non positive-definite during the process, such as snap through problems of shells, cannot be analyzed by the existing computer programs. In addition, structures which develop

large strains under applied load must be avoided, because of the assumed small strain behavior. The former difficulty could be overcome by building in special controls in the program to check the structural stiffness matrix and control the load increments according to the positive or negative-definiteness of the matrix (this consideration is for static case only). To extend the program to account for large strains, nonlinear constitutive relations which are not included in this study would have to be considered.

Another restriction of the present program is that a large amount of computer core storage and computational effort are needed to carry out the analysis. The nonlinear dynamic analysis used in this study requires that the complete structural stiffness matrix be held in core, and the program is therefore limited in capacity. In the Computer Center at the University of California at Berkeley, the CDC 6400 machine with a core storage of 140,000 (in octal) storage spaces is used. The problem in Fig. 6-14b is about the maximum size that can be handled in core by this computer (520 equations and the band width of the structural stiffness matrix is 50). This limitation could be removed by dividing the stiffness matrix into blocks and solving block by block. However, the large amount of computer time needed for the analysis is the cost one has to pay to solve a large problem.

Further modification of the program might include the combination of this shell element with some other elements such as beam elements. This would extend the practical value of the program because many shell structures are constructed with ribs or in combination with frames.

Further research is suggested in the following areas:

i) Development of new shell elements. The most promising one is the curved shell element based on a three-dimensional solid (1).

ii) Study of nonlinear material properties. This is important because in many shell structures collapse is caused by material failure while the deformations of the structure are still small.

REFERENCES

1. Ahmad, S., Irons, B. M., and Zienkiewicz, O. C., "Curved Thick Shell and Membrane Element with Particular Reference to Axi-symmetric Problems," Civil Engineering Research Report, No. C/R/95/68, University of Wales, Swansea, Great Britain.

2. Biggs, J. M., "Introduction to Structural Dynamics," McGraw-Hill, 1964.

3. Carr, A. J., "A Refined Finite Element Analysis of Thin Shell Structures Including Dynamic Loadings," SEL Report, No. 67-9, University of California, Berkeley, 1967.

4. Central Electricity Generating Board (CEGB), "Report of the Committee of Inquiry into Collapse of Cooling Towers at Ferry-bridge," London, Nov. 1965.

5. Clough, R. W., "Analysis of Structural Vibrations and Dynamic Response," Japan-U.S. Seminar on Matrix Method of Structural Analysis and Design, 1969.

6. Clough, R. W., and Felippa, C. A., "A Refined Quadrilateral Element for Analysis of Plate Bending," Proceedings, The Second Conference on Matrix Method in Structural Mechanics, Air Force Flight Dynamics Laboratory, Wright-Patterson Air Force Base, Ohio, Dec. 1969.

7. Clough, R. W., and Tocher, J. L., "Finite Element Stiffness Matrices for the Analysis of Plate Bending," Proceedings, Conference on Matrix Method in Structural Mechanics, Air Force Institute of Technology, Wright-Patterson Air Force Base, Ohio, Oct. 1965.

8. Ergatoudis, J., Irons, B. M., and Zienkiewicz, O. C., "Curved, Isoparametric, Quadrilateral Element for Finite Element Analysis," Int. Journal Solid and Structures, vol. 4, 1968.

9. Farhoomand, I., "Nonlinear Dynamic Stress Analysis of Two-dimensional Solid," Ph.D dissertation, University of California, Berkeley, 1970.

10. Felippa, C. A., "Refined Finite Element Analysis of Linear and Nonlinear Two-dimensional Structures," SEL Report No. 66-22, University of California, Berkeley, 1966.

11. Felippa, C. A., "Plate Bending Finite Elements," Ph.D dissertation, University of California, Berkeley, 1966.

12. Forsberg, K., "A Review of Analytic Methods Used to Determine the Modal Characteristic of Cylindrical Shells," NASA Contractor Report, NASA CR-613, prepared by Lockheed Aircraft Corp., Palo Alto, California, Sept. 1967.

13. Ghosh, S., and Wilson, E. L., "Dynamic Stress Analysis of Axisymetric Structures under Arbitrary Loadings," EERC Report, No. 69-10, University of California, Berkeley, 1969.

14. Greste, O., "Finite Element Analysis of Tubular K Joints," Ph.D dissertation, University of California, Berkeley, 1970.

15. Hildebrand, F. B., "Introduction to Numerical Analysis," McGraw-Hill, 1956.

16. Hurty, W. C., and Rubinstein, M. F., "Dynamics of Structures," Prentice-Hall, 1964.

17. Irons, B. M., and Zienkiewicz, O. C., "The Isoparametric Finite Element System - A New Concept in Finite Element Analysis," Conference on Recent Advances in Stress Analysis, Joint Brit. Comm. Stress Analysis, London, March 1968.

18. Isaacson, E., and Keller, H. B., "Analysis of Numerical Method," John Wiley and Sons, 1966.

19. Johnson, C. P., "The Analysis of Thin Shells by a Finite Element Procedure," Ph.D dissertation, SEL Report, No. 67-22, University of California, Berkeley, 1966.

20. Kao, R., and Perrone, N., "Asymmetric Buckling of Spherical Caps with Asymmetrical Imperfections," The Catholic University of America Report, No. 16, Feb. 1970.

21. Kornishin, H. S., and Isanbaeva, F. S., "Flexible Plates and Panels," (in Russian) Nauka, Moscow, 1968.

22. Kraus, H., "Thin Elastic Shells," John Wiley and Sons, 1967.

23. Laursen, H., "Matrix Analysis of Structures," McGraw-Hill, 1966.

24. Laursen, H. I., "Stability and Nonlinear Analysis of Framed Structures," SEL Report, No. 63-4, University of California, Berkeley, 1963.

25. Martin, H. C., "Large Deflection and Stability Analysis by the Direct Stiffness Method," Jet Propulsion Lab., Technical Report No. 32-931, Pasadena, 1965.

26. Murray, D. W., "Large Deflection Analysis of Plates," SEL Report, No. 67-44, University of California, Berkeley, 1967.

27. Newmark, N. M., "A Method of Computation for Structural Dynamics," Journal, Engineering Mechanics Division, ASCE, No. EM 3, July 1959.

28. Oden, J. T., "Calculation of Geometric Stiffness Matrices for Complex Structures," AIAA Journal, vol. 4, No. 8, 1966.

29. Oden, J. T., "Analysis of Finite Deformations of Elastic Solids by the Finite Element Method," paper prepared for the IUTAM Symposium on High Speed Computing of Elastic Structures, 1969.

30. Powell, G. H., "Theory of Nonlinear Elastic Structures," ASCE Journal, Structural Division, vol. 95, No. ST12, Dec. 1969.

31. Przemieniecki, J. S., "Theory of Matrix Structural Analysis," McGraw-Hill, 1968.

32. Rutishauser, H., "Deflation bei Bandmatrizen," ZAMP, 1959, vol. 10, pp. 314-319.

33. Shilov, G. E., "An Introduction to the Theory of Linear Space," Prentice-Hall, 1965.

34. Stricklin, J. A., Martinez, J. E., Tillerson, J. R., Hong, J. H., and Haisler, W. E., "Nonlinear Dynamic Analysis of Shells of Revolution by Matrix Displacement Method," Texas A&M University Report 69-77, Feb. 1970.

35. Timoshenko, S. P., and Gere, J. M., "Theory of Elastic Stability," McGraw-Hill, 1961.

36. Timoshenko, S. P., and Woinowsky-Krieger, S., "Theory of Plates and Shells," McGraw-Hill, 1959.

37. Tong, K. N., "Theory of Mechanical Vibration," John Wiley and Sons, 1960.

38. Willam, K., "Finite Element Analysis of Cellular Structures," Ph.D dissertation, University of California, Berkeley, 1969.

39. Wilson, E. L., "Elastic Dynamic Response of Axisymmetric Structures," SEL Report, No. 69-2, University of California, Berkeley, 1969.

40. Wilson, E. L., and Clough, R. W., "Dynamic Response by a Step-by-Step Analysis," Proceedings, Symposium on the Use of Computer in Civil Engineering, Lisbon, 1962.

41. Wilson, E. L., Jones, L. R., and Hsueh, T., "Large Displacement Analysis of Axisymmetric Shells," SEL Report, No. 69-13, University of California, Berkeley, 1969.

42. Yaghmai, S., "Incremental Analysis of Large Deformations in Mechanics of Solid with Applications to Axisymmetric Shells of Revolution," SEL Report, No. 68-17, University of California, Berkeley, 1968.

43. Zienkiewicz, O. C., and Cheung, Y. K., "The Finite Element Method in Structural and Continuum Mechanics," McGraw-Hill, 1967.

44. Proceedings of the First and the Second Conferences on Matrix Method in Structural Mechanics, Wright-Patterson Air Force Base, Ohio, 1965 and 1960.